

AD-A094 897

TEXAS UNIV AT AUSTIN APPLIED RESEARCH LABS
THE PERFORMANCE OF A PARAMETRIC RECEIVER IN AN INHOMOGENEOUS ME--ETC(U)

F/G 17/1

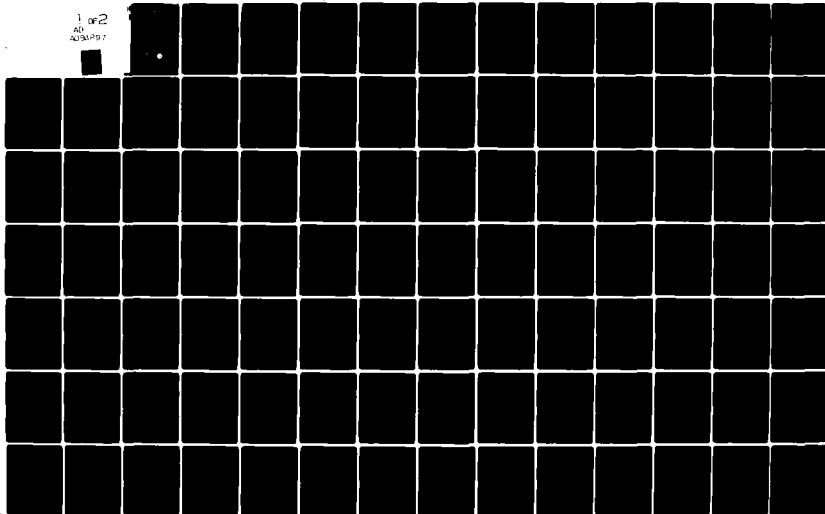
AUG 80 C R CULBERTSON

N00024-79-C-6358

NL

UNCLASSIFIED ARL-TR-80-44

1 of 2
AD
A094897



LEVEL

11
B.S.

ARL-TR-80-44

Copy No. 34

**THE PERFORMANCE OF A PARAMETRIC
RECEIVER IN AN INHOMOGENEOUS MEDIUM**

C. Robert Culbertson

**APPLIED RESEARCH LABORATORIES
THE UNIVERSITY OF TEXAS AT AUSTIN
POST OFFICE BOX 8029, AUSTIN, TEXAS 78712**

18 August 1980

Technical Report

APPROVED FOR PUBLIC RELEASE;
DISTRIBUTION UNLIMITED.

DTIC
ELECTRONIC
FEB 11 1981

Prepared for:

**NAVAL SEA SYSTEMS COMMAND
DEPARTMENT OF THE NAVY
WASHINGTON, DC 20362**

**OFFICE OF NAVAL RESEARCH
DEPARTMENT OF THE NAVY
ARLINGTON, VA 22217**



AD A094897

DDC FILE COPY

Te

81 2 11 046

UNCLASSIFIED

SECURITY CLASSIFICATION OF THIS PAGE (When Data Entered)

| REPORT DOCUMENTATION PAGE | | READ INSTRUCTIONS BEFORE COMPLETING FORM |
|--|---|---|
| 1. REPORT NUMBER | 2. GOVT ACCESSION NO. <i>AD-A094 897</i> | 3. RECIPIENT'S CATALOG NUMBER |
| 4. TITLE (and Subtitle) <i>THE PERFORMANCE OF A PARAMETRIC RECEIVER IN AN INHOMOGENEOUS MEDIUM,</i> | | 5. TYPE OF REPORT & PERIOD COVERED <i>technical report</i> |
| 7. AUTHOR(s) <i>C. Robert Culbertson</i> | | 6. PERFORMING ORG. REPORT NUMBER <i>ARL-TR-80-44</i> |
| 9. PERFORMING ORGANIZATION NAME AND ADDRESS <i>Applied Research Laboratories The University of Texas at Austin Austin, TX 78712</i> | | 8. CONTRACT OR GRANT NUMBER(s) <i>N00024-79-C-6358, and N00014-75-C-0161</i> |
| 11. CONTROLLING OFFICE NAME AND ADDRESS <i>Naval Sea Systems Command Department of the Navy Washington, DC 20362</i> <i>and</i> <i>Office of Naval Research Department of the Navy Arlington, VA 22217</i> | | 10. PROGRAM ELEMENT, PROJECT, TASK AREA & WORK UNIT NUMBERS <i>(12)</i> |
| 16. DISTRIBUTION STATEMENT (of this Report) <i>Approved for public release; distribution unlimited.</i> | | 12. REPORT DATE <i>18 Aug 1980</i> |
| | | 13. NUMBER OF PAGES <i>165</i> |
| | | 15. SECURITY CLASS. (of this report) <i>UNCLASSIFIED</i> |
| 15a. DECLASSIFICATION DOWNGRADING SCHEDULE | | |
| 17. DISTRIBUTION STATEMENT (of the abstract entered in Block 20, if different from Report) | | |
| 18. SUPPLEMENTARY NOTES | | |
| 19. KEY WORDS (Continue on reverse side if necessary and identify by block number) | | |
| 20. ABSTRACT (Continue on reverse side if necessary and identify by block number) <i>This thesis describes a theoretical and experimental study of the effects of medium inhomogeneities on the performance of a parametric receiver.</i> <i>A review is made of the basic principles of parametric receiver operation and of wave propagation in an inhomogeneous medium.</i> <i>A theoretical analysis is presented for the case of a signal wave source located on the axis of the parametric receiver in a weakly inhomogeneous medium. Expressions are developed that predict the level of amplitude fluctuations in</i> | | |

DD FORM 1 JAN 73 1473

EDITION OF 1 NOV 65 IS OBSOLETE

UNCLASSIFIED

SECURITY CLASSIFICATION OF THIS PAGE (When Data Entered)

FOREWORD.

This report is an adaptation of a dissertation submitted to the Faculty of Science and Engineering, University of Birmingham, England, for the degree of Ph.D. The work was supervised by Professor H. O. Berkday and Dr. B. V. Smith. The author expresses his appreciation to Professor H. A. Prime for facilities made available at Birmingham for this work and for permission to publish the dissertation in the present form.

Financial support for the author was provided primarily by the Office of Naval Research. Additional support was provided by the Defense Advance Research Projects Agency, Naval Electronic Systems Command, and Naval Sea Systems Command.

| | |
|--------------------|-------------------------------------|
| Accession For | |
| NTIS GRA&I | <input checked="" type="checkbox"/> |
| DTIC TAB | <input type="checkbox"/> |
| Unannounced | <input type="checkbox"/> |
| Justification | <input type="checkbox"/> |
| By _____ | |
| Distribution/ | |
| Availability Codes | |
| Dist | Avail and/or Special |
| A | |

↓

SYNOPSIS.

This thesis describes a theoretical and experimental study of the effects of medium inhomogeneities on the performance of a parametric receiver.

A review is made of the basic principles of parametric receiver operation and of wave propagation in an inhomogeneous medium.

A theoretical analysis is presented for the case of a signal wave source located on the axis of the parametric receiver in a weakly inhomogeneous medium. Expressions are developed that predict the level of amplitude fluctuations in the second-order pressure at the hydrophone of the parametric receiver. Both collimated and spherically spreading pump waves are considered.

The experimental study reported in this thesis was conducted in a model tank in which an array of immersion heaters and a perforated screen produced a thermal microstructure. Measurements were made of the coefficient of amplitude variation for the signal, pump, and interaction frequency waves associated with both a nearfield and a farfield parametric receiver. Results are compared to theory and discussed.

31

7

TABLE OF CONTENTS.

| | <u>Page</u> |
|--|-------------|
| LIST OF FIGURES | vii |
| LIST OF SYMBOLS | ix |
| CHAPTER 1. INTRODUCTION | 1 |
| 1.1 Nonlinear Acoustics and Parametric Arrays | 1 |
| 1.2 Effects of Medium Inhomogeneities | 4 |
| 1.3 An Overview of the Thesis | 5 |
| CHAPTER 2. THE PARAMETRIC ACOUSTIC RECEIVING ARRAY | 7 |
| 2.1 Introduction | 7 |
| 2.2 Basic Theoretical Concepts | 7 |
| 2.3 The Parametric Array | 11 |
| 2.3.1 The Nearfield Receiving Array | 13 |
| 2.3.2 The Farfield Receiving Array | 18 |
| 2.4 Practical Consideration | 20 |
| 2.4.1 Signal Processing | 20 |
| 2.4.2 Shadowing | 22 |
| 2.4.3 Finite Amplitude Effects | 25 |
| 2.4.4 Sources of Noise that Affect Parametric Reception | 27 |
| 2.4.5 Effect of Turbulence and Medium Inhomogeneities | 29 |
| 2.5 Summary | 29 |
| CHAPTER 3. ACOUSTIC WAVE PROPAGATION IN AN INHOMOGENEOUS MEDIUM | 31 |
| 3.1 Introduction | 31 |
| 3.2 Methods of Describing the Inhomogeneous Medium | 34 |
| 3.3 Turbulence | 37 |
| 3.4 The Wave Equation for an Inhomogeneous Medium | 43 |
| 3.5 Fluctuations in the Amplitude and Phase of the Observed Pressure | 46 |
| 3.5.1 Fluctuations in a Medium Described by a Correlation Function | 48 |

| | <u>Page</u> |
|--|-------------|
| 3.5.2 Fluctuations in a Turbulent Medium | 49 |
| 3.6 Correlation of Fluctuations | 51 |
| 3.7 Summary | 52 |
| CHAPTER 4. THEORETICAL ANALYSIS | 54 |
| 4.1 Introduction | 54 |
| 4.2 Amplitude Fluctuations for a Nearfield Receiving Array | 55 |
| 4.3 Amplitude Fluctuations for a Farfield Receiving Array | 64 |
| 4.4 Approximating the Spatial Correlation Functions | 69 |
| 4.5 Evaluation of Results | 76 |
| 4.5.1 Nearfield Receiving Array | 76 |
| 4.5.2 Farfield Receiving Array | 78 |
| 4.6 Summary and Discussion | 82 |
| CHAPTER 5. EXPERIMENTAL STUDY | 85 |
| 5.1 The Experimental Medium | 85 |
| 5.2 Description of Apparatus | 88 |
| 5.3 Experimental Results | 91 |
| 5.3.1 Measurements of Upper Sideband Pressure | 91 |
| 5.3.2 Procedure for Obtaining Data | 94 |
| 5.3.3 Signal Wave Amplitude Fluctuations | 95 |
| 5.3.4 Pump Wave Amplitude Fluctuations | 100 |
| 5.3.5 Amplitude Fluctuations in the Upper Sideband Wave | 104 |
| 5.3.6 Results for Spherically Spreading Pump Waves | 110 |
| 5.4 Discussion | 113 |
| 5.5 Summary | 114 |

| | <u>Page</u> |
|---|-------------|
| CHAPTER 6. SUMMARY AND DISCUSSION | 116 |
| 6.1 Summary of the Thesis | 116 |
| 6.2 Discussion of Results | 118 |
| 6.3 Conclusions | 120 |
| APPENDIX 1. DERIVATION OF EQUATIONS (4.20) and (4.21) | 122 |
| APPENDIX 2. TRANSVERSE CORRELATION OF FLUCTUATIONS | 125 |
| A.2.1 Transverse Correlation for the Nearfield Case | 125 |
| A.2.2 Transverse Correlation for the Farfield Case | 127 |
| APPENDIX 3. TRANSDUCERS | 128 |
| A.3.1 Signal Source | 128 |
| A.3.2 Pump Transducer for the Nearfield Receiver | 128 |
| A.3.3 Pump Transducer for the Farfield Receiver | 128 |
| A.3.4 Hydrophone | 128 |
| APPENDIX 4. ELECTRONIC RECEIVING SYSTEM | 130 |
| APPENDIX 5. COMPUTER PROGRAMS | 135 |
| AFLUCT | 136 |
| CAVANA | 139 |
| CAVNUM | 142 |
| APPENDIX 6. ANALYSIS OF THE NEARFIELD PARAMETRIC RECEIVER | 151 |
| A.6.1 Second-Order Solution for a Homogeneous Medium | 151 |
| A.6.2 Amplitude Fluctuations in an Inhomogeneous Medium | 156 |
| REFERENCES | 159 |

LIST OF FIGURES.

| <u>Figure</u> | <u>Title</u> | <u>Page</u> |
|---------------|--|-------------|
| 2.1 | Radiation from an Elemental Source | 12 |
| 2.2 | The Nearfield Parametric Receiving Array | 14 |
| 2.3 | Elemental Wafers in the Interaction Region | 16 |
| 2.4 | Sketch of the Filtering Problem | 21 |
| 2.5 | Band Elimination Receiver | 23 |
| 2.6 | Phase-Locked Loop Receiver | 24 |
| 3.1 | Modelling an Inhomogeneity as a Spherical Source | 32 |
| 3.2 | Turbulent Power Density Spectrum | 40 |
| 4.1 | Geometry for Analyzing Nearfield Receiver | 56 |
| 4.2 | Scattering Geometry | 62 |
| 4.3 | Geometry for Analyzing Farfield Receiver | 65 |
| 4.4 | Propagation Paths of Pump and Second-Order Wave | 71 |
| 4.5 | Geometry for Autocorrelation of Second-Order Wave Fluctuations | 75 |
| 4.6 | CAV for Farfield Parametric Receiver Operating in the Ocean | 81 |
| 5.1 | Model Tank | 86 |
| 5.2 | Experimental Apparatus | 90 |
| 5.3 | Arrangement for Measuring Mixing in the Electronic Receiver | 92 |
| 5.4 | Temperature Dependence of 1 MHz Signal Wave Fluctuations | 98 |
| 5.5 | Signal Wave Amplitude Fluctuations | 101 |
| 5.6 | Pump Wave Amplitude Fluctuations | 103 |
| 5.7 | CAV _{USB} for Fixed Array Length and Variable Range | 105 |
| 5.8 | CAV _{USB} for Fixed Range and Variable Array Length | 108 |

| <u>Figure</u> | <u>Title</u> | <u>Page</u> |
|---------------|---|-------------|
| 5.9 | Comparison of Upper Sideband and Signal Wave Fluctuations | 109 |
| 5.10 | CAV for Spherical Pump Waves | 111 |
| A2.1 | Significant Scattering Volumes in Nearfield of Pump | 126 |
| A4.1 | Electronic Receiving System | 131 |
| A4.2 | One Channel of Signal Processing Unit | 132 |
| A4.3 | Receiving System for Farfield Receiver | 133 |
| A6.1 | Model of the Nearfield Parametric Receiver | 152 |

LIST OF SYMBOLS.

Latin Symbols

| | |
|---------------------------|---|
| a | patch radius |
| B | total amplitude fluctuation (sum of B_s , B_p , and B_{\pm}) |
| b | a dimension of the pump transducer, which is usually square with sides $2b \times 2b$ |
| B_p, B_s, B_{\pm} | amplitude fluctuations of 'pump', 'signal', and 'interaction frequency' waves, respectively |
| B_{PR} | amplitude fluctuation of 'interaction frequency' wave at the hydrophone |
| B_t | amplitude fluctuations produced by transition region |
| B/A | parameter of nonlinearity |
| CAV | coefficient of amplitude variation |
| C_n | turbulence parameter |
| c | sound speed |
| c_o | small signal sound speed |
| $c_o = \langle c \rangle$ | mean sound speed (Chapter 3) |
| Δc | random variation in sound speed from mean value |
| D | wave parameter |
| $D(\theta)$ | directivity function |
| d | shadow length |
| $\frac{dx}{dt}$ | propagation speed |
| $EXDB$ | excess attenuation |
| e_x | pump excess |
| f | frequency |
| f_a | aperture factor |
| f_{μ} | normalizing factor |

| | |
|---------------------|---|
| FNR | fluctuation-to-noise ratio |
| \hat{i} | unit vector in the x direction |
| j | $\sqrt{-1}$ |
| k | acoustic wavenumber |
| k_p, k_s, k_{\pm} | acoustic wavenumber at frequencies ω_p , ω_s , and ω_{\pm} , respectively |
| L | characteristic scale of flow (Chapter 3) |
| L | array length |
| L_o | outer scale of turbulence |
| l_o | inner scale of turbulence |
| ℓ | eddy size |
| ΔL | separation |
| M | parameter used in describing the angular response of a parametric receiver (Chapter 2) |
| M | voltage response (Appendix 6) |
| N | correlation function |
| n | refractive index |
| p | acoustic pressure |
| p_F | pressure of the 'interaction frequency' wave for the case of spherical pump waves, with the detector in the pump farfield |
| p_N | pressure of the 'interaction frequency' wave when the detector is in the nearfield of all elemental wafers |
| p_o | equilibrium pressure |
| p_T | total pressure |
| p_n | n^{th} -order pressure |
| q | source density |
| R | correlation coefficient |

| | |
|---------------------|--|
| \vec{R} | unit vector in the propagation direction of the 'signal' wave |
| $\text{Re}(x)$ | real part of x |
| Re | Reynolds number (Chapter 3) |
| R_0 | nearfield limit |
| R_B^L, R_S^L | longitudinal amplitude and phase correlation coefficient, respectively |
| R_B^T, R_S^T | transverse amplitude and phase correlation coefficient, respectively |
| \vec{r} | radius vector of observer |
| \vec{r}' | vector from source point to observer |
| \vec{r}_0 | radius vector of source point |
| S | total phase fluctuation (sum of $S_p, S_s,$ and S_{\pm}) |
| s | entropy (Chapters 1, 2) |
| S_p, S_s, S_{\pm} | phase fluctuations of 'pump', 'signal', and 'interaction frequency' wave, respectively |
| S_{PR} | phase fluctuation of 'interaction frequency' wave at hydrophone |
| S_{μ} | three-dimensional spectral density of refractive index variations |
| t | time |
| T | average kinetic energy |
| T_0 | mean temperature |
| ΔT | deviation from mean temperature |
| u | particle velocity |
| V | volume |
| \bar{x} | shock formation distance |
| Z_s | distance from low frequency signal source to pump transducer |

Greek Symbols

| | |
|------------------------------------|--|
| α | attenuation coefficient |
| $\alpha_p, \alpha_s, \alpha_{\pm}$ | attenuation coefficient at frequencies ω_p , ω_s , and ω_{\pm} , respectively |
| β | a parameter of nonlinearity |
| Γ | Gol'dberg number |
| ϵ | acoustic mach number |
| ϵ | energy dissipated as heat per unit mass per unit time (Chapter 3) |
| η | efficiency |
| θ | phase of 'signal' wave at $z = 0$ |
| κ | spatial wavenumber |
| $\kappa_m, \kappa_t, \kappa_o$ | wavenumbers that are upper boundaries of source, transition, and inertial subranges, respectively |
| λ | acoustic wavelength |
| λ_s | acoustic wavelength at frequency ω_s |
| μ | variation in refractive index from unity |
| ν | kinematic viscosity |
| ρ | excess density |
| $\rho_o = \langle \rho_T \rangle$ | mean density (Chapter 3) |
| ρ_o | equilibrium density |
| ρ_T | total density |
| $\Delta\rho$ | variation in density from mean value |
| σ | normalized range parameter |
| τ | retarded time |
| ϕ_m | magnitude, or maximum value, of the refractive index spectrum |
| ϕ_v | one-dimensional power spectral density |

| | |
|------------------------------------|--|
| ϕ | phase angle |
| ω | angular frequency |
| $\omega_p, \omega_s, \omega_{\pm}$ | angular frequencies of 'pump', 'signal', and 'interaction frequency' waves, respectively |

Units

| | |
|--------------------|--------------------|
| $^{\circ}\text{C}$ | degrees Centigrade |
| cm | centimeters |
| h | hours |
| m | meters |
| MHz | megahertz |
| mV | millivolts |
| mW | milliwatts |
| Pa | Pascals |
| p-p | peak-to-peak |
| rms | root-mean-square |
| V | volts |

Miscellaneous

| | |
|--------------------|----------------------------------|
| $\langle \rangle$ | ensemble average |
| $\overline{\quad}$ | time average |
| x^* | complex conjugate of x |
| \int_V | volume integral |
| ∇ | vector differential operator del |
| \square^2 | the D'Alembertian operator |

The subject considered in this thesis is the performance of a parametric acoustic receiving array in an inhomogeneous medium. Development of this subject requires the synthesis of two branches of acoustics: (1) nonlinear acoustics, from which the concept of the parametric receiver has been developed, and (2) wave propagation in an inhomogeneous medium. Both of these topics have received considerable study in recent years, and it is reasonable to introduce the topics separately before considering their interrelation. In this chapter an introduction is given to nonlinear acoustics and to the effects of medium inhomogeneities. Following this is an introduction to the present investigation, including a description of the aims and the organization of this investigation.

1.1 Nonlinear Acoustics and Parametric Arrays

It has been known theoretically since Stokes' analysis¹ in 1848 that an acoustic wave distorts as it propagates through a fluid. This distortion occurs because the propagation speed of a sound wave is a function of the particle velocity; that is,²

$$\frac{dx}{dt} = c_0 + u(x,t) + \frac{1}{2} \frac{B}{A} u(x,t)^2, \quad (1.1)$$

where

$\frac{dx}{dt}$ is the propagation speed,

c_0 is a constant equal to the sound speed for waves of infinitesimal amplitude,

$\frac{B}{A}$ is a constant that characterizes the nonlinearity of the pressure-density relation, [defined in Eq. (1.2)], and

u is the particle velocity in the x direction.

It can be seen from Eq. (1.1) that there are two effects which contribute

to the variability of the propagation speed. One effect is 'convection' which arises because the particles of the supporting medium are moving in the same direction as the propagating wave. Convection is taken into account in Eq. (1.1) by the term $u(x,t)$, which indicates that the propagation speed is linearly dependent on the particle velocity. A second cause of variations in propagation speed is due to nonlinearity in the pressure-density relation.³ The relation between acoustic pressure and excess density in a liquid may be written as⁴

$$p = c_o^2 \rho + \frac{1}{2} \frac{c_o^2}{\rho_o} \left(\frac{B}{A} \right) \rho^2, \quad (1.2)$$

where

$$p = p_T - p_o \quad \text{is acoustic pressure,}$$

$$\rho = \rho_T - \rho_o \quad \text{is excess density,}$$

$$\frac{B}{A} = \frac{\rho_o}{c_o^2} \left(\frac{\partial^2 p}{\partial \rho^2} \right)_{o,S}$$

S is entropy, and

the subscripts zero and T denote equilibrium and total values, respectively.

The quantity B/A is a measure of the nonlinearity of a fluid. In Eq. (1.1) the effect of this nonlinearity on the propagation speed is accounted for by the term $\frac{1}{2} \frac{B}{A} u(x,t)$. For water, B/A has a value of the order of 5.2 while for air, B/A approximately equals 0.4.³ It can be seen by substituting these values of B/A into Eq. (1.1) that convection is the dominant effect in distorting airborne sound waves, while fluid nonlinearity dominates in the distortion of sound waves in water.

As a result of the nonlinear character of acoustic wave propagation, when two waves propagate simultaneously in a fluid, interaction-frequency components are generated.⁵ Difference frequency tones have been observed

by musicians⁶⁻⁸ since 1745, and it was the observation of a difference frequency sound beam⁹ that led Westervelt¹⁰ to formulate the concept of the parametric array in 1960. This concept can be summarized as follows. If pressure waves* of frequencies f_1 and f_2 insonify a common region of fluid, there arise in that region secondary sound sources of frequency $|f_1 \pm f_2|$. These secondary sources act as an array which can be used to transmit or receive directive beams of sound.

In the transmitting application, the 'primary waves' (i.e., the waves of frequency f_1 and f_2) are launched from a common transducer, and the effective array length is controlled by attenuation in the medium. Such a parametric transmitter can be used to generate a directive beam with negligible sidelobe levels¹¹ at frequencies $|f_1 \pm f_2|$.

In the receiving application, one primary wave is usually a low frequency acoustic signal arriving at the parametric receiver from some distant source. This signal interacts with a locally generated 'pump' wave to form sum and difference frequency sources in the region common to both waves. The radiation from these sources is detected by a hydrophone placed in the pump beam. The array length in this instance is determined by the separation, L , between the pump transducer and hydrophone. The parametric receiver acts as a conventional end-fire linear array of length L , operating at the frequency of the signal to be detected. The advantages of directivity offered by an end-fire array (i.e., reduction of interference due to ambient noise and multipath signals) are achieved by the parametric receiver, but only two transducers are required to 'construct' the array.

Further discussion of the basic principles of the parametric acoustic receiving array, as well as an outline of the history of its development, is given in Chapter 2.

*The waves are assumed to be such that their propagation vectors are at angles of less than 90° to one another.

1.2 Effects of Medium Inhomogeneities

The variability of sound transmission in the sea is a topic that has received a great deal of study in the last 30 years. There is a variety of mechanisms that can cause fluctuations in the amplitude and phase of an acoustic signal.¹² For example, if an acoustic source or receiver is mounted on a ship, then irregular motion of the platform can give rise to fluctuations. If surface reflections contribute to the received signal, then changes in the surface due to wave motion will cause phase and amplitude variations. Even when the source and receiver are fixed and there are no surface reflections involved, signal fluctuations will still occur. Fluctuations having frequencies of the order of cycles per hour to cycles per day will result from internal waves and internal tides,¹³ while fluctuations with frequencies in the range of cycles per second to cycles per minute will result from scattering by random inhomogeneities in the sea.¹⁴ Although these inhomogeneities may be due to turbulence, thermal microstructure, air bubbles, or biological matter, they may all be treated as variations in the sound velocity (or refractive index) of the medium. The sea can then be crudely modelled as a medium containing 'patches' of variable refractive index which scatter a propagating acoustic wave. Usually the principal cause of scattering is the thermal microstructure, as we will see in Chapter 3.

Numerous theoretical studies have appeared that predict the amount of amplitude and phase fluctuations in an acoustic wave when the statistical nature of the thermal microstructure is known (see, for example, references¹⁵⁻¹⁹). Some results of these theoretical studies which are pertinent to the present investigation will be discussed in Chapter 3.

As discussed in the previous section, there are three acoustic waves associated with the parametric receiver: the incoming 'signal' wave, the pump wave with which the signal interacts, and the interaction frequency

wave which arises from the nonlinear interaction. It is reasonable to expect that each of these waves would be scattered in an inhomogeneous medium, and consequently, there would be three components of fluctuation in the output* of the parametric receiver. These fluctuations can have a significant effect on the performance of a parametric receiver in detecting and resolving low-level acoustic signals. In anticipating practical applications in the ocean, it is therefore desirable to know the effects that medium inhomogeneities have on the performance of a parametric receiver. It is the aim of the investigation reported in this thesis to determine these effects.

1.3 An Overview of the Thesis

These introductory considerations of the parametric receiver and of the effects of medium inhomogeneities are extended in Chapters 2 and 3, respectively. Both of these chapters contain a literature survey and a review of basic principles for their respective topics.

In Chapter 4, the analytical methods described in Chapters 2 and 3 are used to develop a theory which predicts amplitude fluctuations in the interaction frequency pressure at the hydrophone of the parametric receiver. It is assumed in this analysis that the amplitude and phase fluctuations are small compared to unity, and that the signal source is located on the main beam of the parametric receiver. With these assumptions, integral expressions are derived for the coefficient of amplitude variation for the cases of collimated planar and spherically spreading pump waves. Approximate solutions to these integral expressions are obtained by making a number of assumptions regarding the spatial correlation functions contained in these expressions.

*The parametric receiver 'output' may be taken to be the sum or difference frequency pressure at the hydrophone.

An experimental investigation is reported in Chapter 5. The experiments were conducted in a model tank in which an array of immersion heaters and a screen mesh were used to generate a thermal microstructure. Measurements are discussed in Chapter 5 that were made to determine the coefficient of amplitude variation for the signal, pump, and interaction frequency waves of a model parametric receiver. These results are then compared to theoretical predictions based on the analysis developed in Chapter 4.

In the final chapter, Chapter 6, the results of this study are summarized and discussed.

CHAPTER 2. THE PARAMETRIC ACOUSTIC RECEIVING ARRAY

2.1 Introduction

The purpose of this chapter is to explain the basic principles of the parametric acoustic receiving array, and to outline the history of its development. The theoretical development of the parametric acoustic array was based upon Lighthill's study^{20,21} of sound generated aerodynamically. Westervelt applied Lighthill's results to the problem of scattering of sound by sound^{22,23} and later¹⁰ extended this work to the parametric array. In formulating the theory of the parametric array, Westervelt developed an inhomogeneous wave equation that describes the second-order sound field. A brief sketch of the development of this wave equation, as well as a discussion of the physical significance of Westervelt's results, will be given in the next section of this chapter. Solutions of the second-order wave equation for various configurations of the parametric receiving array will then be discussed. Finally, practical matters such as signal processing, shadowing, finite amplitude effects, and the effects of noise on the performance of the parametric receiver are considered.

2.2 Basic Theoretical Concepts

We will begin discussion of the parametric acoustic array by turning briefly to some of the first principles of acoustics. Acoustic wave propagation in a lossless medium is governed by the following equations of fluid mechanics:²⁴

Continuity Equation

$$\frac{\partial \rho_T}{\partial t} + \nabla \cdot (\rho_T \vec{u}) = 0 \quad , \quad (2.1)$$

Momentum Equation

$$\frac{\partial}{\partial t} (\rho_T \vec{u}) + \rho_T \vec{u} (\nabla \cdot \vec{u}) + (\vec{u} \cdot \nabla) \rho_T \vec{u} + \nabla p = 0 \quad ; \quad (2.2)$$

Isentropic Equation of State

$$p = p(\rho)_S \quad ;$$

where

ρ_T is the total density,

∇ is the vector differential operator del,

\vec{u} is the particle velocity,

p is the acoustic pressure, and

the subscript S denotes constant entropy.

The isentropic equation of state may be expanded in a Taylor series about the ambient density of the fluid, giving

$$p_T = p_o + c_o^2 (\rho_T - \rho_o) + \frac{1}{2} \frac{c_o^2}{\rho_o} \left(\frac{B}{A} \right) (\rho_T - \rho_o)^2 \quad , \quad (2.3)$$

where the terms higher than second-order have been neglected. It may be noted that Eqs. (2.3) and (1.2) are identical, except for a change of variables.

The field variables ρ_T , \vec{u} , and p appearing in these fundamental equations can be expanded in series such that

$$\begin{aligned} \rho_T &= \rho_o + \rho_1 + \rho_2 + \dots + \rho_n \quad , \\ \vec{u} &= \vec{u}_o + \vec{u}_1 + \vec{u}_2 + \dots + \vec{u}_n \quad , \quad \text{and} \\ p_T &= p_o + p_1 + p_2 + \dots + p_n \quad . \end{aligned} \quad (2.4)$$

The physical meaning of, for example, the various pressure terms in Eqs. (2.4) is as follows. The zeroth-order, or static component, p_0 , is the pressure of the fluid in the absence of a sound wave. The first-order term, p_1 , is the pressure associated with a wave propagating linearly through the fluid. The higher order components are due to the nonlinear nature of acoustic wave propagation, as discussed in Section 1.1. Under the limitations of perturbation theory for which the acoustic signals are sufficiently small that

$$p_0 \gg p_1 \gg p_2 \gg \dots \gg p_n \quad ,$$

terms higher than second order are neglected.²⁵ Neglecting these terms is effectively the same as assuming that no nonlinear interactions occur beyond those which give rise to the second-order field; i.e., the second-order radiation is assumed to propagate linearly.

First and second-order wave equations can be derived by substituting the series expressions in Eq. (2.4) into the fundamental equations, Eqs. (2.1)-(2.3), and then retaining only terms of first or second order, respectively. The parametric acoustic array utilizes the second-order field variables, so the second-order wave equation is of particular interest, and is given by^{10,26}

$$\square^2 p_2 = - \frac{\beta}{\rho_0 c_0^4} \frac{\partial^2 p_1^2}{\partial t^2} \quad , \quad (2.5)$$

where

$$\square^2 = \nabla^2 - \frac{1}{c_0^2} \frac{\partial^2}{\partial t^2} \text{ is the D'Alembertian operator, and}$$

$$\beta = 1 + \frac{B}{2A} \quad .$$

This inhomogeneous wave equation has a source term on the right hand side that is a function of the first-order pressure field and some constants. Apparently to emphasize the physical meaning of this wave equation, Westervelt rewrote Eq. (2.5) in terms of the source strength density, q , as follows:

$$\square^2 p_2 = - \rho_0 \frac{\partial q}{\partial t} \quad , \quad (2.6)$$

where

$$q = \frac{\beta}{\rho_0 c_0^4} \frac{\partial p_1^2}{\partial t} \quad .$$

Equation (2.6) has the same form as the linear (first-order) wave equation in which there are real mass sources present, the sources having source strength density, q . By analogy with such a linear wave equation, Eq. (2.6) describes the propagation of second-order acoustic waves that are generated by the nonlinear interaction of first-order acoustic waves. The sources that generate the secondary pressure field are not real, but are 'virtual' sources produced by the nonlinear properties of acoustic wave propagation. These sources are distributed throughout the region of space in which the nonlinear interaction of the primary field occurs. The general solution for the pressure p_2 in Eq. (2.6) is²⁷

$$p_2(\vec{r}, t) = \frac{\rho_0}{4\pi} \int_V \frac{1}{r'} \frac{\partial}{\partial t} q(\vec{r}_0, \tau) dv \quad , \quad (2.7)$$

where

\vec{r} is the observation point,

\vec{r}_0 is the source point,

$$\vec{r}' = \vec{r} - \vec{r}_0 \quad ,$$

$$r' = |\vec{r}'| \quad ,$$

$\tau = t - \frac{r'}{c_0}$ is the retarded time,

V is the interaction volume, and the geometry of Fig. 2.1 applies.

This result can be summarized qualitatively as follows. Whenever some first-order pressure p_1 is present at a point in the medium, a second-order virtual source will arise at that point having a source strength qdv . The second-order pressure at an observation point \vec{r} will be the sum of all sources in the interaction volume; this pressure is given by Eq. (2.7). In the next few sections, we will discuss specific solutions for p_2 for given first-order pressure fields.

2.3 The Parametric Array

Two practical applications for the second-order sound field described by Eq. (2.7) were proposed by Westervelt.¹⁰ He noted that if two plane harmonic waves of frequencies ω_1 and ω_2 are projected by a common transducer, an array of virtual sources will be established in the beam of the transducer, radiating at sum and difference frequencies $\omega_1 \pm \omega_2$. The array would be phased in an end-fire manner, and its radiation pattern would have negligible sidelobe levels. This concept of a parametric transmitting array was confirmed experimentally by Bellin and Beyer,²⁸ and led to further studies of this application by Berkday,²⁹ Berkday and Smith,³⁰ Hobaek,³¹ Zverev and Kalachev,³² Muir and Blue,³³ Muir,¹¹ and Smith.^{25,34}

In addition to its use as a transmitter, Westervelt also suggested using the parametric array as an acoustic receiver. In this application some distant signal would interact nonlinearly with a locally generated signal. The second-order pressure arising from this interaction would then be detected by a hydrophone placed in the vicinity of the locally generated wave. Several studies were also prompted by this possibility.³⁵⁻⁴⁴ The findings of some of these studies will be discussed in the following sections.

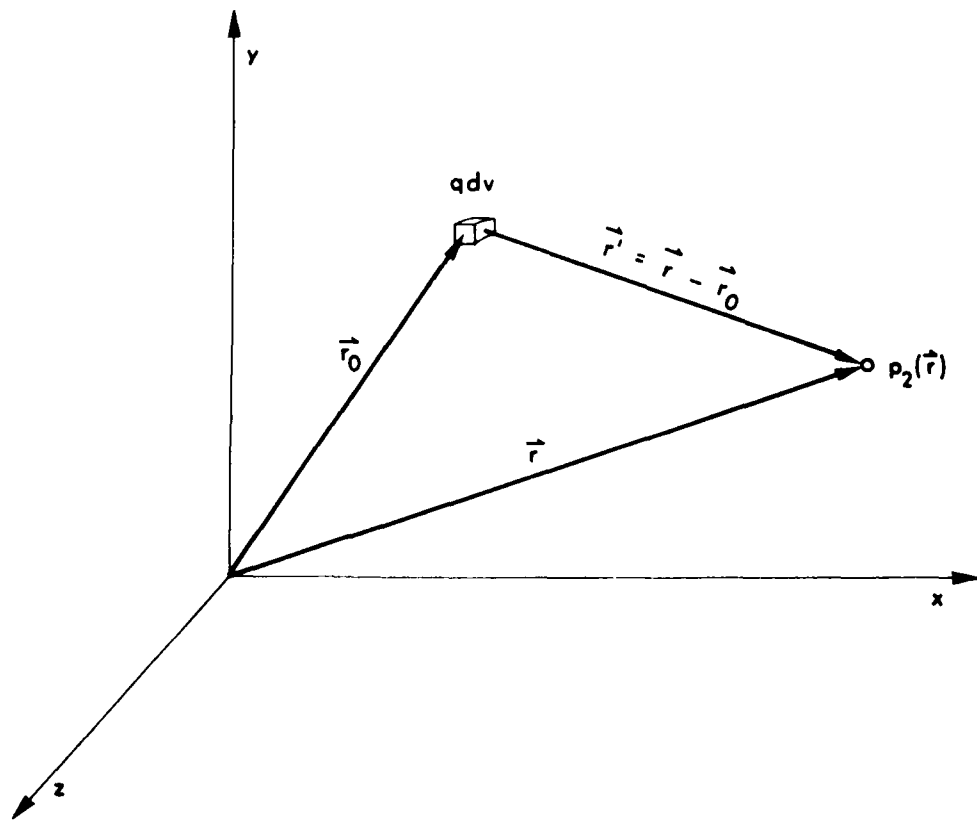


FIGURE 2.1
RADIATION FROM AN ELEMENTAL SOURCE

2.3.1 The Nearfield Receiving Array

As an illustration of the parametric receiving array, consider the arrangement shown in Fig. 2.2. A pump transducer of dimensions $2b \times 2b$ is situated at the origin and radiates a wave of frequency ω_p along the x-axis. A signal wave with frequency ω_s propagates in a direction given by the unit vector

$$\vec{R} = \vec{i} \cos\theta + \vec{j} \sin\theta \quad , \quad (2.8)$$

where \vec{i} and \vec{j} are unit vectors in the x and y directions, respectively.

The second-order pressure produced by interaction of the pump and signal waves is detected by a hydrophone placed at $x = L$. It is assumed that the detector is in the nearfield of the pump transducer, so that the pump radiation may be approximated by a plane wave.⁴⁵ The signal source is assumed to be located so distantly that the signal wave is planar in the vicinity of the pump. With these considerations, the pump and signal pressures are described by

$$\text{Pump:} \quad p_p(x,t) = P_p e^{j(\omega_p t - k_p x)} e^{-\alpha_p x} \quad (2.9)$$

$$\text{Signal:} \quad p_s(x,t) = P_s e^{j(\omega_s t - k_s x)} e^{-\alpha_s R} \quad (2.10)$$

where P_p is the pressure amplitude of the pump wave in the nearfield of the pump transducer,

P_s is the pressure amplitude of the signal wave at the origin, α_p and α_s are attenuation coefficients for the pump and signal waves, respectively, and

$$R = x \cos\theta + y \sin\theta \quad .$$

In writing Eqs. (2.9) and (2.10), it has been assumed that the attenuation coefficients are constants because the waves are each of single frequency.

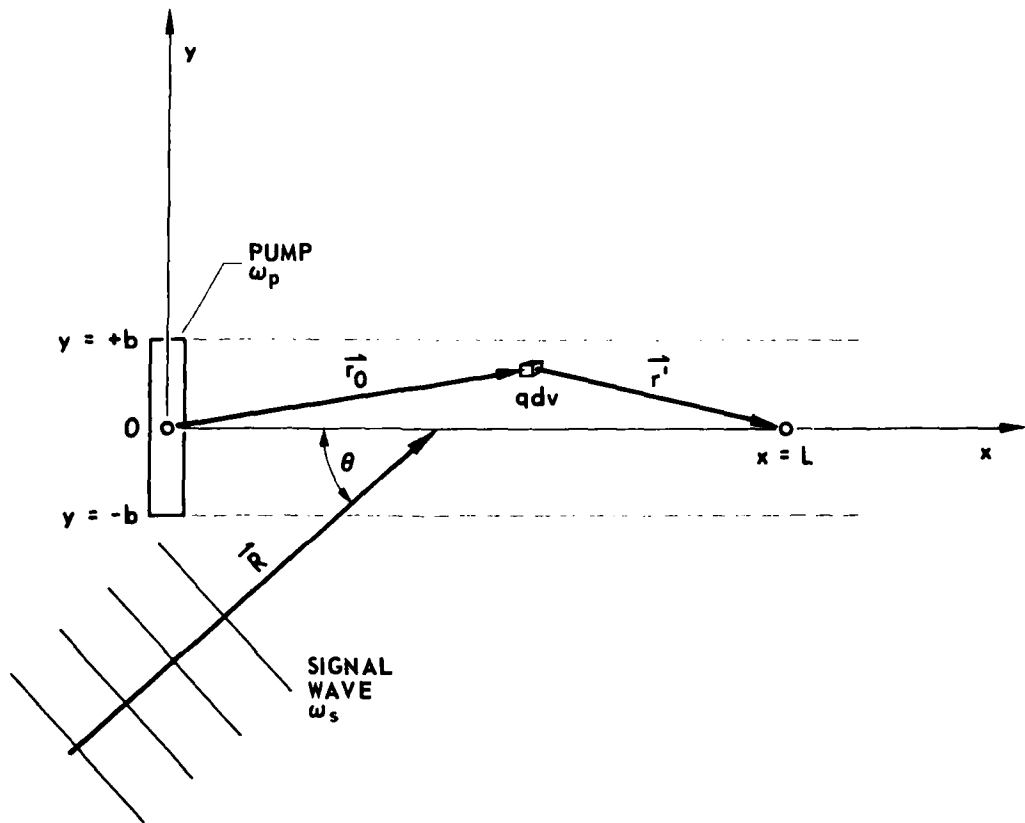


FIGURE 2.2
THE NEARFIELD PARAMETRIC RECEIVING ARRAY

Also, the phase of the signal wave has arbitrarily been set to zero at the origin.

The total first-order pressure at any point in the pump column (i.e., the region indicated by dashed lines in Fig. 2.2) is

$$P_1 = P_p + P_s \quad (2.11)$$

The second-order pressure detected by the hydrophone at $x = L$ can be calculated by substituting Eq. (2.11) into Eqs. (2.7) and (2.8). If only the sum and difference frequency terms are retained, the result is

$$P_{\pm}(L) = \frac{\omega_{\pm}^2 \beta_p P_p P_s}{4\pi\rho_o c_o^4} \int_0^L \int_{-b}^b \int_{-b}^b e^{-j(k_p x \pm k_s R)} e^{-(\alpha_p x + \alpha_s R)} \times \frac{e^{-(\alpha_{\pm} + jk_{\pm})\sqrt{(L-z)^2 + y^2 + z^2}}}{\sqrt{(L-z)^2 + y^2 + z^2}} dx dy dz, \quad (2.12)$$

where $\omega_{\pm} = \omega_p \pm \omega_s$, α_{\pm} is the attenuation coefficient at frequency ω_{\pm} (a constant), k_{\pm} is the acoustic wavenumber at frequency ω_{\pm} , and the time dependence has been suppressed.

This integral is not easy to evaluate directly, but Berklay⁴⁶ has devised a method for simplifying the integration which will now be adopted. The interaction region in front of the pump transducer can be regarded as a series of elemental wafers of thickness dx and cross-sectional dimensions $2b \times 2b$ (see Fig. 2.3). Each of these wafers is insonified by the first-order sound field and will radiate at the frequency ω_{\pm} . These wafers will produce nearfield, planar radiation at a range less than R_o from the wafer, and farfield, spherically spreading radiation at ranges greater than R_o . Using Freedman's⁴⁵ description of radiation from a square piston, Berklay and Al-Temimi³⁸ choose R_o to be

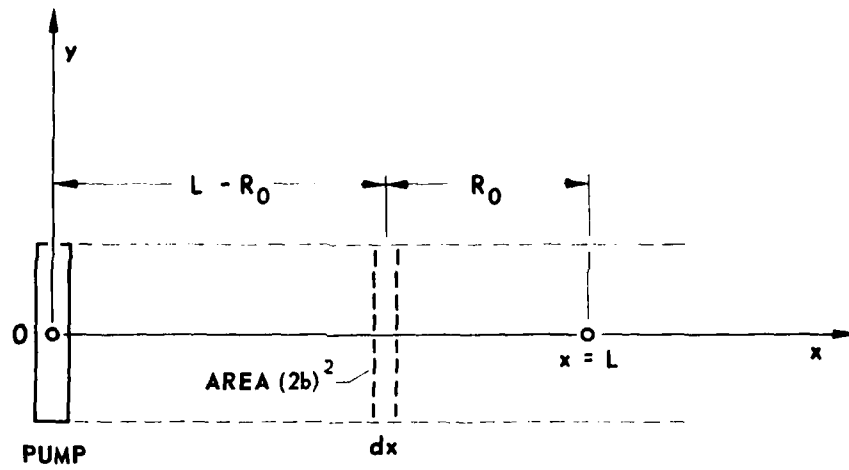


FIGURE 2.3
ELEMENTAL WAFERS IN THE INTERACTION REGION

$$R_0 = 1.3 b/\lambda_3 \quad , \quad (2.13)$$

where λ_s is the acoustic wavelength at frequency ω_s .

The detected second-order pressure may be considered to have two components: (1) nearfield radiation from wafers within a distance R_0 of the detector and (2) farfield radiation from wafers at a distance greater than R_0 from the detector. For this illustration assume that $L < R_0$ so that all wafers are in the nearfield of the detector. With the further assumption that absorption along the y-axis is negligible compared to that in the x direction, so that $\alpha_s R$ can be approximated by $\alpha_s x \cos\theta$, Berktaf and Al-Temini³⁸ evaluate Eq. (2.12) with the result

$$p_N(L, \theta) = \frac{-j\omega_s P P_s \beta L}{2\rho_o c_o^3} \cdot \left[\exp -(\alpha_{\pm} + jk_{\pm})L \right] \cdot \exp[\mp jM] \cdot \frac{\sin M}{M} \quad , \quad (2.14)$$

where

the subscript N indicates that the result is valid only when the detector is in the nearfield of all elemental wafers, and

$$M = \frac{1}{2} k_s L(1 - \cos\theta). \quad (2.15)$$

The pressure detected by the hydrophone can be expressed in terms of the on-axis pressure amplitude, $P_N(L, 0)$, and the directivity, $D(\theta)$, as follows:

$$p_N(L, \theta) = P_N(L, 0) \cdot D(\theta) \quad , \quad (2.16)$$

where
$$P_N(L, 0) = \frac{\omega_s P P_s \beta L}{2\rho_o c_o^3} \exp(-\alpha_{\pm} L) \quad , \quad (2.17)$$

and
$$D(\theta) = \frac{\sin M}{M} \quad . \quad (2.18)$$

Experimental confirmation of the validity of Eqs. (2.17) and (2.18) is reported by Berktaý and Al-Temini.^{37,38,47}

The directivity function is identical to that of a continuous end-fire array of length L , realized from elements operating at frequency ω_s . It is this directional property of the parametric receiver that makes it an attractive device for the reception of underwater signals. It offers the same capabilities as the conventional end-fire array as regards directional detection of signals; yet the parametric device requires only two transducers in its construction.

These conclusions have been based on results obtained assuming that the hydrophone is placed in the nearfield of the pump transducer. In applications requiring high directivity, and consequently large values of L , it is likely that the hydrophone will be placed well in the farfield of the pump. The next section extends the discussion to this situation.

2.3.2 The Farfield Receiving Array

In 1972, Barnard et al.³⁹ considered a case in which the hydrophone is placed in the farfield of the pump transducer. Their analysis assumed interaction between a plane signal wave and a spherical pump wave produced by a baffled circular piston. Prediction of the interaction frequency pressure was given by a numerical solution to Eq. (2.12). The results of the integration were tested against experiment for the sum frequency, with good agreement between theory and experiment.

A closed-form solution for parametric reception with spherically spreading pump waves is given by Berktaý and Shooter.⁴³ The analysis is similar to that for the nearfield receiving array, but rather than having planar elemental wafers, the interaction frequency sources are assumed to be cophasal along the spherical wavefronts. The received pressure at the interaction frequency ω_{\pm} can be written^{42,43}

$$p_F(L, \theta) = \frac{-\omega_{\pm} P'_p s^3}{2\rho_o c_o^3} \exp \left[\mp (\alpha_{\pm} + jk_{\pm})L \mp jM \right] D(\theta) \quad , \quad (2.19)$$

where

$p_F(L, \theta)$ is the pressure of the interaction frequency signal at $x = L$,
for the case of spherical pump waves,

P'_p is the on-axis farfield pump pressure amplitude referred to 1 meter,

$D(\theta) = \sin M/M$ is the directivity function, and

$$M = \frac{1}{2} k_s L (1 - \cos \theta).$$

In comparing results for the collimated pump [Eq. (2.14)] and the spherically spreading pump [Eq. (2.19)], it can be seen that the directivity patterns for the two cases are identical. The pressure amplitude for the case of the spherically spreading pump is, with the exception of absorption, independent of array length, whereas for the collimated pump, the pressure amplitude increases with L .

The directivity function of the pump transducer does not enter into the result for the farfield parametric receiver, but it has been assumed in the analysis that the pump beamwidth is less than the beamwidth of the parametric receiver.⁴³ The directivity function of the parametric receiver for both the collimated and spherically spreading pump is independent of pump frequency, and is the same whether the sum or difference frequency signal is used.

Berktaf and Shooter⁴³ compared the closed-form solution [Eq. (2.19)] to results obtained by the numerical integration of Barnard et al.³⁹ and found that agreement between the predictions was good. Computed results of Eq. (2.19) were also found to be in good agreement with experimental measurements.^{42,43} These results show that the amplitude of the interaction frequency signal component can be made approximately equal to the original signal amplitude by proper choice of pump source level and array length so that no loss in signal level is experienced in parametric reception.

Truchard^{36,44} solved the problem of a parametric receiving array with an arbitrarily shaped planar piston pump as follows. He first analyzed the interaction of a high frequency spherical wave from a point source and a low frequency plane wave. The solution for pump transducers of two or three dimensions was then obtained by summing the point source solution over the active face or volume of the pump transducer. In this manner Truchard analyzed the following situations: (1) a point pump source with a line hydrophone, (2) a rectangular pump with a point hydrophone, and (3) a circular piston pump with a point hydrophone. Truchard also studied these situations experimentally and obtained very good agreement between his theoretical and experimental results.

2.4 Practical Considerations

2.4.1 Signal Processing

In practical applications there are factors which make detection of the interaction frequency signal difficult. Since $\omega_s \ll \omega_p$, the interaction frequency $\omega_p \pm \omega_s$ is very close to the pump frequency ω_p . Also the pump amplitude P_p is generally much greater than either of the amplitudes, P_s and P_{\pm} . This situation is illustrated by the sketch of Fig. 2.4. The quantity e_x shown in the figure is the 'pump excess,' defined by Berklay and Muir⁴² to be the ratio of the pump pressure at the hydrophone to the amplitude of the interaction frequency signal. For the case of spherical pump waves⁴²

$$e_x \doteq 2\rho_o c_o^3 / (\omega_p \pm \omega_s) \beta L P_s \quad . \quad (2.20)$$

The signal processing problem is to reject the high amplitude pump signal and retain one or both of the interaction frequency signals. Since a pump excess on the order of 160 dB may be encountered in practice,⁴⁸ careful design of the signal processing system may be required in applications of the parametric receiver.

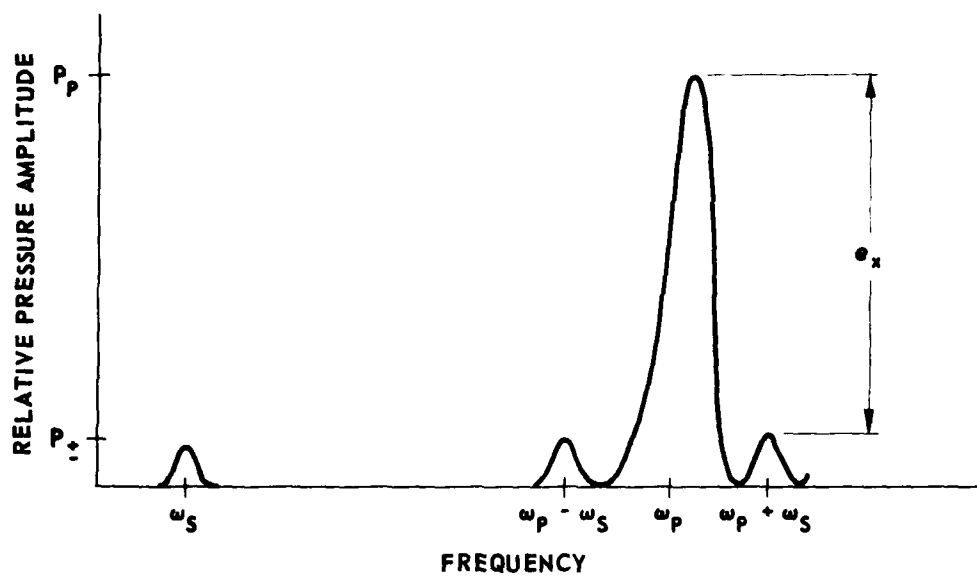


FIGURE 2.4
SKETCH OF THE FILTERING PROBLEM

There are three basic types of signal processing systems that have been used with the parametric receiving array: the band pass receiver, the carrier rejection or band elimination receiver, and the phase-locked loop receiver. The band pass receiver is relatively simple to design and construct and is adequate in applications where the pump excess is low and the interaction frequency is well separated from the pump frequency. This type of receiver was used in the present study, and is described in Chapter 5.

For applications involving a high pump excess and low signal frequencies, the band elimination receiver is suitable. This type of receiver may be described using the block diagram of Fig. 2.5. The design uses a cascade of two crystal notch filters and two preamplifiers to reduce the level of the carrier, and to amplify the interaction frequency (i.e., sideband) components. The signal is then split into its in-phase and quadrature components, and these components are processed to give the upper and lower sideband signals. Rohde *et al.*⁴⁸ report this method of signal processing to be useful in a parametric receiver with carrier to sideband ratios approaching 180 dB.

A third type of signal processing system is the phase-locked loop (PLL) receiver, shown in Fig. 2.6. This system operates as a closed loop servo system with phase as the controlled variable.⁴⁹ The input of the PLL receiver is connected to the hydrophone of the parametric receiving array. With the voltage controlled oscillator operating nominally at the pump frequency, and with the loop bandwidth less than the lowest modulation frequency of interest, the error voltage $r(t)$ contains the demodulated signal. This type of receiver is useful in minimizing the effects of low frequency noise, such as due to transducer vibration.^{49,50} This point will be further discussed in Section 2.4.5.

2.4.2 Shadowing

Any time that an obstacle significantly large with respect to wavelength

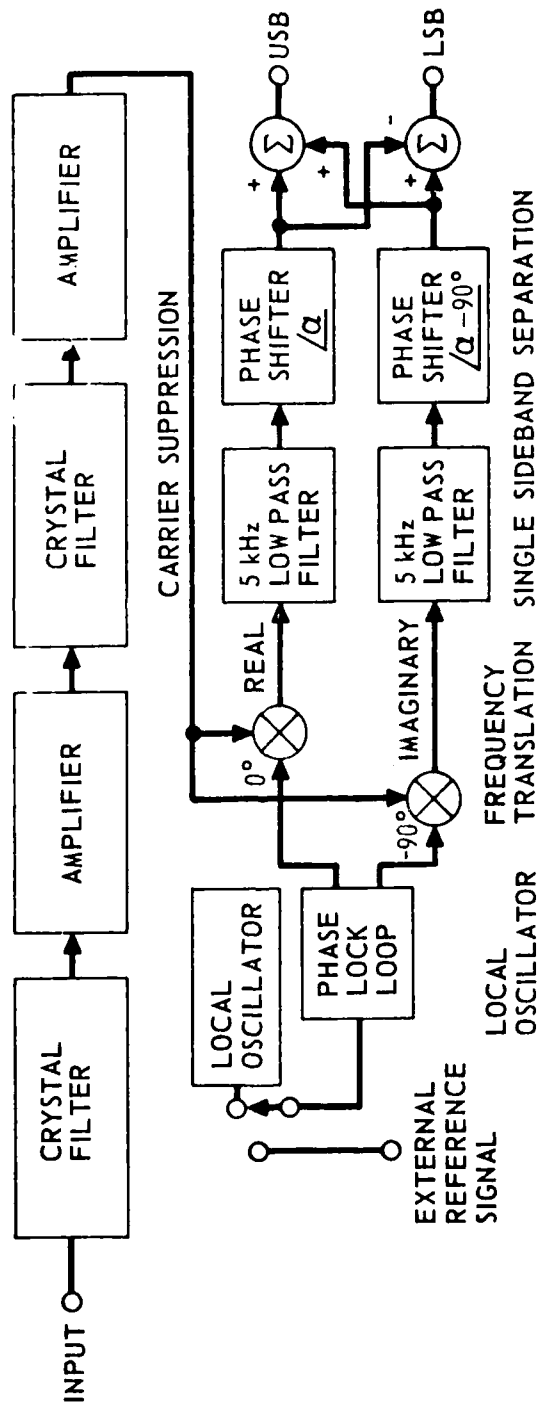


FIGURE 2.5
BAND ELIMINATION RECEIVER
(From Ref. 48)

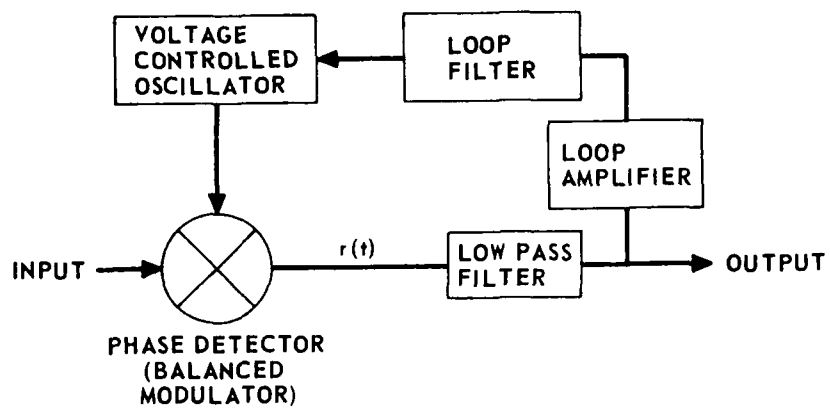


FIGURE 2.6
PHASE-LOCKED LOOP RECEIVER

is placed in the path of a propagating wave, shadows may form in the region behind the obstacle. In the case of the parametric receiver, the pump transducer and its mounting obstruct the incoming signal wave and form a shadow in the array interaction region. This shadow has the effect of truncating the array length, with consequent effects on the sensitivity and the directivity function of the array.

Al-Temimi^{47,51} has done a theoretical and experimental study of the effects of shadows on the performance of parametric receivers. One important result of his work is a description of the condition for which acoustic shadows cause no appreciable deterioration of array performance and hence may be neglected. This condition is that the shadow length d be kept below 5% of the array length L ; i.e.,

$$d < 0.05 L, \quad (2.21)$$

where

$$d \doteq 1.25 b^2 / \lambda_s, \quad (2.22)$$

and $2b$ is the length of each side of a square transducer.

2.4.3 Finite Amplitude Effects

It was noted in Chapter 1 that a finite amplitude acoustic wave distorts as it propagates, this distortion being due to the dependence of the phase velocity on the particle velocity; i.e.,

$$\left(\frac{dx}{dt} \right)_u = c_0 + \beta u(x,t), \quad (2.23)$$

where

c_0 is the sound speed with respect to the fluid particles,

$\left(\frac{dx}{dt}\right)_u$ is the phase (or propagation) velocity of a given point on a sound waveform, and

u is particle velocity.

The distortion of an initially sinusoidal acoustic wave gives rise to harmonic components. Energy is transferred from the fundamental component of the wave to the harmonics as the wave is progressively distorted, so the fundamental is attenuated by this effect. If the wave experiences enough distortion for a discontinuity or 'shock' to develop, the situation becomes more complex. When the acoustic wave is 'weak,' i.e., $u_0/c_0 < 0.1$, then a method known as 'weak-shock theory' can be used to describe the wave propagation.^{52,53} We will not discuss this theory in any detail, but merely note that when a shock forms, dissipation may be assumed to occur at the shock front to the degree that the waveform never becomes multivalued.⁵²

In general, there are three mechanisms that attenuate an acoustic wave: geometrical spreading, absorption by the medium, and the 'excess attenuation' due to energy transfer from fundamental to harmonic components as the wave is distorted. The spreading and absorption mechanisms, by reducing the amplitude of an acoustic wave, tend to reduce the nonlinear distortion process considerably. For example, a spherically spreading wave will have a value of u that reduces as $\frac{1}{r}$, so that the importance of the second term in Eq. (2.23) diminishes with range. Absorption will similarly reduce the effects of nonlinearity. It can be seen, therefore, that excess attenuation will only be significant in the case of waves with initially large amplitudes.

The excess attenuation for a plane wave propagating through a lossy medium is calculated by Blackstock⁵⁴ in terms of the Gol'dberg number, Γ , and the normalized range parameter, σ . These quantities are:

$$\Gamma = \frac{\rho_0 \epsilon k}{\alpha} \quad , \quad (2.24)$$

where

$$\epsilon = \frac{u_0}{c_0} ,$$

u_0 being the particle velocity at the transducer face,

and

$$\sigma = \frac{x}{\beta \epsilon k} . \quad (2.25)$$

The value of the excess attenuation EXDB in the fundamental component can be read from curves given in reference 54. An approximate solution, said to be accurate to within 1 dB of Blackstock's results, is given by^{55,56}

$$\text{EXDB} = 10 \log \left\{ 1 + \left(\frac{\Gamma}{4} \right)^2 [1 - \exp(-2\sigma/\Gamma)]^2 \right\} . \quad (2.26)$$

Some effects of finite amplitude attenuation on the performance of a parametric receiver have been studied by Berktaf and Al-Temimi.^{38,47} They found that for the case of the nearfield array, excess attenuation of the pump wave can bring about saturation in the sensitivity of the parametric receiver.

It was found by Al-Temimi⁴⁷ that finite amplitude attenuation had little effect on the parametric receiver directivity. The combination of shadowing and finite amplitude attenuation, both dependent on frequency, can reduce the bandwidth of the receiver. The effect is particularly significant when a great deal of extra attenuation occurs in the shadow region of the pump, so that the pump wave is well attenuated before entering the interaction volume.⁴⁷

2.4.4 Sources of Noise that Affect Parametric Reception

Any noise in the acoustic environment at frequencies ω_s and $\omega_p \pm \omega_s$ will be detected by the parametric receiver. The signal frequency noise component (at ω_s) will be up-converted along with the desired signal, and

the interaction frequency noise component (at $\omega_p \pm \omega_s$) will be detected directly by the receiving transducer. The parametric receiver, by virtue of its directivity at ω_s , discriminates against the low frequency noise. Some rejection of the interaction frequency noise is provided by the receiving transducer directivity. An analysis of the effects of ambient noise on parametric reception may be found in Berkta's papers.^{37,57,58} Effects of ambient noise were an important consideration in the parametric receiver design described by Goldsberry,^{59,60} who discusses in Ref. 61 an extensive experimental program which studied the performance of the parametric receiver in a fresh water lake.

In addition to noise in the acoustic environment, electronic noise in the pump signal source will contribute to the overall noise level of the parametric receiver. This noise is due to the fact that the pump transducer does not radiate at a single frequency, but over a frequency band, and if $\omega_s \ll \omega_p$, then there is very likely to be energy radiated by the pump at $\omega_p \pm \omega_s$, which will be detected by the hydrophone. This radiation depends primarily on the sideband noise produced by the pump oscillator, and must be minimized if low-level, low frequency signals are to be detected by the parametric receiver. A crystal oscillator developed for the purpose of minimizing the noise of the pump source is reported to have a sideband noise level (measured in a 1 Hz band) of -160 dB referenced to the carrier level, measured at 100 Hz from the carrier frequency.^{61,62}

Another kind of noise may arise due to transducer vibration. If the pump transducer and hydrophone are mounted such that they move relative to one another because of vibration, then the array length will be varied by this motion. As a result the pump and interaction frequency signals will be phase modulated. This modulation produces undesirable sidebands in the hydrophone output which may appear as spurious low frequency signals that are indistinguishable from acoustic signals.⁶¹ The response of a parametric

receiver to transducer vibration has been studied analytically and experimentally by Reeves et al.^{63,64} and by Lamb.⁴⁹ Lamb has demonstrated the usefulness of the phase-locked loop receiver, discussed in Section 2.4.1, in minimizing the noise due to transducer vibration.

2.4.5 Effect of Turbulence and Medium Inhomogeneities

Another factor which may affect receiver performance is the signal fluctuation due to turbulence and medium inhomogeneities. Both turbulence and inhomogeneities in the medium produce random scattering of an acoustic signal. The various scattered components interfere at an observation point to produce amplitude and phase fluctuations in the observed signal. For the parametric receiver there are three signal components which undergo fluctuations: the incoming low frequency signal, the pump signal, and the interaction frequency signal. In a severely inhomogeneous or turbulent medium, the composite effect of these fluctuations could prove prohibitive to the detection of low-level signals. This is a problem that has received little attention to date, and it is the principal topic with which this thesis will be concerned.

2.5 Summary

In this chapter, the basic concepts of the parametric receiver have been discussed and an outline of the historical highlights of its development presented. Of necessity, topics have been treated briefly. Some topics, such as the use of arrays of parametric receivers,⁴² the phase modulation model of the parametric receiver,⁴¹ and the effects of having the signal source located in the nearfield of the parametric receiver,⁶⁵ have been omitted, as they do not directly bear upon the present study.

It has been shown in this chapter that the parametric array makes use of the second-order sound field generated by nonlinear interaction of a low frequency signal wave and a locally generated pump wave. A second-order

wave equation [Eq. (2.6)] was presented, the solution to which is dependent upon the geometry of the interaction region. Solutions to the wave equation for the cases of the nearfield and farfield parametric receiver were discussed. It was seen from these solutions that the parametric receiver has the same directivity characteristics of an end-fire array of equal length, realized by continuous elements. Thus the advantages of directivity offered by the end-fire array are achieved by the parametric receiver, which requires only two transducers for its construction. Finally, practical considerations regarding signal processing, shadowing, finite amplitude effects, and the effects of noise were discussed briefly. It was noted that one remaining topic for study regarding practical application of the parametric receiver is the effects of medium inhomogeneities; this is the topic for this thesis.

3.1 Introduction

The discussion of the parametric receiver in the previous chapter implicitly assumed that the acoustic medium is homogeneous. This assumption is usually unrealistic in practice. The ocean, for example, may contain one or more of a variety of inhomogeneities: fish, bubbles, algae, thermal microstructure, and turbulent eddies. These inhomogeneities scatter the energy of an acoustic wave and, as they move about in the medium, produce random fluctuations in the amplitude and phase of the transmitted wave. In many instances the effects of fish, bubbles, and algae can be ignored because these kinds of scatterers occur in small quantities. More widespread are thermal inhomogeneities and turbulent eddies which can cause significant fluctuations in a transmitted signal.¹⁴ Both of these inhomogeneities can be modelled as regions or 'patches' of variable refractive index.

Thermal patches are usually the principal cause of scattering in the ocean.¹⁴ The dimensions of these patches are generally large compared to the acoustic wavelength, in which case, as a first approximation, they may be treated as spherical sound sources of radius a , where a is the mean radius of the thermal patches.^{14,17} Scattered sound from the patches will propagate in the same direction as the incident wave, and with a farfield beam angle of $1/ka$ radians, where k is the acoustic wavenumber¹⁷ (see Fig. 3.1).

The region in front of the patch out to a distance ka^2 is taken to be the 'ray region' of the scattered radiation.¹⁷ In this region the patch will behave like a lens, focusing or defocusing the scattered rays according to whether the sound velocity in the patch is smaller or larger than the average value, respectively.¹⁷ In 1946, a 'ray theory' was developed by Bergman¹⁵ which predicted that a wave propagating over a distance less than ka^2 would undergo amplitude fluctuations proportional to the three-halves power of the range.

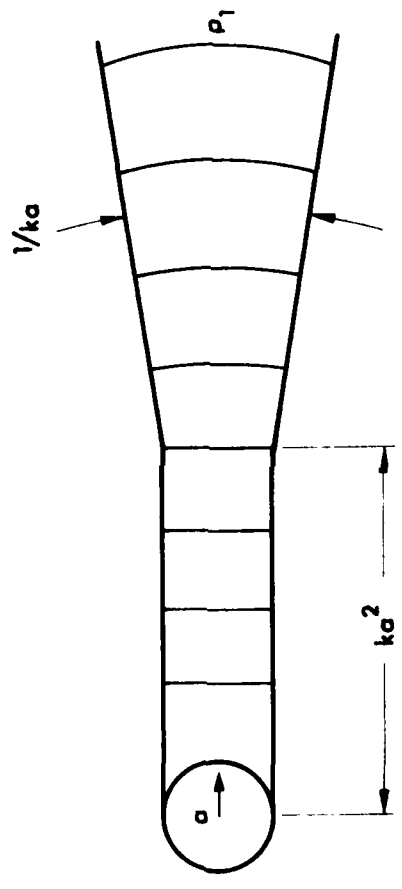


FIGURE 3.1
MODELLING AN INHOMOGENEITY AS A SPHERICAL SOURCE

The region beyond a distance ka^2 from the patch is the 'wave region' of the scattered radiation. At ranges greater than ka^2 from a source, interference will occur between waves scattered by various patches in the medium. For these ranges the theory of Mintzer¹⁶ predicts mean square amplitude fluctuations in the acoustic signal which increase linearly with range. Mintzer's prediction of range dependence is in good agreement with the experimental data of Sheehy,⁶⁶ who measured fluctuations in a 24 kHz pulsed signal transmitted over ranges of approximately 30 to 3000 meters. Further verification of this theoretical range dependence was given by the model tank experiments of Stone and Mintzer.⁶⁷ Chernov¹⁸ reproduced the Bergmann and Mintzer results and in addition calculated the transverse and longitudinal spatial correlation of the fluctuations. Chernov's analysis of fluctuations and their correlation was extended to the case of spherical waves by Karavainikov.⁶⁸

All of the theoretical studies mentioned above assumed that the refractive index field in the acoustic medium could be described by an exponential or Gaussian spatial correlation function. Measurements of thermal microstructure in the Pacific Ocean were reported by Liebermann⁶⁹ in 1951, and his results agreed reasonably well with the exponential function, $e^{-x/a}$, where a is the mean radius of the thermal patches. (Liebermann measured a mean patch size of 0.6 meters.) When Whitmarsh et al.¹⁴ made simultaneous measurements of acoustic fluctuations and thermal microstructure in 1957, however, they found that the Kolmogorov theory of turbulence provided a more accurate description of the thermal structure of the sea than did the exponential or Gaussian functions. Whitmarsh et al. suggest that the agreement of the Kolmogorov theory with their experimental results was a consequence of the 'freezing' of the thermal patches after their turbulent motion has been damped out. They reason as follows:

Since the static heat conductivity is almost 1000 times smaller than the turbulent conductivity, the patches continue to exist, even after the turbulent motion has disappeared. This stability seems to lead to excellent statistical conditions and to a temperature distribution that agrees with the experimental results....¹⁴

This 'Kolmogorov' model of the medium has been used by Tatarski¹⁹ and Medwin⁷⁰ to predict sound phase and amplitude fluctuations in a turbulent medium. The Kolmogorov model will be used in the present study, so a brief description of turbulence theory, and some of the results of Tatarski and Medwin, will be presented later in this chapter.

The research cited above all deals with situations in which the total fluctuations imposed on the propagating wave are sufficiently small that only single scattering is involved. By the end of the 1960s, work had begun on the more difficult problem of multiple scattering, where fluctuations in the wave parameters can become large. Multiple scattering is discussed at some length in the books of Tatarski,⁷¹ Uscinski,⁷² and Ishimaru.⁷³ In this thesis we will be concerned only with single scattering. More detailed surveys of theoretical work for both single and multiple scattering, including extensive bibliographies, may be found in Ishimaru⁷⁴ and Barabanenkov et al.⁷⁵

3.2 Methods of Describing the Inhomogeneous Medium

A theoretical analysis of the propagation of linear acoustic waves in an inhomogeneous medium requires statistical methods for describing the medium. The medium may be modelled as a randomly varying field of refractive index, or equivalently, of sound speed. The sound speed is then given by

$$c = c(x, y, z, t) \quad ,$$

and the refractive index is

$$n(x,y,z,t) = \frac{c_0}{c(x,y,z,t)} = 1 + \mu(x,y,z,t) \quad , \quad (3.1)$$

where

$c_0 = \langle c \rangle$ is the mean sound speed,

$\langle \rangle$ denotes ensemble averaging, and

$\mu(x,y,z,t)$ is the deviation from unity in the refractive index.

Variations in the refractive index are usually very small; for example, Urick and Searfoss⁷⁶ measured a value of $\langle \mu^2 \rangle = 8 \times 10^{-10}$ at a depth of about 6 meters in a mixed layer off Key West, Florida. Liebermann⁶⁹ observed mean square refractive index variations of $\langle \mu^2 \rangle = 5 \times 10^{-9}$ at a depth of 50 meters off the coast of California. Because the quantities c and n are random variables, a description of their spatial dependence requires statistical parameters such as the correlation function and its Fourier transform, the spatial wavenumber spectrum. Both the correlation function and the wavenumber spectrum are used frequently in what follows, so we will define each of these parameters.

If $\mu(x,y,z,t)$ may be assumed to be an ergodic process, then the fluctuations may be characterized by the correlation function⁷⁷

$$N_{12} = \overline{\mu(x_1, y_1, z_1, t) \mu(x_2, y_2, z_2, t)} \quad , \quad (3.2)$$

where the overbar denotes time averaging. Because of the ergodic hypothesis, ensemble averaging and time averaging are equivalent. If it is further required that the process be spatially homogeneous, then the correlation function depends only upon the separations Δx , Δy , and Δz , where $\Delta x = x_2 - x_1$, $\Delta y = y_2 - y_1$, and $\Delta z = z_2 - z_1$. When points (x_1, y_1, z_1) and (x_2, y_2, z_2) are the same, so that $\Delta x = \Delta y = \Delta z = 0$, then the correlation function has a maximum value of $\overline{\mu^2}$. As the separation between the two points is increased,

the correlation function decreases in value until, at infinite separation, N_{12} becomes zero.

If the variations in refractive index are isotropic as well as homogeneous, then the correlation function will depend only upon the magnitude of the separation between points. This condition may be written as

$$N_{12} = N_{12}(\rho) \quad ,$$

where

$$\rho = \sqrt{(\Delta x)^2 + (\Delta y)^2 + (\Delta z)^2} \quad .$$

It is useful to normalize the correlation function by dividing N_{12} by $\overline{\mu^2}$. This results in the correlation coefficient R , given by

$$R = N_{12} / \overline{\mu^2} \quad .$$

Two correlation coefficients frequently used to describe the refractive index variations in the ocean are the exponential function,

$$R(\rho) = \exp(-\rho/a) \quad , \quad (3.3)$$

and the Gaussian function,

$$R(\rho) = \exp(-\rho^2/a^2) \quad , \quad (3.4)$$

where a is a constant corresponding to the mean patch radius. It should be noted⁷⁷ that the derivative of the exponential function, which may be found from Eq. (3.3) to be

$$\frac{dR}{d\rho} = -\frac{1}{a} \exp(-\rho/a) \quad ,$$

has a nonzero value at $\rho = 0$. This implies a discontinuity in the correlation function at $\rho = 0$, which is possible only if the variation in refractive index, $\mu(\rho)$, is discontinuous, a condition which is unrealistic in the ocean.¹⁷ The Gaussian function, Eq. (3.4), does not exhibit this discontinuity, and in this respect is a more realistic representation of the refractive index fluctuations than is the exponential function.

An alternate way to describe spatial variations in refractive index is to use a spatial wavenumber spectrum. Physically, this spectrum characterizes the distribution of patch sizes that are present in an inhomogeneous medium. As mentioned in Section 3.1, the distribution of thermal patches in the ocean is a result of turbulent mixing. Similarly, the thermal microstructure in a model tank such as used in the present study is generated by turbulent mixing. Before returning to our discussion of acoustic wave propagation in an inhomogeneous medium, we will consider some basic concepts of turbulence theory.

3.3 Turbulence

The theory of turbulence^{19,71,78,79} is used, in general, to describe viscous fluid flow for large Reynolds numbers. The Reynolds number, Re , is defined as

$$Re = \frac{Lv}{\nu} ,$$

where

L is the characteristic scale of flow,

v is the characteristic flow velocity, and

ν is the kinematic viscosity of the fluid.

For small values of Re , the fluid flow is orderly or laminar. When the Reynolds number exceeds a critical value, Re_{cr} , the flow becomes unstable and breaks up into turbulent eddies. Each eddy of size ℓ will have

associated with it a local Reynolds number, Re_ℓ . If Re_ℓ also exceeds Re_{cr} , the eddy will further break down into smaller eddies. This process will continue until the eddies are small enough that viscous dissipation balances out the energy being supplied to the eddies from the external source. When this occurs, the turbulence reaches steady state, and a range of eddy sizes exists such that

$$l_o < \ell < L_o \quad ,$$

where

L_o is the outer scale of turbulence, and

l_o is the inner scale of turbulence.

The outer scale, L_o , is determined by the boundary conditions of the fluid flow. In an acoustics application, L_o may generally be taken to be the dimension from the acoustic source or receiver to the nearest boundary of the medium. The inner scale, l_o , is shown by Tatarski⁸⁰ to be

$$l_o = \sqrt[4]{\nu^3/\epsilon} \quad , \quad (3.5)$$

where

ϵ is the energy dissipated as heat per unit mass per unit time.

This qualitative description may be summarized in terms of energy as follows: an external energy source supplies energy to eddies of size L_o which transfer this energy down a chain of successively smaller eddies, the energy finally being dissipated as heat due to the viscous losses associated with the smallest eddies.

In describing turbulence it is often convenient to deal with the wavenumber, κ , associated with an eddy rather than use its characteristic dimension, ℓ . The wavenumber is inversely proportional to the eddy size

and may be written as⁸¹

$$\kappa = \frac{2\pi}{\lambda} \quad (3.6)$$

It can be seen that large wavenumbers correspond to small eddy sizes, and vice versa. Because the kinetic energy of the flow is distributed throughout a spectrum of eddy sizes, it is possible to define a power spectral density for the flow. The average kinetic energy of the flow is then the sum of the energy associated with all the eddies; i.e.,⁸²

$$T = \int_0^{\infty} \phi_v(\kappa) d\kappa \quad ,$$

where

T is the average kinetic energy per unit mass per unit time, $\phi_v(\kappa)$ is the one dimensional power spectral density, and the flow is assumed to be homogeneous and isotropic.

The quantity $\phi_v(\kappa)$ is related to the velocity fluctuations in the flow, but because temperature may usually be treated as a passive additive to the turbulence, the spectra of the temperature and refractive index variations are usually assumed to have the same shape as $\phi_v(\kappa)$.⁷⁰

A spectrum proposed by Medwin⁷⁰ for describing refractive index variations is shown in Fig. 3.2. In the figure, the range of wavenumbers corresponding to large, anisotropic eddies is labelled the 'source' sub-range, as these eddies supply energy to the entire spectrum. The energy of the source eddies gradually becomes less anisotropic (directional) in the transition subrange, until, in the inertial subrange, the energy is isotropic and homogeneous. In the inertial subrange, the spectral density is given by the simple relation:⁷⁰

$$\phi_v(\kappa) = b\kappa^{-5/3} \quad , \quad (3.7)$$

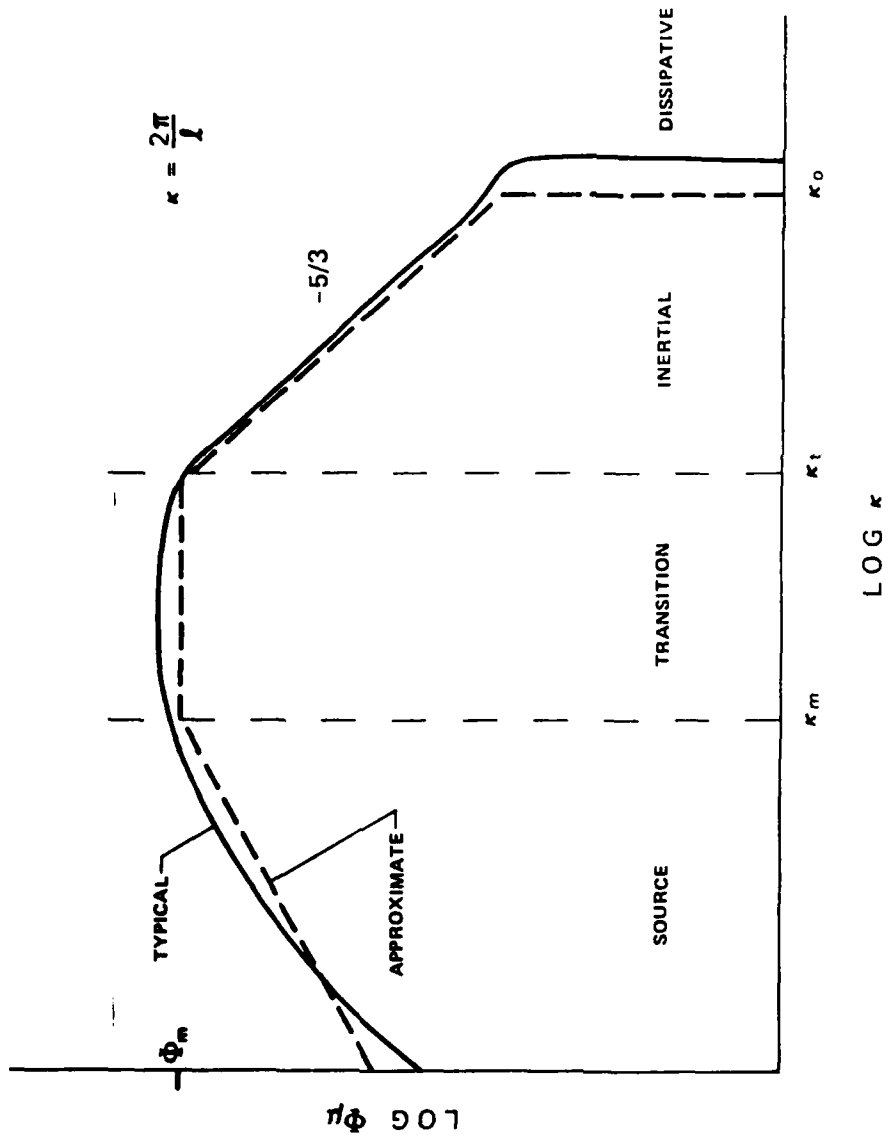


FIGURE 3.2
TURBULENT POWER DENSITY SPECTRUM

where

b is a function of the viscosity, ν , and the energy dissipation rate, ϵ .

The $-5/3$ power law expressed by Eq. (3.7) was originally proposed by Kolmogorov,⁸³ and has been experimentally verified in a number of studies.^{70,71,78} The turbulent energy of the flow is finally lost to heat in the 'dissipation' subrange, where viscous forces become dominant.

The various subranges of the spectrum in Fig. 3.2 are bounded by the wavenumbers κ_m , κ_t , and κ_o . Medwin defines these boundary wavenumbers as follows:⁷⁰

$$\kappa_m = \frac{\pi}{2D} \quad \text{where } D = \text{depth}, \quad (3.8)$$

$$\kappa_o = (\epsilon/\nu^3)^{1/4}, \quad \text{and} \quad (3.9)$$

$$\kappa_t = 0.5(\kappa_o \kappa_m)^{1/2}. \quad (3.10)$$

The wavenumber κ_m , defined by Eq. (3.8), depends only upon the depth of the acoustic experiment. In the upper ocean, the sea surface will be the nearest physical boundary to the acoustic experiment, so it seems reasonable that this boundary will determine the maximum significant eddy size. The effect on the acoustic experiment of eddy sizes corresponding to wavenumbers less than κ_m may be assumed to be negligible.⁷⁰

The lower limit of the inertial subrange, κ_t , is an empirical value that is shown by Medwin to obey the relation expressed in Eq. (3.10). The upper limit of the inertial subrange is the Kolmogorov wavenumber, κ_o , given by Eq. (3.9). Medwin assumes that the spectrum can be truncated at κ_o , and that the effects of the dissipation subrange upon an acoustic experiment can be ignored.⁷⁰ However, the results of Chotiros and Smith⁸⁴ suggest that

for the model tank used in the present investigation it is more reasonable to assume that the truncation wavenumber of Pao⁸⁵ is valid. Pao's theory assumes that the spectrum of the thermal microstructure in the dissipation subrange departs from that of turbulence and is controlled by the diffusivity. Pao suggests that the -5/3 power law continues to be valid in the dissipation subrange, with a truncation wavenumber given by

$$\kappa_p = (\varepsilon/D^3)^{1/4} \quad , \quad (3.11)$$

where

D is the diffusivity.

When κ_p is used to truncate the spectrum rather than κ_o , the wavenumber κ_t will become:⁸⁴

$$\kappa_t = 0.5(\kappa_p \kappa_m)^{1/2} \quad . \quad (3.12)$$

In this section and the previous section, two alternative methods of describing an inhomogeneous medium have been presented: the method of the correlation function and that of the spectral density function. The two methods are not independent, however; they are related by the Fourier transform theorem. In three dimensions, for a homogeneous medium this relation may be written as:

$$N_{12}(\Delta x, \Delta y, \Delta z) = \iiint_{-\infty}^{\infty} S_{\mu}(\kappa_1, \kappa_2, \kappa_3) \times \exp[j(\kappa_1 \Delta x + \kappa_2 \Delta y + \kappa_3 \Delta z)] d\kappa_1 d\kappa_2 d\kappa_3 \quad , \quad (3.13)$$

where

$S_{\mu}(\kappa_1, \kappa_2, \kappa_3)$ is the three dimensional spectrum of the refractive index variations, and

κ_1 , κ_2 , and κ_3 are wavenumbers in the x , y , and z dimensions, respectively.

For an isotropic medium Eq. (3.13) becomes⁷⁰

$$N_{12}(\rho) = \int_0^{\infty} \frac{\sin \kappa \rho}{\kappa \rho} \phi_{\mu}(\kappa) d\kappa, \quad (3.14)$$

where the one-dimensional spectral density is related to the isotropic three-dimensional spectral density by

$$\phi_{\mu}(\kappa) = 4\pi\kappa^2 S_{\mu}(\kappa) .$$

3.4 The Wave Equation for an Inhomogeneous Medium

In the preceding sections we have discussed some of the causes of acoustic signal fluctuations and have presented two methods that are useful in describing the inhomogeneous medium in which these fluctuations occur. Now we will consider in more detail the way in which medium inhomogeneities produce variations in the amplitude and phase of a propagating wave. The acoustic wave equation for an inhomogeneous medium has been derived by a number of people, including Rayleigh.⁸⁶ The discussion in this section will be based on Chernov's⁸⁷ development.

It is assumed that the medium is lossless and is in a state of equilibrium so that, ignoring the force of gravity, the ambient pressure p_0 is constant throughout the medium. The only inhomogeneities present in the medium are those in temperature and density; the effects of bubbles, biological matter, etc., are neglected. Temperature and density variations are not independent quantities. In order for the pressure to remain constant, the changes in temperature at any point in the medium will be accompanied by a related change in density. In the ocean, it would be expected that the temperature inhomogeneities would be moved about in the medium by

current flow and convective motion. It is assumed that these types of motion are slow compared to the velocity of sound so that the inhomogeneities can be regarded as fixed during the time required for an acoustic wavefront to propagate through a patch of diameter $2a$. This condition is what Chernov calls the 'quasi-static' condition.

The wave equation for the situation described above is

$$\frac{1}{c^2} \frac{\partial^2 p}{\partial t^2} - \nabla^2 p + \nabla \log \rho_T \cdot \nabla p = 0 \quad , \quad (3.15)$$

where

$c = c(x,y,z) = c_0 + \Delta c$ is the sound speed,

$c_0 = \langle c \rangle$ is the mean sound speed,

$\Delta c = \Delta c(x,y,z)$ is the random variation in sound speed,

p is the acoustic pressure,

$\rho_T = \rho_T(x,y,z) = \rho_0 + \Delta \rho$ is the total density,

$\rho_0 = \langle \rho_T \rangle$ is the mean density, and

$\Delta \rho = \Delta \rho(x,y,z)$ is the random variation in density.

This equation differs from the homogeneous wave equation in two respects: (1) the sound velocity is not constant, but varies spatially in a random manner; and (2) there is an additional term, $\nabla \log \rho_T \cdot \nabla p$, which arises as a result of the random variations in density. It is assumed that the variations in sound speed and density are small; i.e., $\Delta c \ll c_0$ and $\Delta \rho \ll \rho_0$.

When some 'primary' acoustic wave is transmitted through the inhomogeneous medium described above, each element of the medium becomes a source of 'secondary' scattered waves. For example, suppose a harmonic plane wave propagates in the x direction. This primary or incident wave can be described by

$$p_i = P_i \exp[j(\omega t - kx)] \quad , \quad (3.16)$$

where

ω is the angular frequency, and

$k = \frac{\omega}{c_0}$ is the wave number.

If the scattering elements are associated with the coordinates (ξ, η, ζ) and the observation point is designated by (x, y, z) , then the distance from a scattering element to the observation point will be

$$r = \sqrt{(x - \xi)^2 + (y - \eta)^2 + (z - \zeta)^2} \quad . \quad (3.17)$$

The total scattered pressure at the observation point will be given by the solution to Eq. (3.15), which Chernov expresses as:

$$p_{sc} = -\frac{p_i}{4\pi} \int_V \left\{ 2k^2 \frac{\Delta c}{c_0} - \frac{jk}{\rho_0} \frac{\partial(\Delta\rho_T)}{\partial\xi} \right\} \cdot \frac{1}{r} \exp[-jk(r + \xi)] dv \quad , \quad (3.18)$$

where

\int_V denotes integration over the volume of scatterers.

[In Eq. (3.18) and hereafter the factor $e^{j\omega t}$ is dropped.] The first term in curly brackets [Eq. (3.18)] is associated with scattering of sound by spatial variations in the sound velocity, while variations in the density give rise to the second term. In the ocean, the density fluctuations may be assumed to be negligible in comparison to the sound speed fluctuations, so the second term in curly brackets [Eq. (3.18)] can be omitted in approximating the scattered pressure.

One further modification of Eq. (3.18) can be made as follows. From Eq. (3.1) we can write the refractive index variations as

$$\mu = \frac{c_0}{c} - 1 = \frac{c_0}{(c_0 + \Delta c)} - 1 \quad , \quad (3.19)$$

where $c = c_0 + \Delta c$. Some algebraic manipulation of Eq. (3.19) gives

$$\mu = - \frac{\Delta c}{(c_0 + \Delta c)} \doteq - \frac{\Delta c}{c_0} \quad , \quad (3.20)$$

where, as mentioned above, $\Delta c \ll c_0$. Substitution of this result for $\frac{\Delta c}{c_0}$ in Eq. (3.18) leads to the following expression for the scattered pressure:

$$p_{sc} = \frac{k^2 p_i}{2\pi} \int_V \frac{\exp[-jk(r + \xi)]}{r} \mu(\xi, \eta, \zeta) dv \quad . \quad (3.21)$$

The physical significance of this result can be summarized as follows: A scattering element with volume dv and refractive index variation μ is located at point (ξ, η, ζ) . Due to the influence of an incident wave p_i , the scattering element acts as a secondary sound source which radiates a pressure wave dp_{sc} . The total scattered pressure, p_{sc} , received at the observation point (x, y, z) is the sum of the contributions from all scattering elements in the volume V . The result expressed by Eq. (3.21) can be used to calculate the amplitude and phase fluctuations of the pressure wave at the observer, as will now be discussed.

3.5 Fluctuations in the Amplitude and Phase of the Observed Pressure

The total pressure at the observation point will be the sum of the primary pressure and the scattered pressure,

$$p = P e^{-j\phi} = p_i + p_{sc} \quad ,$$

where

P and ϕ are the amplitude and phase of the total pressure, p .

As the inhomogeneities move about in the medium, the amplitude and phase of the observed pressure will vary randomly about their mean values. It is

convenient to define the fluctuation in observed pressure amplitude and phase about their mean values as

$$B = \ln\left(\frac{P}{\langle P \rangle}\right), \text{ and} \quad (3.22)$$

$$S = \phi - \langle \phi \rangle, \quad (3.23)$$

where

B is the logarithmic fractional variation of the instantaneous pressure amplitude, P , from its mean value, $\langle P \rangle$, and

S is the variation of the instantaneous phase, ϕ , from its mean value, $\langle \phi \rangle$.

The \ln operator in Eq. (3.22) is a consequence of using Rytov's method, also known as the method of smooth perturbations, in calculating the fluctuations.⁸⁸ In this thesis we will be concerned with amplitude fluctuations sufficiently small to make the approximation

$$B = \ln\left(\frac{P}{\langle P \rangle}\right) \approx \frac{P - \langle P \rangle}{\langle P \rangle}; \quad B \ll 1.$$

The average values of B and S are zero, so it is necessary to use the mean square fluctuations, $\langle B^2 \rangle$ and $\langle S^2 \rangle$, to characterize the level of fluctuations caused by the inhomogeneities. There are a variety of analytical expressions in the literature that relate the mean square fluctuations to the statistical parameters used to describe the inhomogeneous medium. In the next two sections we consider expressions for $\langle B^2 \rangle$ and $\langle S^2 \rangle$ when the medium is described by a Gaussian correlation function, and when the medium is described by a spectral density function.

3.5.1 Fluctuations in a Medium Described by a Correlation Function

In the case of plane waves propagating through a statistically isotropic inhomogeneous medium, Chernov⁸⁹ obtained solutions for $\langle B^2 \rangle$ and $\langle S^2 \rangle$ in terms of a wave parameter, D , given by

$$D = \frac{4L}{ka^2} ,$$

where

L is the propagation distance of the acoustic wave through the medium. Chernov's analysis assumes that the inhomogeneities are large compared to an acoustic wavelength ($ka \gg 1$), and that the propagation distance is large compared to the scale of the inhomogeneities ($L \gg a$).

For large values of the wave parameter, which corresponds to the wave region of the patches, Chernov obtains:

$$\langle B^2 \rangle = \langle S^2 \rangle = \langle \mu^2 \rangle k^2 L \int_0^\infty R(\rho) d\rho , \quad D \gg 1 . \quad (3.24)$$

If the correlation coefficient is Gaussian, given by Eq. (3.4), then Eq. (3.24) becomes

$$\langle B^2 \rangle = \langle S^2 \rangle = \frac{\sqrt{\pi}}{2} \langle \mu^2 \rangle k^2 aL , \quad D \gg 1 . \quad (3.25)$$

Mintzer has shown^{16,67} that these same results, Eqs. (3.24) and (3.25), are valid for a spherical wave in the wave region when

$$k^2 \langle \mu^2 \rangle aL \ll 1 .$$

For small values of the wave parameter, corresponding to the ray region of the patches, Chernov shows the mean square amplitude

fluctuations for a plane wave to be

$$\langle B^2 \rangle = \frac{1}{6} \langle \mu^2 \rangle L^3 \int_0^\infty \nabla^2 \nabla^2 R(\rho) d\rho, \quad D \ll 1, \quad (3.26)$$

which, for a Gaussian correlation coefficient, becomes

$$\langle B^2 \rangle = \frac{8\sqrt{\pi}}{3} \langle \mu^2 \rangle \frac{L^3}{a}, \quad D \ll 1. \quad (3.27)$$

The phase fluctuations for $D \ll 1$ have been shown⁸⁹ to be twice their values when $D \gg 1$ (i.e., double the results in Eqs. (3.24) and (3.25)).

Finally, when the wave parameter is of the order of unity, Chernov obtains

$$\langle B^2 \rangle = \frac{\sqrt{\pi}}{2} \langle \mu^2 \rangle k^2 a L \left(1 - \frac{1}{D} \arctan D \right), \quad (3.28)$$

$$\langle S^2 \rangle = \frac{\sqrt{\pi}}{2} \langle \mu^2 \rangle k^2 a L \left(1 + \frac{1}{D} \arctan D \right), \quad (3.29)$$

where a Gaussian correlation coefficient has been assumed. For small and large values of D , these last two results become equivalent to the ray and wave region solutions, respectively.

Using the same conditions and assumptions as Chernov, Karavainikov⁹⁰ obtained a similar set of results for the amplitude and phase fluctuations in a propagating spherical wave. For the wave region of the inhomogeneities, $D \gg 1$, Karavainikov's result is identical to Eq. (3.25).

3.5.2 Fluctuations in a Turbulent Medium

In the case of a medium whose random refractive index field is determined by turbulence, Tatarski^{19,71} has found expressions for amplitude fluctuations in terms of a turbulence parameter, C_n . For propagation distances L such that $L_0 \gg \sqrt{\lambda L} \gg l_0$, where l_0 and L_0 are the inner and outer scales of turbulence, respectively, and λ is the acoustic wavelength,

Tatarski shows

$$\langle B^2 \rangle = 0.13 C_n^2 k^{7/6} L^{11/6} \quad (3.30)$$

for spherical waves, and

$$\langle B^2 \rangle = 0.31 C_n^2 k^{7/6} L^{11/6} \quad (3.31)$$

for plane waves. The quantity C_n is related to the spectral function $S_\mu(\kappa)$ by⁹¹

$$S_\mu(\kappa) = 0.033 C_n^2 \kappa^{-11/3}, \quad \kappa_t < \kappa < \kappa_p.$$

An assumption made in deriving Eqs. (3.30) and (3.31) is that only the inertial range of the spectrum contributes to the acoustic fluctuations. If the spectrum is of the form shown in Fig. 3.2, so that there is an approximately flat transition region, then there is an additional contribution from the transition region to the amplitude fluctuations of an amount⁸⁴

$$\langle B_t^2 \rangle \doteq \frac{\pi}{480} \phi_m L^3 (\kappa_t^4 - \kappa_m^4) \quad (3.32)$$

for spherical waves, and

$$\langle B_t^2 \rangle \doteq \frac{\pi}{48} \phi_m L^3 (\kappa_t^4 - \kappa_m^4) \quad (3.33)$$

for plane waves. As shown in Fig. 3.2, ϕ_m is the maximum value of the spectral density function ϕ_μ . The total mean square amplitude fluctuations, when there is a contribution due to the transition region, is $\langle B^2 \rangle + \langle B_t^2 \rangle$.

Often the amplitude fluctuations are expressed in terms of the coefficient of amplitude variation, CAV, because this parameter is easy to calculate from a record of pulsed data. The coefficient of amplitude variation, which is essentially the standard deviation of the pressure amplitude, is defined as⁶⁷

$$\text{CAV}^2 = \frac{\langle P^2 \rangle - \langle P \rangle^2}{\langle P \rangle^2}, \quad (3.34)$$

where P is the amplitude of the observed pressure. For small amplitude fluctuations, $\langle B^2 \rangle$ and CAV^2 are approximately equal.

3.6 Correlation of Fluctuations

In addition to the mean-square fluctuations, it is useful to know the spatial correlation of the fluctuations. As will be seen in Chapter 4, these correlations are important quantities in developing a theory of parametric reception in a random medium. In this section, we present some of the correlation functions that will be useful in this study. There are two types of spatial correlations that are of interest: longitudinal correlation, which is the correlation of fluctuations between two point receivers, separated a distance ΔL , and both located on the axis of the propagating wave; and transverse correlation, which is the correlation of fluctuations between two point receivers separated a distance $\Delta \rho$ in a direction transverse to the acoustic axis.

For a plane wave in a Gaussian medium, the longitudinal correlation coefficients for the amplitude and phase fluctuations are given by⁹²

$$R_B^L = R_S^L = \left[1 + \left(\frac{2\Delta L}{ka^2} \right)^2 \right]^{-1}, \quad D \gg 1 \quad (3.34)$$

for the wave region of the inhomogeneities, and by⁹³

$$R_B^L = \left(1 + \frac{3\Delta L}{2L_1}\right) \left(1 + \frac{\Delta L}{L_1}\right)^{-3/2}, \quad D \gg 1 \quad (3.35)$$

$$R_S^L = \left[1 + \left(\frac{2\Delta L}{ka^2}\right)^2\right]^{-1} \left(1 + \frac{\Delta L}{L_1}\right)^{-1/2}, \quad D \ll 1 \quad (3.36)$$

in the ray region. In these expressions L_1 refers to the propagation distance to the receiver nearest the signal source. Similar expressions for the transverse correlation coefficients for a plane wave in a Gaussian medium are:⁹²

$$R_B^T = R_S^T = \exp[-(\Delta\rho)^2/a^2], \quad D \gg 1 \quad (3.37)$$

$$R_B^T = \exp[-(\Delta\rho)^2/a^2] \cdot \left\{1 - 2[(\Delta\rho)^2/a^2] + \frac{1}{2}[(\Delta\rho)^2/a^2]^2\right\}, \quad D \ll 1 \quad (3.38)$$

$$R_S^T = \exp[-(\Delta\rho)^2/a^2], \quad D \ll 1 \quad (3.39)$$

There are also published results describing the correlation of fluctuations for spherical waves⁹⁰ and for turbulent media.^{19,94} These results in general involve complicated expressions from which it is difficult to gain a physical understanding, and we will not reproduce them here.

3.7 Summary

In this chapter, a review of the basic theory of acoustic wave propagation in an inhomogeneous medium has been presented. The material has been selected on the basis of its relevance to the theoretical analysis of parametrically received signal fluctuations to be discussed in the following chapter.

It was seen in Section 3.1 that the principal cause of scattering in the ocean is the thermal microstructure. Thermal patches can be treated as sound sources of radius a . The scattered radiation from these patches has

a nearfield extending to a distance ka^2 ; from that distance onward the radiation is spherically spreading with a beamwidth of $1/ka$ radians. At any point in the medium the observed pressure is the sum of the unscattered pressure p_i and the scattered pressure p_{sc} . Due to random changes in the characteristics of the scattered pressure field, the observed pressure is a randomly fluctuating quantity.

In Section 3.2 two methods were discussed that can be used to describe an inhomogeneous medium. One method uses a correlation function for the variations of refractive index, and the other method uses a spatial wave-number spectrum. Because the spectral composition of the inhomogeneities is determined by turbulence, Section 3.3 gave a brief summary of some concepts from the theory of turbulence.

The wave equation for an inhomogeneous medium and its integral solution were discussed in Section 3.4. A summary of expressions for the amplitude and phase fluctuations of the observed pressure, as well as for the correlation of these fluctuations, was presented in the remainder of the chapter.

The background material discussed in Chapters 2 and 3 will now be used to develop a theory of parametric reception in an inhomogeneous medium.

4.1 Introduction

In Chapter 2, expressions were given for the second-order pressure associated with both nearfield and farfield parametric receivers. The results assumed the parametric receiver to be operating in a medium containing no inhomogeneities. In this chapter, some effects of medium inhomogeneities will be taken into account, and an expression will be derived that describes amplitude fluctuations in the second-order pressure wave of a parametric receiver.

Before beginning a formal analysis, it may be helpful to consider some general aspects of the problem. There are three separate signals which will be affected by the inhomogeneities. One is the low-frequency signal that is to be detected by the receiver. In practice this signal may be expected to propagate a significant distance through the ocean, and as a result of scattering, it will arrive at the receiver as a randomly varying signal. The pump wave will also be scattered as it travels through the interaction region, so nonlinear interaction will be occurring between two fluctuating first-order signals. The resulting second-order signal can be expected to vary in a manner that is related to the first-order fluctuations. Also, the second-order signal will be scattered as it propagates from each source point to the observer, and further fluctuations will result.

Analyses have been reported by Smith^{95,96} and by Chotiros and Smith^{84,97} describing the performance of a parametric transmitting array in a random medium but, to date, there is no similar study for receiving arrays. In this chapter, the methods developed by Smith and Chotiros are used to study the effects of medium inhomogeneities on parametric reception. It will be assumed in this analysis that the signal source is located in the main beam of the parametric receiver. Expressions

predicting the amplitude fluctuations for the second-order pressure will be developed for both collimated and spherically spreading pump waves.

4.2 Amplitude Fluctuations for a Nearfield Receiving Array

We will begin our analysis with the simple case of the nearfield parametric receiver shown in Fig. 4.1. A signal wave originates at a source located on the acoustic axis of the parametric receiver at $z = -Z_s$; the source is sufficiently far removed from the pump transducer that its radiation may be treated as being planar in the vicinity of the parametric receiver. In rectangular coordinates, the signal wave may be represented by

$$p_s(z,t) = P_s [1 + B_s(x,y,z,t)] e^{-\alpha_s z} \times \exp\{j[\omega_s t - k_s z - \phi_0 - S_s(x,y,z,t)]\}, \quad (4.1)$$

where

$P_s = \overline{P_s(t)}$ is the mean pressure amplitude at the pump transducer,

$B_s = \frac{P_s(t) - P_s}{P_s}$ is the amplitude fluctuation,

$S_s = \phi(t) - k_s z$ is the phase fluctuation,

α_s is the attenuation coefficient at the signal frequency,

ϕ_0 is the phase of the wave at $z = 0$, which may be set to zero, and

the overbar indicates time averaging.

Now assume that the hydrophone is situated in the nearfield of the pump transducer; i.e., that

$$L \leq 4b^2/\lambda_p,$$

where

$z = L$ is the location of the hydrophone,

$2b \times 2b$ are the dimensions of the pump transducer, and

λ_p is the wavelength of the pump wave.

For this case the pump radiation in the interaction volume of the parametric receiver may be assumed to be approximately planar and may be written as

$$p_p(z,t) = P_p [1 + B_p(x,y,z,t)] e^{-\alpha_p z} \times \exp\{j[\omega_p t - k_p z - S_p(x,y,z,t)]\}, \quad (4.2)$$

where

P_p is the mean pressure amplitude,

B_p represents the amplitude fluctuations,

α_p is the attenuation coefficient at the pump frequency, and

S_p represents the phase fluctuations.

The source density for the second-order radiation can be found by substituting the total first-order pressure field, $p_1 = p_s + p_p$, into the equation,

$$q(\vec{r}_o, t) = \frac{\beta}{\rho_o^2 c_o^4} \frac{\partial}{\partial t} [p_1(\vec{r}_o, t)^2],$$

where

\vec{r}_o gives the location of a source point, as shown in Fig. 4.1, and the remaining terms are defined in Section 2.2.

The result, using Eqs. (4.1) and (4.2) for p_s and p_p , is

$$q(\vec{r}_o, t) = \frac{j\beta P_s P_p \omega_{\pm}}{\rho_o^2 c_o^4} (1 + B_s)(1 + B_p) e^{-(\alpha_s + \alpha_p)z} \times \exp\{j[\omega_{\pm} t - k_{\pm} z - (S_s \pm S_p)]\}, \quad (4.3)$$

where

$$\omega_{\pm} = \omega_p \pm \omega_s, \text{ and}$$

$$k_{\pm} = k_p \pm k_s.$$

Inclusion of the attenuation coefficients as constant terms as in Eq. (4.3) requires that the time fluctuations in amplitude and phase are slowly varying when compared to the signal frequencies. This requirement ensures that frequency broadening of the signals due to the fluctuations is negligible, so that the approximation of the attenuation coefficients as constants is valid.

The stipulation that B and S be slowly varying also permits their

time derivatives to be neglected when calculating the source density. Such an approximation is reasonable in situations where the signal frequencies involved are much higher than any frequency component in the fluctuation spectra.

The interaction frequency pressure produced at the observation point, \vec{r} , due to radiation of the virtual source, qdv , will be given by

$$dp_{\pm}(\vec{r}, t) = -\frac{\rho_0}{4\pi r'} (1 + B_{\pm}) e^{-jS_{\pm}} e^{-\alpha_{\pm} r'} \times \left[\frac{\partial}{\partial t} q(\vec{r}_0, \tau) \right] dv, \quad (4.4)$$

where

$$r' = |\vec{r}'|,$$

B_{\pm} and S_{\pm} are the amplitude and phase fluctuations produced in the interaction frequency wave as it propagates from source point to observation point, and

$$\tau = t - \frac{r'}{c_0} \text{ is the retarded time.}$$

An attenuation term, $e^{-\alpha_{\pm} r'}$, has been included ad hoc in Eq. (4.4) to account for attenuation of the interaction frequency wave. Substitution of Eq. (4.3) for the source density in Eq. (4.4), and integration over the interaction volume, V , gives the following expression for the second-order pressure at the observer:

$$p_{\pm}(\vec{r}, t) = \frac{\beta P_s P_p k_{\pm}^2}{\rho_0 c_0^2} \int_V e^{-(\alpha_s + \alpha_p)z} e^{-\alpha_{\pm} r'} \times (1 + B_s) (1 + B_p) (1 + B_{\pm}) e^{-j(S_s \pm S_p + S_{\pm})} \times e^{-jk_{\pm}z} e^{-jk_{\pm}r'} \frac{1}{4\pi r'} dv. \quad (4.5)$$

This expression for p_{\pm} can be simplified in the following way. First, assume that the amplitude and phase fluctuations are small compared to unity; i.e.,

$$B_s \ll 1, \quad S_s \ll 1,$$

$$B_p \ll 1, \quad S_p \ll 1,$$

$$B_{\pm} \ll 1, \quad S_{\pm} \ll 1.$$

Then the amplitude fluctuation terms can be expanded and, retaining only terms of first order in fluctuations,

$$(1 + B_s)(1 + B_p)(1 + B_{\pm}) \doteq 1 + B, \quad (4.6)$$

where

$$B \equiv B_s + B_p + B_{\pm}.$$

Similarly, the phase fluctuation term can be approximated as

$$e^{-j(S_s \pm S_p + S_{\pm})} \doteq 1 - jS \quad (4.7)$$

where

$$S \equiv S_s \pm S_p + S_{\pm}.$$

Next, assume that the signal frequency is much lower than the pump frequency, and that the pump and interaction frequencies are approximately equal;

$$\omega_s \ll \omega_p, \text{ and}$$

$$\omega_p \doteq \omega_{\pm}.$$

It may then be expected that the absorption coefficients corresponding to these frequencies will obey the relations

$$\alpha_s \ll \alpha_p, \text{ and} \quad (4.8)$$

$$\alpha_p \doteq \alpha_{\pm}. \quad (4.9)$$

Furthermore, if the transverse dimensions of the interaction region remain small compared to the longitudinal dimension, then

$$r' \doteq (L - z),$$

so that

$$e^{-\alpha_{\pm} r'} \doteq e^{-\alpha_{\pm} (L - z)}. \quad (4.10)$$

Using these approximations [Eqs. (4.8) - (4.10)], the attenuation terms in Eq. (4.5) can be written as

$$\begin{aligned}
e^{-(\alpha_s + \alpha_p)z} e^{-\alpha_{\pm} r'} &\doteq e^{-\alpha_s z} e^{-(\alpha_p - \alpha_{\pm})z} e^{-\alpha_{\pm} L} \\
&\doteq e^{-\alpha_{\pm} L}.
\end{aligned} \tag{4.11}$$

Now Eqs. (4.6), (4.7), and (4.11) can be used to rewrite the expression for the second-order pressure [Eq. (4.5)] as

$$p_{\pm}(\vec{r}, t) = A \int_V (1 + B)(1 - jS) e^{-jk_{\pm}(z + r')} \frac{1}{r'} dv, \tag{4.12}$$

where, for convenience,

$$A \equiv \frac{\beta P_s P_p k_{\pm}^2}{4\pi \nu_o c_o^2} e^{-\alpha_{\pm} L}.$$

In addition to Eq. (4.12), we can also write p_{\pm} explicitly in terms of the fluctuations of the second-order pressure. Thus, if B_{PR} and S_{PR} are the amplitude and phase fluctuations of the interaction frequency pressure at the observation point, then p_{\pm} can be written as

$$p_{\pm}(\vec{r}, t) = p_H (1 + B_{PR}) e^{-jS_{PR}}, \tag{4.13}$$

where

$$p_H = A \int_V e^{-jk_{\pm}(z + r')} \frac{1}{r'} dv$$

is the second-order pressure that would be produced at the observation point if the medium were homogeneous. For phase fluctuations small compared to unity, the exponential term in Eq. (4.13) can be approximated by

$$e^{-jS_{PR}} \doteq 1 - jS_{PR},$$

so that the interaction frequency pressure becomes

$$p_{\pm}(\vec{r}, t) \doteq p_H (1 + B_{PR} - jS_{PR}), \tag{4.14}$$

where only terms to first-order in fluctuations are retained.

It is now possible to solve for the amplitude and phase fluctuations, B_{PR} and S_{PR} , as follows. First we equate Eqs. (4.12) and (4.14)

$$p_H (1 + B_{PR} - jS_{PR}) = A \int_V (1 + B - jS) e^{-jk_{\pm}(z + r')} \frac{1}{r'} dv, \tag{4.15}$$

where only terms to first order in fluctuations have been retained from Eq. (4.12). Next the homogeneous component of the pressure, p_H , is subtracted from both sides of Eq. (4.15), leaving

$$B_{PR} - jS_{PR} = \frac{1}{H} \int_V (B - jS) e^{-jk_{\pm}(z + r')} \frac{1}{r'} dv, \quad (4.16)$$

where

$$H = \int_V e^{-jk_{\pm}(z + r')} \frac{1}{r'} dv.$$

The amplitude and phase fluctuations of the interaction frequency wave at the hydrophone may now be found by equating the real and imaginary parts of Eq. (4.16); i.e.,

$$B_{PR} = \text{Re} \left\{ \frac{1}{H} \int_V (B - jS) e^{-jk_{\pm}(z + r')} \frac{1}{r'} dv \right\}, \quad (4.17)$$

$$\text{and } S_{PR} = -\text{Im} \left\{ \frac{1}{H} \int_V (B - jS) e^{-jk_{\pm}(z + r')} \frac{1}{r'} dv \right\}.$$

In this analysis we will be concerned only with the amplitude fluctuations, given by Eq. (4.17). Since B_{PR} is a random variable, it will be useful to find its mean-square value, $\langle B_{PR}^2 \rangle$. By assuming that B_{PR} is ergodic, it will be possible to take the (spatial) ensemble average rather than a time average. Thus, we form the average of the product,

$B_{PR1} B_{PR2}$, where

$$B_{PR1} = \text{Re} \left\{ \frac{1}{H} \int_V (B_1 - jS_1) e^{-jk_{\pm}(z_1 + r'_1)} \frac{1}{r'_1} dv_1 \right\},$$

$$B_{PR2} = \text{Re} \left\{ \frac{1}{H} \int_V (B_2 - jS_2) e^{-jk_{\pm}(z_2 + r'_2)} \frac{1}{r'_2} dv_2 \right\},$$

and the geometry of Fig. 4.2 applies. The mean-square amplitude fluctuation, $\langle B_{PR}^2 \rangle$, is given by*

*In forming the product $B_{PR1} B_{PR2}$ the following relation

between complex numbers a and b is used:

$$\text{Re} \{ a \} \cdot \text{Re} \{ b \} = \frac{1}{2} \text{Re} \{ a(b + b^*) \},$$

where the asterisk denotes the complex conjugate.

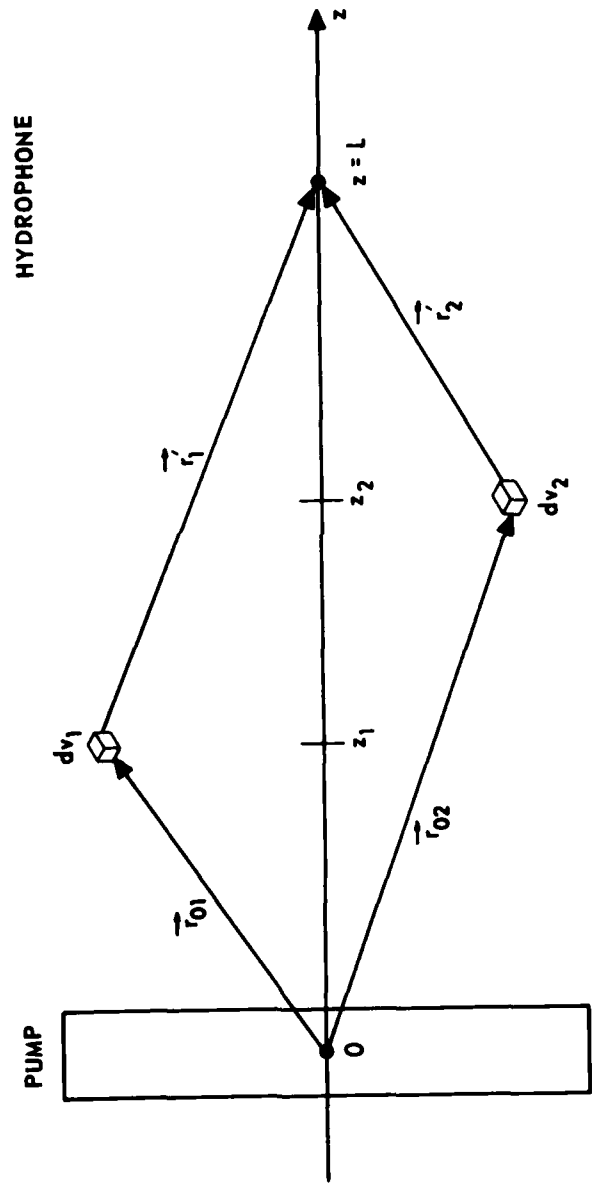


FIGURE 4.2
SCATTERING GEOMETRY

$$\begin{aligned}
\langle B_{PR}^2 \rangle &= \langle B_{PR1} B_{PR2} \rangle \\
&= \frac{1}{2} \operatorname{Re} \left\{ \frac{1}{H^2} \iint_V \langle (B_1 - jS_1)(B_2 - jS_2) \right. \\
&\quad \times e^{-jk_{\pm}(z_1 + z_2 + r'_1 + r'_2)} \frac{1}{r'_1 r'_2} dv_1 dv_2 \\
&\quad \left. + \frac{1}{HH^*} \iint_V \langle (B_1 - jS_1)(B_2 + jS_2) \rangle e^{-jk_{\pm}(z_1 - z_2 + r'_1 - r'_2)} \right. \\
&\quad \left. \times \frac{1}{r'_1 r'_2} dv_1 dv_2 \right\} \quad (4.18)
\end{aligned}$$

This result is not easy to use as it will require numerical integration for its evaluation. However, Eq. (4.18) can be simplified considerably if it is assumed that the amplitude and phase fluctuations have complete transverse correlation in the interaction volume. With this assumption, B_1 , B_2 , S_1 , and S_2 become independent of the variables x and y , and the expressions for $\langle B_{PR}^2 \rangle$ become

$$\begin{aligned}
\langle B_{PR}^2 \rangle &= \frac{1}{2} \operatorname{Re} \left\{ \frac{1}{H^2} \int_0^L \int_0^L \langle (B_1 B_2 - jB_1 S_2 - jB_2 S_1 - S_1 S_2) \rangle e^{-jk_{\pm}(z_1 + z_2)} I_1 I_2 dz_1 dz_2 \right. \\
&\quad \left. + \frac{1}{HH^*} \int_0^L \int_0^L \langle (B_1 B_2 + jB_1 S_2 - jB_2 S_1 + S_1 S_2) \rangle e^{-jk_{\pm}(z_1 - z_2)} I_1^* I_2^* dz_1 dz_2 \right\} \quad (4.19)
\end{aligned}$$

$$\text{where } I = \int_{-b}^b \int_{-b}^b \exp\{-jk_{\pm}[(L-z)^2 + x^2 + y^2]^{\frac{1}{2}}\} [(L-z)^2 + x^2 + y^2]^{-\frac{1}{2}} dx dy \quad .$$

An approximate expression for I , valid in the nearfield of the pump transducer, is shown in Appendix 1 to be

$$I \doteq -\frac{j\pi}{k_{\pm}} e^{-jk_{\pm}(L-z)} \quad (4.20)$$

A similar result is obtained in Appendix 1 for H ; namely,

$$H \doteq -\frac{j\pi L}{k_{\pm}} e^{-jk_{\pm}L} \quad (4.21)$$

Substitution of Eqs. (4.20) and (4.21) into Eq. (4.19) leads to the result

$$\begin{aligned} \langle B_{PR}^2 \rangle &= \frac{1}{2} \operatorname{Re} \left\{ \frac{1}{L^2} \int_0^L \int_0^L \langle (B_1 B_2 - j B_1 S_2 - j B_2 S_1 - S_1 S_2) \rangle dz_1 dz_2 \right. \\ &\quad \left. + \frac{1}{L^2} \int_0^L \int_0^L \langle (B_1 B_2 + j B_1 S_2 - j B_2 S_1 + S_1 S_2) \rangle dz_1 dz_2 \right\} \\ &= \frac{1}{2} \operatorname{Re} \left\{ \frac{1}{L^2} \int_0^L \int_0^L (2 \langle B_1 B_2 \rangle - j 2 \langle B_2 S_1 \rangle) dz_1 dz_2 \right\}. \end{aligned}$$

Because $\langle B_1 B_2 \rangle$ and $\langle B_2 S_1 \rangle$ are real numbers, this expression reduces to

$$\langle B_{PR}^2 \rangle = \frac{1}{L^2} \int_0^L \int_0^L \langle B_1 B_2 \rangle dz_1 dz_2. \quad (4.22)$$

This result for the mean-square amplitude fluctuations of the second-order pressure wave can be evaluated by developing an expression for the correlation term, $\langle B_1 B_2 \rangle$, as a function of z_1 and z_2 , and performing the integration. We will return to the matter of evaluating and interpreting Eq. (4.22) below, but first a similar expression for $\langle B_{PR}^2 \rangle$ will be developed assuming that the pump wave is spherically spreading rather than collimated and planar.

4.3 Amplitude Fluctuations for a Farfield Receiving Array

An analysis similar to that in the previous section can be developed for a parametric receiver with spherically spreading pump waves. The geometry used is shown in Fig. 4.3. As for the nearfield analysis, the signal source is located on the axis of the parametric receiver and is sufficiently far from the pump that its radiation may be assumed to be planar in the vicinity of the parametric receiver. The signal wave may be represented as

$$p_s = P_s [1 + B_s(z + Z_s)] e^{-\alpha_s z} \exp \{ j[\omega_s t - k_s z - S_s(z + Z_s)] \},$$

and the pump wave is

$$p_p = j(P_p'/r)D(\gamma)[1 + B_p(r)] e^{-\alpha_p r} \exp \left\{ j[\omega_p t - k_p r - S_p(r)] \right\},$$

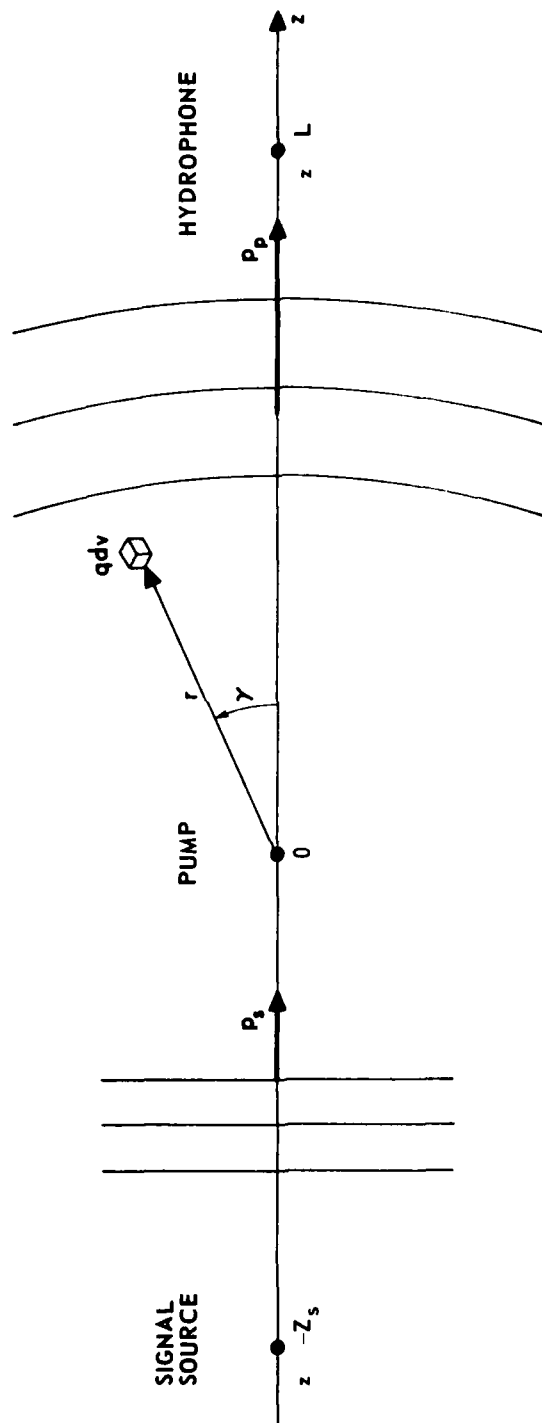


FIGURE 4.3
GEOMETRY FOR ANALYZING FARFIELD RECEIVER

where

P'_p is the mean pump wave pressure amplitude at $\gamma = 0$, $r = 1$ m, and

$D(\gamma)$ is the directivity function for the pump transducer.

In writing the signal wave fluctuation terms, B_s and S_s , as independent of γ , complete transverse correlation of B_s and S_s in the interaction volume has been assumed. Similarly, it is assumed that the pump wave fluctuation terms, B_p and S_p , are completely correlated along the spherical wavefronts within the pump beam so that B_p and S_p are independent of γ . These assumptions are discussed in more detail in Appendix 2.

The source density function at point (r, γ) can be found in the same way as in the nearfield case [Eq. (4.3)]; the result is

$$q = \frac{-\beta P'_s P'_p \omega_{\pm}}{\rho_o c_o^2 r} e^{-\alpha_s z} e^{-\alpha_p r} D(\gamma) \times (1 + B_s)(1 + B_p) e^{-j(S_p \pm S_s)} e^{-j(k_p r \pm k_s z)} e^{j\omega_{\pm} t}. \quad (4.23)$$

This expression can be used to find the second-order pressure at the observer in the same way as in the previous section. In the case of spherically spreading pump waves, however, a solution can be obtained more simply by adopting a procedure developed by Berktaf and Shooter.⁴³ They assume that the sphericity of the pump wave within the beam is small compared to the wavelength at the signal frequency, so that, for the signal source located on the Z axis, the source functions q_{\pm} can be assumed to be cophasal on the spherical wavefronts. The frequency of the second-order radiation is nearly equal to the pump frequency, so the second-order waves will radiate spherically, with the same beam pattern as for the pump wave. These assumptions are used to calculate the second-order pressure at the observer as follows.

The elemental particle velocity at r due to a spherical shell of sources of thickness δr is

$$\delta u_r = \frac{1}{2} q(r) \delta r,$$

where the source density function is given by Eq. (4.23). The contribution of these sources to the particle velocity at $(L,0)$ will be

$$\delta u_L = (\tau/L) \delta u_r (1 + B_u) e^{-jS_u} \exp[-(\alpha_{\pm} + jk_{\pm})(L - r)],$$

where

$$B_u = \frac{U(t) - \overline{U(t)}}{\overline{U(t)}} \quad \text{is the amplitude fluctuation,}$$

$$S_u = \phi_u(t) - k_{\pm} r \quad \text{is the phase fluctuation, and}$$

$U(t)$ and $\phi_u(t)$ are the amplitude and phase of the particle velocity, respectively.

The total particle velocity at $(L,0)$ is the sum of contributions from all sources in the interaction region, i.e.,

$$U_{\pm}(L,0) = (2L)^{-1} \exp[-(\alpha_{\pm} + jk_{\pm})L] \int_0^L (1 + B_u) \times e^{-jS_u} q(r) r \exp[(\alpha_{\pm} + jk_{\pm})r] dr. \quad (4.24)$$

The second-order pressure at the point $(L,0)$ can now be found by using the far-field relation, $p = \rho_0 c u$, in connection with Eq. (4.24). The result is

$$p_{\pm}(L,0) = \frac{-\beta P_s P' \omega_{\pm}}{2 \rho_0 c_0^3 L} \exp[-(\alpha_{\pm} + jk_{\pm})L] \times \int_0^L (1 + B_s)(1 + B_p)(1 + B_{\pm}) e^{-j(S_p \pm S_s + S_{\pm})} \times \exp[-(\alpha_s + \alpha_p - \alpha_{\pm})r] dr, \quad (4.25)$$

where B_{\pm} and S_{\pm} are amplitude and phase fluctuations, respectively, for the interaction frequency pressure wave.*

*It may be shown that the amplitude fluctuations in the pressure and particle velocity are equal: i.e., $B_u = B_{\pm}$. Similarly, $S_u = S_{\pm}$.

For small fluctuations this result becomes

$$p_{\pm}(L,0) \approx A_s \int_0^L (1+B)(1-jS)dr, \quad (4.26)$$

where

$$A_s = \frac{-\beta P_s P' \omega_{\pm}}{2 \rho_o c_o^3 L} e^{-(\alpha_{\pm} + jk_{\pm})L}$$

$$B = B_s + B_p + B_{\pm}, \text{ and}$$

$$S = S_s \pm S_p + S_{\pm}.$$

In obtaining Eq.(4.26), the attenuation terms have been approximated by Eq.(4.11).

As in the case of the nearfield parametric receiver, the second-order pressure can be written in terms of a homogeneous and fluctuating component,

$$p_{\pm} = p_H(1 + B_{PR}) e^{-jS_{PR}}, \quad (4.27)$$

where

$$p_H = A_s \int_0^L dr = A_s L.$$

Eqs.(4.26) and (4.27) may be equated, and if the fluctuations are small compared to unity, we obtain

$$p_H(1 + B_{PR} - jS_{PR}) = A_s \int_0^L (1+B-jS)dr. \quad (4.28)$$

The homogeneous component is subtracted from both sides of Eq.(4.28), and the real and imaginary components of the result are equated to give

$$B_{PR} = \frac{1}{L} \int_0^L B dr, \text{ and}$$

$$S_{PR} = \frac{1}{L} \int_0^L S dr.$$

The mean-squared amplitude fluctuations, $\langle B_{PR}^2 \rangle$, for the farfield receiver are therefore

$$\langle B_{PR}^2 \rangle = \frac{1}{L^2} \int_0^L \int_0^L \langle B_1 B_2 \rangle dr_1 dr_2. \quad (4.29)$$

This result differs from the solution for the nearfield receiver

[Eq.(4.22)] only in that $\langle B_1 B_2 \rangle$ here is the correlation function for

spherically spreading waves rather than plane waves. In form the solutions are identical.

In the next section we will examine the components of the correlation term, $\langle B_1 B_2 \rangle$, in Eqs.(4.22) and (4.29) so that these results may be evaluated.

4.4 Approximating the Spatial Correlation Functions

The evaluation of Eqs.(4.22) and (4.29) requires the calculation of nine correlation terms; viz.,

$$\begin{aligned}
 \langle B_1 B_2 \rangle &= \langle [B_s(z_1) + B_p(z_1) + B_{\pm}(L - z_1)][B_s(z_2) + B_p(z_2) + B_{\pm}(L - z_2)] \rangle \\
 &= \langle B_s(z_1) B_s(z_2) \rangle + \langle B_s(z_1) B_p(z_2) \rangle + \langle B_s(z_1) B_{\pm}(L - z_2) \rangle \\
 &+ \langle B_p(z_1) B_s(z_2) \rangle + \langle B_p(z_1) B_p(z_2) \rangle + \langle B_p(z_1) B_{\pm}(L - z_2) \rangle \\
 &+ \langle B_{\pm}(L - z_1) B_s(z_2) \rangle + \langle B_{\pm}(L - z_1) B_p(z_2) \rangle \\
 &+ \langle B_{\pm}(L - z_1) B_{\pm}(L - z_2) \rangle.
 \end{aligned} \tag{4.30}$$

These correlation terms fall into three categories: (1) cross correlation between the low frequency signal fluctuations and fluctuations in the pump or interaction frequency waves; (2) cross correlation between pump fluctuations and interaction frequency fluctuations; and (3) autocorrelation of the pump, low frequency, and interaction frequency amplitude fluctuations. These categories are discussed separately below.

(1) The signal wave and pump wave traverse different parts of the medium, which implies that the volume of scatterers associated with these waves will be significantly different. Also, it has been assumed that $\omega_p \gg \omega_s$, which implies that there will be little frequency correlation between signal and pump wave. For these reasons it may be assumed that the signal and pump amplitude fluctuations will be uncorrelated in the interaction region; i.e.,

$$\langle B_s(z_1)B_p(z_2) \rangle \doteq \langle B_p(z_1)B_s(z_2) \rangle \doteq 0. \quad (4.31)$$

A similar argument can be applied to the signal and interaction frequency fluctuations, so that

$$\langle B_s(z_1)B_{\pm}(L - z_2) \rangle \doteq \langle B_{\pm}(L - z_1)B_s(z_2) \rangle \doteq 0. \quad (4.32)$$

(2) The term $\langle B_p(z_1)B_{\pm}(L - z_2) \rangle$ represents cross correlation between pump pressure amplitude fluctuations at the point (z_1) and interaction frequency amplitude fluctuations at $(L - z_2)$. The frequencies of the two waves are approximately equal ($\omega_p \doteq \omega_{\pm}$) so we may assume that complete frequency correlation exists between B_p and B_{\pm} .

The propagation paths associated with the pump and interaction frequency waves are shown in Fig. 4.4. The term $B_p(z_1)$ is due to scattering of the pump wave as it propagates from the origin to $z = z_1$. The fluctuations in the interaction frequency wave, $B_{\pm}(L - z_2)$, are due to scattering of the second-order radiation as it propagates from a source at point z_2 to the hydrophone at $z = L$. Both z_1 and z_2 may vary between 0 and L, so there will be situations in which the two propagation paths overlap ($z_1 > z_2$) and situations in which they are separate ($z_1 < z_2$).

An exact evaluation of Eqs. (4.22) and (4.29) would require an expression for the correlation term, $\langle B_p B_{\pm} \rangle$, for all values of z_1 and z_2 , and for both nearfield and farfield receiving arrays. This is essentially a problem of calculating the correlation of amplitude fluctuations at two receivers when there are two sources generating separate waves. The solution to this problem is not available in the literature, nor is it readily obtained, so we will resort to the following simplified approximation.

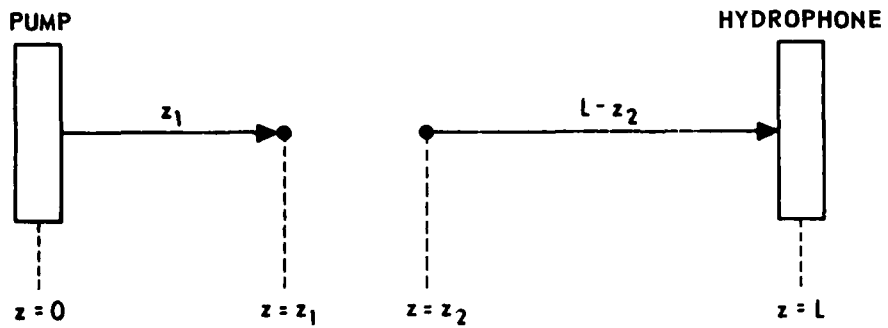


FIGURE 4.4
PROPAGATION PATHS OF PUMP AND SECOND-ORDER WAVE

We will consider two conditions, one in which the array length L is much less than the longitudinal correlation distance l_p , and the other in which the array length is much greater than the pump correlation distance. First assume that $L \ll l_p$. In this case the separation between the 'receivers' at z and L is less than the pump correlation distance; i.e.,

$$L - z_1 \ll l_p, \quad (4.33)$$

where l_p is the distance at which the correlation coefficient for the pump wave amplitude fluctuations equals $1/e$. When Eq.(4.33) applies, the amplitude fluctuations of the pump wave at z_1 and the interaction frequency wave at $z \leq L$ will be highly correlated. We approximate their correlation coefficient by unity; i.e.,

$$R_{p,\pm} = \frac{\langle B_p(z_1)B_{\pm}(L - z_2) \rangle}{[\langle B_p^2(z_1) \rangle \langle B_{\pm}^2(L - z_2) \rangle]^{1/2}} \doteq 1, \quad L \ll l_p.$$

From this expression the cross correlation between pump and interaction frequency fluctuations can be written as

$$\langle B_p(z_1)B_{\pm}(L - z_2) \rangle \doteq [\langle B_p^2(z_1) \rangle \langle B_{\pm}^2(L - z_2) \rangle]^{1/2}. \quad (4.34)$$

This equation is in terms of mean-squared amplitude fluctuations, and can be calculated using the results discussed in Chapter 3. A similar approximation can be made for the remaining cross correlation term in Eq.(4.30), namely

$$\begin{aligned} \langle B_p(z_2)B_{\pm}(L - z_1) \rangle &\doteq \left[\langle B_p^2(z_2)B_{\pm}^2(L - z_1) \rangle \right]^{1/2} R_{p,\pm}, \\ &\doteq [\langle B_p^2(z_2) \rangle \langle B_{\pm}^2(L - z_1) \rangle]^{1/2}. \end{aligned} \quad (4.35)$$

Again we note that Eqs.(4.34) and (4.35) apply only for short array lengths ($L \ll l_p$). In general, if the array length is not sufficiently short that $L \ll l_p$, then $R_{p,\pm}$ is less than unity, and we have the less restrictive approximations

$$\langle B_p(z_2)B_{\pm}(L - z_1) \rangle \doteq [\langle B_p^2(z_2) \rangle \langle B_p^2(L - z_1) \rangle]^{1/2} R_{p,\pm}, \quad (4.36)$$

and

$$\langle B_p(z_1)B_{\pm}(L - z_2) \rangle \doteq [\langle B_p^2(z_1) \rangle \langle B_p^2(L - z_2) \rangle]^{1/2} R_{p,\pm}. \quad (4.37)$$

Now consider the situation when the array length is much greater than the pump longitudinal correlation distance ($L \gg l_p$). Most separations, $L - z_1$, will be greater than the correlation distance l_p , and therefore the fluctuations will (on the average) have very little correlation. For $L \gg l_p$ we therefore approximate the correlation coefficient by zero and obtain

$$\langle B_p(z_1)B_{\pm}(L - z_2) \rangle \doteq 0, \quad (4.38)$$

and

$$\langle B_p(z_2)B_{\pm}(L - z_1) \rangle \doteq 0, \quad L \gg l_p. \quad (4.39)$$

These results are used in Eq.(4.30) for long array lengths.

(3) The third category of correlation terms in Eq.(4.30) are autocorrelation functions for the signal, pump, and interaction frequency fluctuations.

The pump autocorrelation function will be given by

$$\langle B_p(z_1)B_p(z_2) \rangle = [\langle B_p^2(z_1) \rangle \langle B_p^2(z_2) \rangle]^{1/2} R_p, \quad (4.40)$$

where R_p is the longitudinal correlation coefficient for pump wave fluctuations at z_1 and z_2 . For short lengths ($L \ll l_p$), R_p can be approximated as unity. For longer array lengths the results of Chernov¹⁸ or Eliseevnin⁹⁴ can be used to estimate R_p .

Similarly, the autocorrelation function for the signal wave will be

$$\langle B_s(Z_s + z_1)B_s(Z_s + z_2) \rangle = [\langle B_s^2(Z_s + z_1) \rangle \langle B_s^2(Z_s + z_2) \rangle]^{1/2} R_s, \quad (4.41)$$

where R_s is the longitudinal correlation coefficient for signal wave fluctuations at z_1 and z_2 . Here again the correlation coefficient can be approximated as unity for short array lengths ($L \ll l_s$; l_s is the signal wave correlation distance). For $L > l_s$, theoretical

results available in the literature^{18,94} can be used to predict R_s .

The autocorrelation function for the interaction frequency wave is somewhat different from that for the pump or signal wave. Rather than originating at a common source point and being received at different observation points, as are the signal and pump waves, the interaction frequency waves originate at different source points and are received at a common observation point. This is sketched in Fig. 4.5. The waves originate at z_1 and z_2 , and are both received at $z = L$. While there is no explicit analysis of this situation in the literature, Chotiros and Smith^{91,97} have demonstrated that the principle of reciprocity applies as follows. If a wave of frequency ω_{\pm} is projected from the transducer at $z = L$, then the correlation of amplitude fluctuations received at points z_1 and z_2 will be $\langle B_r(L - z_1) B_r(L - z_2) \rangle$. By the reciprocity principle, this correlation will be identical to that for waves originating at z_1 and z_2 , and received at $z = L$; i.e.,

$$\langle B_{\pm}(L - z_1) B_{\pm}(L - z_2) \rangle = \langle B_r(L - z_1) B_r(L - z_2) \rangle,$$

where the subscript r indicates that the positions of sources and receivers have been interchanged. This result is useful because it allows us to write

$$\langle B_{\pm}(L - z_1) B_{\pm}(L - z_2) \rangle = \left[\langle B_{\pm}^2(L - z_1) \rangle \langle B_{\pm}^2(L - z_2) \rangle \right]^{\frac{1}{2}} R_r, \quad (4.42)$$

where R_r is the longitudinal correlation coefficient for interaction frequency waves originating at $z = L$ and received at points z_1 and z_2 . When the array length is short ($L \ll l_p$), the correlation coefficient is $R_r \doteq 1$. For longer array lengths, the results of Chernov¹⁸ or Eliseevnin⁹⁴ may be used to calculate R_r . Because complete frequency correlation has been assumed for the pump and interaction frequency waves, the coefficient R_r will be equal to the longitudinal correlation coefficient for a wave at frequency ω_p received at ranges $L - z_1$ and $L - z_2$; i.e.,

$$R_r = R_p(L - z_1, L - z_2).$$

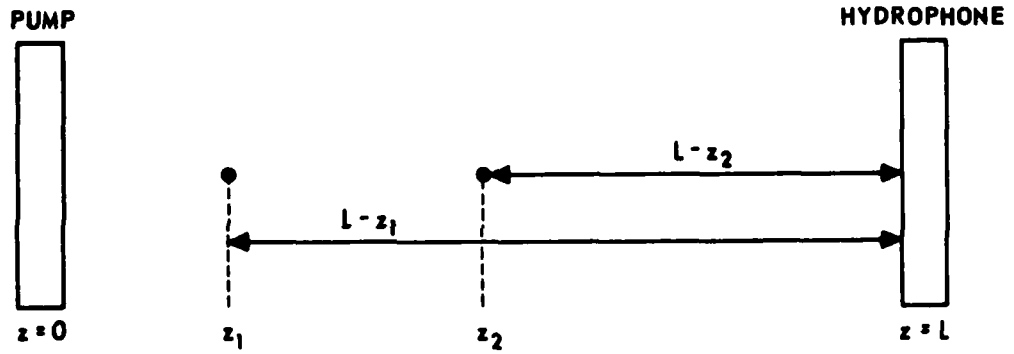


FIGURE 4.5
GEOMETRY FOR AUTOCORRELATION OF
SECOND-ORDER WAVE FLUCTUATIONS

The mean-squared fluctuation terms in Eq. (4.42) are for waves of frequency ω_{\pm} traversing paths of lengths $L - z_1$ and $L - z_2$ and may be calculated using Tatarski's formulae.¹⁹

4.5 Evaluation of Results

In the previous section we examined the nine correlation terms that are required in the evaluation of Eqs. (4.22) and (4.29). Now we will develop expressions for the amplitude fluctuations of the second-order wave for specific types of nearfield and farfield receiving arrays. Before proceeding, we recall that for small fluctuations the rms amplitude fluctuations are approximately equal to the coefficient of amplitude variation. Therefore, it is possible to rewrite Eqs. (4.22) and (4.29) in terms of the coefficient of amplitude variation as follows:

$$\text{CAV}_{\text{PR}}^2 \doteq \frac{1}{L^2} \int_0^L \int_0^L \langle B_1 B_2 \rangle dz_1 dz_2 \quad (4.43)$$

for the nearfield receiving array, and

$$\text{CAV}_{\text{PR}}^2 \doteq \frac{1}{L^2} \int_0^L \int_0^L \langle B_1 B_2 \rangle dr_1 dr_2 \quad (4.44)$$

for the farfield receiving array, where CAV_{PR} is the coefficient of amplitude variation for a parametric receiver.

4.5.1 Nearfield Receiving Array

The coefficient of amplitude variation for the nearfield receiver can be evaluated by substituting Eq. (4.30) for $\langle B_1 B_2 \rangle$ in Eq. (4.43), and then making the approximations given in Eqs. (4.31), (4.32), (4.36), (4.37), and (4.40) - (4.42). The result is

$$\begin{aligned} \text{CAV}_{\text{PR}}^2 \doteq & \int_0^L \int_0^L \left\{ \left[\langle B_p^2(z_1) \rangle \langle B_{\pm}^2(L - z_2) \rangle \right]^{\frac{1}{2}} R_p + \left[\langle B_p^2(z_2) \rangle \langle B_{\pm}^2(L - z_1) \rangle \right]^{\frac{1}{2}} R_p \right. \\ & + \left[\langle B_p^2(z_1) \rangle \langle B_p^2(z_2) \rangle \right]^{\frac{1}{2}} R_p + \left[\langle B_s^2(z_s + z_1) \rangle \langle B_s^2(z_s + z_2) \rangle \right]^{\frac{1}{2}} R_s \\ & \left. + \left[\langle B_{\pm}^2(L - z_1) \rangle \langle B_{\pm}^2(L - z_2) \rangle \right]^{\frac{1}{2}} R_{\pm} \right\} dz_1 dz_2 \quad (4.45) \end{aligned}$$

where, due to the high frequency correlation of the pump and interaction frequency waves, we have assumed that $R_{p,\pm} \doteq R_p$.

An example of the evaluation of Eq. (4.45) will now be given for the restricted condition that the array length is much less than either correlation length l_p or l_s ($L \ll l_s$ and $L \ll l_p$). For this case R_p and R_s are approximated by unity. If the pump and interaction frequency waves are planar, and if

$$L_o \gg \sqrt{\lambda_p} L \gg l_o \quad ,$$

then the amplitude fluctuations will be of the form

$$\langle B_p^j \rangle = 0.31 C_n^2 k_p^{7/6} z^{11/6} \quad , \quad (4.46)$$

and

$$\langle B_{\pm}^2 \rangle = 0.31 C_n^2 k_{\pm}^{7/6} (L - z)^{11/6} \quad . \quad (4.47)$$

We further stipulate that, for purposes of illustration, the signal source propagates a distance $Z_s + z$ that obeys the relation

$$L_o \gg \sqrt{\lambda_s (Z_s + z)} \gg l_o \quad ,$$

where L_o and l_o are outer and inner scales of turbulence, respectively.

Then the signal wave amplitude fluctuation will be of the form

$$\langle B_s^2 \rangle = 0.13 C_n^2 k_s^{7/6} (Z_s + z)^{11/6} + \frac{\pi}{480} \phi_m (Z_s + z)^3 (\kappa_t^4 - \kappa_m^4) \quad . \quad (4.48)$$

It may be noted that Eq. (4.48) is for a spherical wave. This is because the low frequency signal wave will propagate as a spherical wave, although it is assumed to be sufficiently far from the parametric receiver that the wavefront curvature and spreading loss are negligible in the interaction region. Making use of Eqs. (4.46)-(4.48) and assuming that $k_p \doteq k_{\pm}$, we write Eq. (4.45) as

$$\begin{aligned}
C_{PR}^2 &\doteq \frac{1}{L^2} \int_0^L \int_0^L \left\{ 0.31 C_n^2 k_p^{7/6} \left[z_1^{11/12} (L - z_2)^{11/12} + z_2^{11/12} (L - z_1)^{11/12} \right. \right. \\
&+ z_1^{11/12} z_2^{11/12} + (L - z_1)^{11/12} (L - z_2)^{11/12} \left. \right\} \\
&+ \left[0.13 C_n^2 k_s^{7/6} (z_s + z_1)^{11/6} + \frac{\pi}{480} \phi_m (z_s + z_1)^3 (\kappa_t^4 - \kappa_m^4) \right]^{1/2} \\
&\times \left[0.13 C_n^2 k_s^{7/6} (z_s + z_2)^{11/6} + \frac{\pi}{480} \phi_m (z_s + z_2)^3 (\kappa_t^4 - \kappa_m^4) \right]^{1/2} dz_1 dz_2.
\end{aligned}$$

This expression appears somewhat unwieldy, but the integration is straightforward and gives

$$CAV_{PR}^2 \doteq 0.3375 C_n^2 k_p^{7/6} L^{11/6} + \frac{1}{L^2} \frac{4}{9b^2} \left[(a + bL)^{3/2} - a^{3/2} \right]^2, \quad (4.49)$$

where

$$\begin{aligned}
a &= 0.13 C_n^2 k_s^{7/6} z_s^{11/6} + \frac{3\pi}{480} \phi_m (\kappa_t^4 - \kappa_m^4) z_s^3, \text{ and} \\
b &= \frac{11}{6} (0.13 C_n^2 k_s^{7/6}) z_s^{5/6} + \frac{3\pi}{480} \phi_m (\kappa_t^4 - \kappa_m^4) z_s^2.
\end{aligned}$$

This result will be useful in Chapter 5, where we will compare Eq. (4.49) to data from an experiment that approximates the conditions assumed in deriving this equation.

4.5.2 Farfield Receiving Array

An expression similar to Eq. (4.45) can be derived for the farfield receiving array by substituting Eq. (4.30) for $\langle B_1 B_2 \rangle$ in Eq. (4.44), and then making the approximations given in Eqs. (4.31), (4.32), (4.38), (4.39), and (4.40) - (4.42). The coefficient of amplitude variation obtained is

$$\begin{aligned}
\text{CAV}_{\text{PR}}^2 &= \frac{1}{L^2} \int_0^L \int_0^L \left\{ \left[\langle B_s^2(z_s + z_1) \rangle \langle B_s^2(z_s + z_2) \rangle \right]^{1/2} R_s \right. \\
&\quad + \left[\langle B_p^2(z_1) \rangle \langle B_p^2(z_2) \rangle \right]^{1/2} R_p + \left[\langle B_p^2(z_1) \rangle \langle B_{\pm}^2(L - z_2) \rangle \right]^{1/2} R_{p,\pm} \\
&\quad + \left. \left[\langle B_{\pm}^2(L - z_1) \rangle \langle B_p^2(z_2) \rangle \right]^{1/2} R_{p,\pm} + \left[\langle B_{\pm}^2(L - z_1) \rangle \langle B_{\pm}^2(L - z_2) \rangle \right]^{1/2} R_p \right\} dz_1 dz_2,
\end{aligned}
\tag{4.50}$$

where $dz = dr$ on the axis of the array. We will examine the restricted case where the pump and interaction frequency fluctuations are completely correlated in the interaction region so that $R_p \doteq R_{p,\pm} \doteq 1$; we assume that the range of the signal source is much greater than the array length so the $Z_s \gg z_1$ and $Z_s \gg z_2$. This allows us to make the approximation

$$\langle B_s^2(z_s + z) \rangle \doteq \langle B_s^2(Z_s) \rangle, \quad z \ll Z_s.$$

In computing the pump and interaction frequency fluctuations, it is assumed that

$$L_o \gg \sqrt{\lambda_p L} \gg l_o,$$

so that the amplitude fluctuations are of the form

$$\begin{aligned}
\langle B_p^2(z) \rangle &= 0.13 C_n^2 k_p^{7/6} z^{11/6}, \text{ and} \\
\langle B_{\pm}^2(L - z) \rangle &= 0.13 C_n^2 k_{\pm}^{7/6} (L - z)^{11/6}.
\end{aligned}$$

The signal source is assumed to be at a sufficiently long range that

$$\sqrt{\lambda_s Z_s} \gg L_o,$$

so that the signal wave amplitude fluctuations are given by

$$\langle B_s^2(z_s) \rangle = \frac{\sqrt{\pi}}{2} \langle \mu^2 \rangle k_s^2 z_s a,$$

where a is Medwin's⁷⁰ effective Gaussian refractive index correlation distance.

Finally, we approximate the correlation coefficient, R_s , by Chernov's result⁹²

$$R_s = \left[1 + \left(\frac{2\Delta L}{ka^2} \right)^2 \right]^{-1},$$

where ΔL is the separation between receivers.

With these approximations the coefficient of amplitude variation becomes

$$\begin{aligned} \text{CAV}_{\text{PR}}^2 &\doteq \frac{\sqrt{\pi}}{2} \langle \mu^2 \rangle k_s^2 a z_s L^{-2} \int_0^L \int_0^L \left\{ 1 + \left[\frac{2(z_2 - z_1)}{k_s a^2} \right]^2 \right\}^{-1} dz_1 dz_2 \\ &+ 0.1415 C_n^2 k_p^{7/6} L^{11/6}. \end{aligned}$$

By making the change of coordinates, $z = z_2 - z_1$, and integrating, we obtain

$$\text{CAV}_{\text{PR}}^2 \doteq \frac{\sqrt{\pi}}{2L} k_s^3 a^3 \langle \mu^2 \rangle z_s \tan^{-1} \left(\frac{2L}{k_s a^2} \right) + 0.1415 C_n^2 k_p^{7/6} L^{11/6}. \quad (4.51)$$

As a numerical example, consider a parametric receiver with pump frequency $f_p = 100$ kHz used to detect a distant signal source in the ocean. For the medium parameters, we will use the values $\langle \mu^2 \rangle = 5 \times 10^{-9}$, as measured by Lieberman⁶⁹, and $a = 0.25$ m and $C_n = 9.30 \times 10^{-5}$ as computed by Medwin's methods⁷⁰. A plot of CAV_{PR} as a function of array length is shown in Fig. 4.6. It can be seen from the figure that there is little difference in the value of CAV_{PR} for the 1 kHz signal when the range, z_s , is extended from 10 km to 100 km. Also, at the longer array lengths ($L > 50$ m), there is little difference in CAV_{PR} when the signal frequency is increased from 1 kHz to 5 kHz, with $z_s = 10$ km. These results indicate that CAV_{PR} is independent of f_s and z_s at the longer array lengths, at least for the

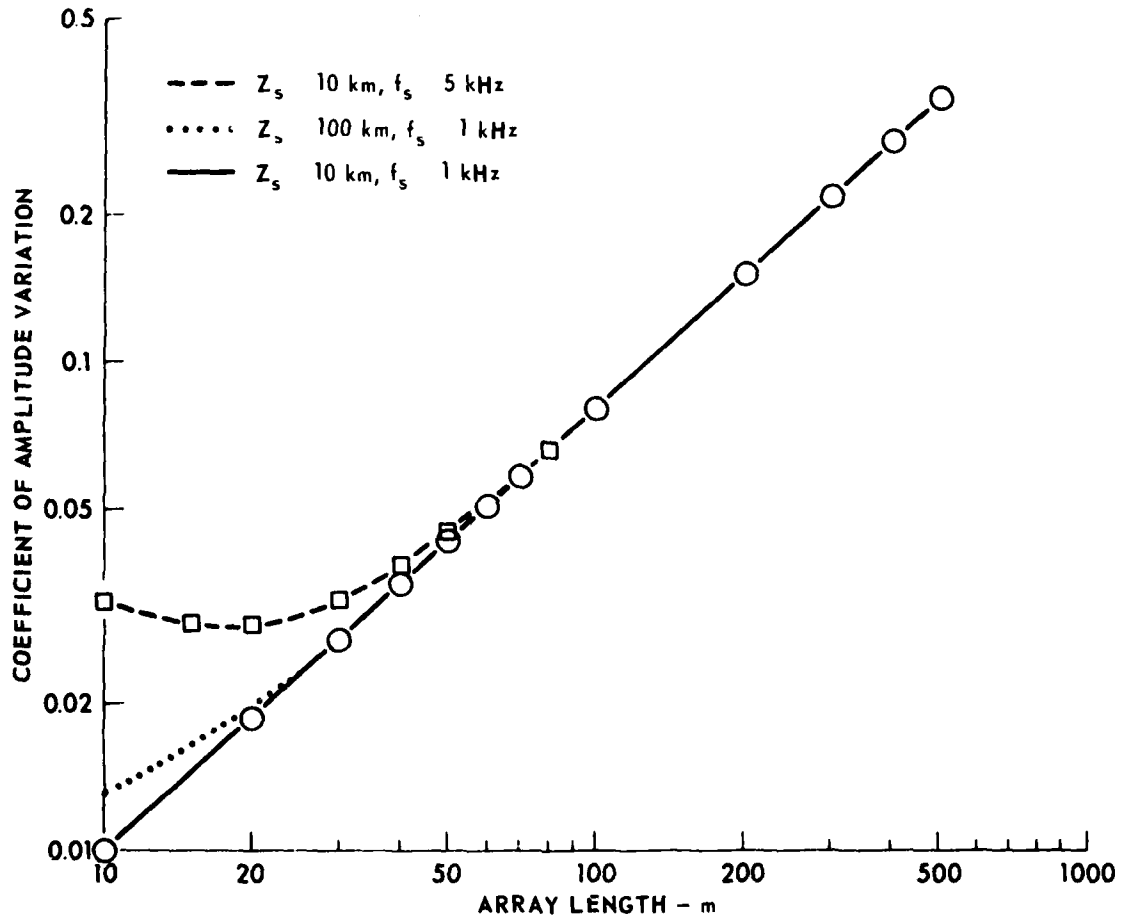


FIGURE 4.6
CAV FOR FARFIELD PARAMETRIC RECEIVER OPERATING IN THE OCEAN

values considered in this example. It can be seen from Fig. 4.6 that CAV_{PR} is greater than 0.1 only at array lengths longer than about 200 m. This means that an rms variation in amplitude of approximately 10% is expected for the sideband signals of a 200 m long parametric receiver operating in the ocean. This is greater than the level of amplitude fluctuations for a 1 kHz signal received by a point hydrophone, which would have, ignoring the effects of multipath signals, rms amplitude variations of approximately 1.4% at $Z_s = 10$ km and 4.4% at $Z_s = 100$ km.

4.6 Summary and Discussion

In the preceding sections an analysis has been developed for the parametric receiver operating in an inhomogeneous medium. The principal assumptions used in the analysis are: (1) the signal source is located on the main beam of the parametric receiver, (2) there is complete transverse correlation of amplitude and phase fluctuations in the interaction region of the parametric receiver, and (3) the amplitude and phase fluctuations are small compared to unity (i.e., the medium is weakly scattering). With these assumptions we were able to derive integral expressions for the coefficient of amplitude variation for the nearfield receiver [Eq. (4.22)] and the farfield receiver [Eq. (4.29)]. By making a number of assumptions regarding the spatial correlation functions contained in these expressions, it was possible to obtain results in terms of the parameters of the medium in which the parametric receiver operates. In this section we will discuss the results of the analysis from a qualitative viewpoint.

For purposes of discussion, the coefficient of amplitude variation for both nearfield and farfield receivers can be written in the following form

AD-A094 897

TEXAS UNIV AT AUSTIN APPLIED RESEARCH LABS

F/G 17/1

THE PERFORMANCE OF A PARAMETRIC RECEIVER IN AN INHOMOGENEOUS ME--ETC(U)

AUG 80 C R CULBERTSON

N00024-79-C-6358

UNCLASSIFIED

ARL-TR-80-44

NL

2 of 2
AD
ADM 997

END

DATE

FILMED

3-11

DTIC

$$CAV_{PR}^2 = \frac{1}{L^2} \int_0^L \int_0^L (\langle B_1 B_2 \rangle_H + \langle B_1 B_2 \rangle_S) dz_1 dz_2, \quad (4.52)$$

where $\langle B_1 B_2 \rangle_H = \langle B_p(z_1) B_p(z_2) \rangle + \langle B_p(z_1) B_{\pm}(L - z_2) \rangle$

$$+ \langle B_{\pm}(L - z_1) B_p(z_2) \rangle + \langle B_{\pm}(L - z_1) B_{\pm}(L - z_2) \rangle, \text{ and}$$

$$\langle B_1 B_2 \rangle_S = \langle B_s(z_1) B_s(z_2) \rangle.$$

Here the correlation functions have been divided into high frequency components, $\langle B_1 B_2 \rangle_H$, that are due to scattering in the interaction region of the parametric receiver, and signal frequency components, $\langle B_1 B_2 \rangle_S$, that are due to scattering of the signal wave.

The high frequency components increase with f_p and L , and the signal frequency component increases with f_s and Z_s . For sufficiently long ranges and short array lengths, the high frequency components, $\langle B_1 B_2 \rangle_H$, will be negligible compared to $\langle B_1 B_2 \rangle_S$, and the coefficient of variation becomes

$$CAV_{PR}^2 \doteq \frac{1}{L^2} \int_0^L \int_0^L \langle B_s(z_1) B_s(z_2) \rangle dz_1 dz_2. \quad (4.53)$$

It can be shown that Eq. (4.53) is also the coefficient of variation for a continuous end-fire array of length L . Thus it can be concluded that, in an inhomogeneous medium the parametric receiver performs like an end-fire array if the correlation terms due to pump and second-order waves are negligible. It can also be shown that, if the array length is very short, then the coefficient of variation becomes identical to that for a point hydrophone; viz.,

$$\text{CAV}_{\text{PR}}^2 \doteq \langle B_s^2 \rangle \quad (L \neq 0).$$

In a practical example, such as the one discussed in Section 4.5.2, the high frequency components, $\langle B_1 B_2 \rangle_H$, may not be negligible, and may even dominate the value of CAV_{PR} . In this case the parametric receiver will not perform as well as a continuous end-fire array, inasmuch as the parametric receiver will have a higher coefficient of amplitude variation.

Having developed a theory for predicting the performance of a parametric receiving array in an inhomogeneous medium, we will discuss in the next chapter some experiments that were conducted to test the theory.

Several experimental studies^{67,84,91,98-101} of the effects of medium inhomogeneities on acoustic wave propagation have been conducted using modelled acoustic and thermal conditions. An advantage of model experiments (i.e., experiments at small acoustic wavelengths) is that the properties of the acoustic medium can be carefully controlled. It is possible in a model experiment to minimize the effects of time-varying surface reflections and transducer movement, which produce fluctuations in an acoustic wave that are extraneous to the study. Also, the characteristics of the medium in a model tank may be assumed to be essentially constant from day to day, so that different experiments can be conducted under similar conditions.

In the present investigation, model experiments were conducted to measure the effect of medium inhomogeneities on parametric reception. The investigation will be described in this chapter as follows. First, a description is given of the experimental medium and of the apparatus used. Measurements made of the coefficient of amplitude variation for the signal, pump, and upper sideband waves of a model parametric acoustic receiving array are then discussed. These measurements are compared to theoretical predictions using the analysis developed in Chapter 4. Finally, the experimental results are summarized and discussed.

5.1 The Experimental Medium

A water tank with a width of 0.9 m, length of 1.8 m, and a depth of 0.8 m was used in this experimental study. The thermal microstructure was generated by an array of immersion heaters located along the bottom of the tank (see Fig. 5.1), the total heating power of the array being 4.5 kW. The flow of rising heated water was broken up into patches by a perforated aluminium sheet mounted about 5 cm above the heated array.

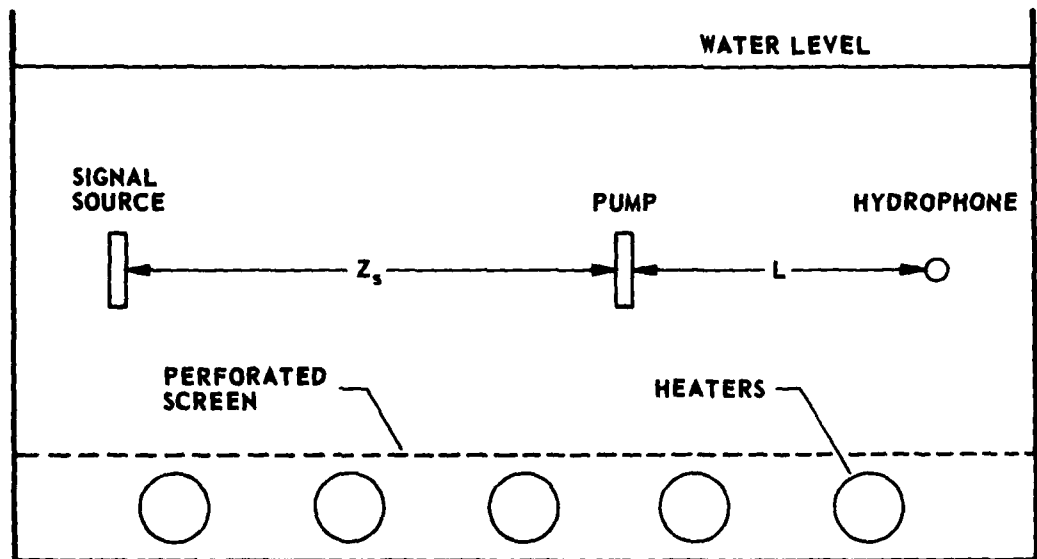


FIGURE 5.1
MODEL TANK

The model tank just described has been used as a research tool for a number of years, and the characteristics of its thermal microstructure are well documented.^{84,95} During the course of this study, measurements of the rate of temperature increase and the standard deviation of temperature were made to insure that the tank was operating as in previous studies. The rate of temperature increase was measured using a mercury thermometer suspended in the water at mid-depth. The result, $1.1 \times 10^{-3} \text{ }^\circ\text{Cs}^{-1}$, agrees to within 10% of the results of Smith and Weston-Bartholomew⁹⁵ and Chotiros and Smith.⁸⁴ A measurement of temperature variations was made using a thermistor placed in the center of the tank. Measurements were begun 1 hour after turning on the tank heaters. This permitted thorough mixing of the water so that the thermal activity would be uniform throughout the tank. The standard deviation of temperature computed from nine such measurements is $0.023 \text{ }^\circ\text{C}$, which is less than the value, $0.032 \text{ }^\circ\text{C}$, measured by Chotiros and Smith,⁸⁴ but is of the same order of magnitude. The results of these measurements of heating rate and standard deviation of temperature allow us to conclude that the tank is operating essentially as reported previously. Consequently, we will adopt the methods developed by Chotiros and Smith^{91,84} for describing the field of inhomogeneities in the tank.

As discussed in Chapter 3, an inhomogeneous medium can be described by a turbulent power density spectrum. The magnitude of the spectrum, ϕ_m , is a function of the mean-squared refractive index change, $\langle \mu^2 \rangle$. Each of these parameters depends upon the standard deviation of the temperature, and hence will be calculated from the measurements of temperature variations made in this study. The boundary wavenumbers, κ_m , κ_p , and κ_p , depend upon the physical dimensions of the tank, the diffusivity, and the rate of kinetic energy dissipation per unit mass. We will assume that these parameters are unchanged since the investigation of Chotiros and Smith,⁸⁴ and will use their values of κ_m , κ_t , and κ_p .

A list of parameters used to describe the inhomogeneous medium in the model tank is given in Table 5.1. These parameters varied with position throughout the tank; their values at the center of the tank are shown in the table. These values will be used as discussed below in making theoretical predictions for the acoustic waves propagating in the tank.

5.2 Description of Apparatus

A model parametric receiver was constructed by placing a pump transducer and a hydrophone at mid-depth in the tank, as shown in Fig. 5.1. The array length was varied by changing the separation, L , between the two transducers. A source of acoustic signals to be detected with the parametric receiver was located on the main axis of the parametric receiver, and at a distance, Z_s , from the pump transducer.

The apparatus used to generate and receive the acoustic waves for this study is shown in the block diagram of Fig. 5.2. To minimize the problems of electronic feedover and acoustic multipaths, both the signal and pump waves were pulsed, the pulses being typically 100 μ sec in duration. There was a time delay, τ_d , in the generation of the pump frequency wave; this was to synchronize the pulses so that they occur simultaneously in the interaction region of the array. The pump and signal frequencies were maintained at 10 MHz and 1 MHz, respectively, throughout the experimental study. Details of the transducers used to generate the signal and pump waves are given in Appendix 3.

The pressure detected by the hydrophone was separated into three components (f_u , f_p , and f_s) by the arrangement of filters and tuned amplifiers shown in Fig. 5.2. A signal processing unit sampled a 10 μ sec segment of each pulse and detected the peak value of this segment. The amplitude of each sampled pulse was then recorded by a data logging unit for later off-line computer processing. Further details of the receiving apparatus may be found in Appendix 4.

| Parameter | Value and Units at 30° C |
|-------------------------------|---|
| $\langle \mu^2 \rangle^{1/2}$ | 3.54×10^{-5} (dimensionless) |
| ϕ_m | 2.80×10^{-12} m |
| C_n | 1.96×10^{-4} m ^{-2/3} |
| κ_m * | 22.9 m ⁻¹ |
| κ_t * | 179 m ⁻¹ |
| κ_p * | 5600 m ⁻¹ |

*From reference 91

$$\langle \mu^2 \rangle^{1/2} = \frac{1}{c} \frac{\partial c}{\partial T} \langle (\Delta T)^2 \rangle^{1/2}$$

$$\phi_m = \frac{\langle \mu^2 \rangle}{(5/2)\kappa_t}$$

$$C_n^2 = \frac{\langle \mu^2 \rangle}{(0.33\pi) \kappa_t^{-2/3}}$$

TABLE 5.1

PARAMETERS DESCRIBING THE INHOMOGENEOUS MEDIUM

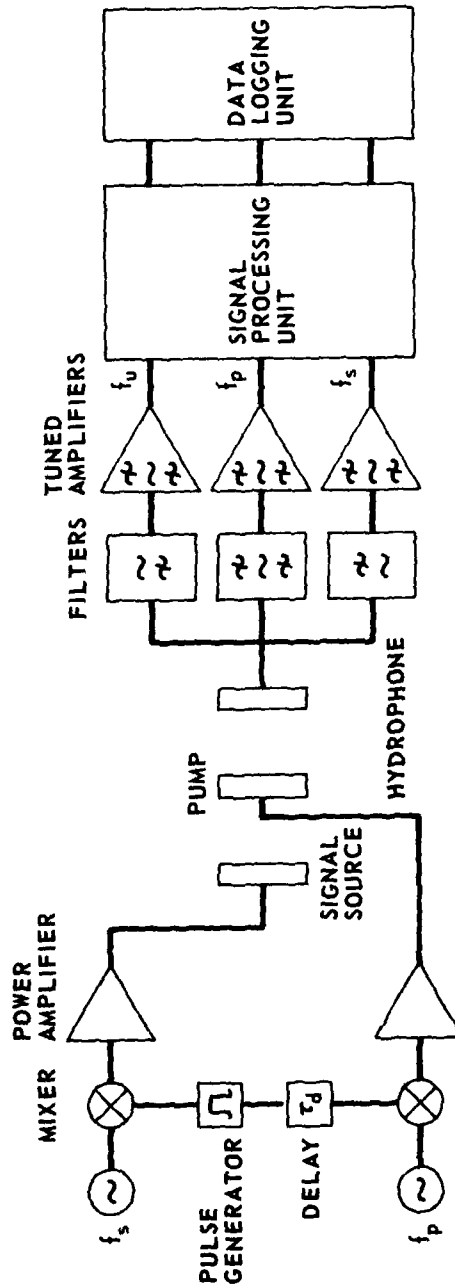


FIGURE 5.2
EXPERIMENTAL APPARATUS

5.3 Experimental Results

In this section we will discuss some experiments conducted in the model tank using the apparatus just described. Since we are particularly interested in the behavior of the upper sideband component, p_u , of the second-order pressure field, we will first measure the amplitude of p_u in a homogeneous medium to verify that it is being generated as predicted by theory. Then we will examine the amplitude fluctuations in the pump, signal, and upper sideband waves for a variety of experimental conditions and compare the results to theoretical predictions based on the analysis of Chapter 4.

5.3.1 Measurements of Upper Sideband Pressure

Aside from nonlinear acoustic interaction, there are four ways in which voltages at the upper sideband frequency may appear at the input of the signal processor. When two pressure waves are incident on the face of the hydrophone, mechanical mixing occurs and an upper sideband voltage is generated by the hydrophone. (This extraneous signal is called pseudosound.) Also, the pressure waves may be received by the hydrophone and then mixed in the electronic receiving apparatus. Another possibility is that the two signals may be transmitted electromagnetically and then mixed in the electronic receiving system. Finally, a harmonic of the signal source may be radiated which is at the upper sideband frequency.

Tests were conducted to ensure that the 11 MHz signal detected by the hydrophone was being generated by acoustic nonlinear interaction. The signal disappeared when either the signal or pump transducer was blocked off, indicating that it was not produced by electromagnetic pickup or by harmonic radiation of the signal source.

A measurement of mixing in the electronic receiver was conducted using the arrangement shown in Fig. 5.3. With oscillator 2 set to zero output voltage, oscillator 1 was adjusted to provide a voltage V_{in} that was of the order of the hydrophone output voltage when receiving the pump wave directly.

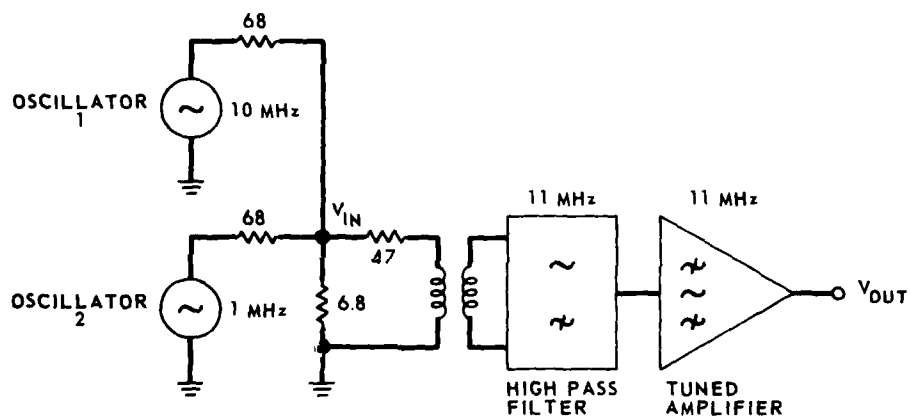


FIGURE 5.3
ARRANGEMENT FOR MEASURING MIXING
IN THE ELECTRONIC RECEIVER

Similarly, oscillator 2 was adjusted to simulate the hydrophone output when receiving the 1 MHz signal. The 68 Ω resistors served to decouple the oscillators. With both oscillators on, the upper sideband voltage, V_{out} , was more than 50 dB below the level observed when the input voltages were generated acoustically. This test confirmed that the upper sideband signal detected by the hydrophone was not produced by mixing in the electronic receiver.

The interaction frequency pressure component of pseudosound produced by two collinear plane waves incident at the hydrophone surface has a pressure amplitude, P' , given by¹⁰²

$$P' = P_1 P_2 / \rho_o c_o^2, \quad (5.1)$$

where P_1 and P_2 are the pressure amplitudes of the two waves. As the upper sideband pressure amplitude measured in the present experiments was four orders of magnitude greater than the level predicted by Eq. (5.1), it was demonstrated that the contribution of pseudosound was negligible in these experiments.

The tests and measurements described in the previous three paragraphs assure us that the upper sideband pressure wave measured in this study was generated by nonlinear interaction of the pump and signal waves, and not by extraneous effects. Next we will discuss the amplitude of this wave. The on-axis pressure amplitude of the interaction frequency wave of a nearfield parametric receiver is given by Eq. (2.17), and is

$$P_N = \frac{\omega_{\pm} P_p P_s \beta L}{2 \rho_o c_o^3} \exp(-\alpha_{\pm} L) \quad (5.2)$$

This expression predicts a pressure amplitude of $P_u \doteq 1.0 \times 10^4$ Pa at the hydrophone of the parametric receiver for the following conditions:

$f_u = 11$ MHz, $P_p = 7.01 \times 10^4$ Pa, $P_s = 3.85 \times 10^4$ Pa, and $L = 0.5$ m. This

result, however, does not take into account the shadowing effect of the pump transducer, which may be expected to reduce the effective array length by an amount^{47,51}

$$d \doteq \frac{1.25b^2}{\lambda_s}$$

where b is the radius of the pump transducer housing. Also, the presence of the pump transducer was observed to reduce the pressure of the 1 MHz signal wave at the hydrophone by 3.3 dB, to $P_s = 2.63 \times 10^4$ Pa. Taking these effects of shadowing into account, and using a measured value of attenuation of $\alpha_{\pm} \doteq 3.79$ neper/m, the upper sideband pressure theoretically should be $P_u = 6.27 \times 10^3$ Pa. The upper sideband pressure amplitude was measured to be $P_u = 6.11 \times 10^3$ Pa, which is in good agreement with the predicted value. Similar results were obtained for a 10 cm array length.

We have determined by the measurements discussed in this section that the parametric receiver is functioning as expected in a homogeneous medium. Now we will proceed to a discussion of some experiments conducted to determine the effects of inhomogeneities on its operation.

5.3.2 Procedure for Obtaining Data

The procedure used in measuring amplitude fluctuations in the signal, pump, and upper sideband waves may be described as follows. The transducers shown in Fig. 5.1 were aligned in the desired geometry at mid-depth in the tank. Using the apparatus described in Section 5.2, and with the tank heaters turned off, recordings were made of the amplitudes of the signal, pump, and upper sideband pulses. These measurements obtained with the heaters off are amplitude fluctuations produced by the electronic apparatus and by any 'ambient' inhomogeneities in the tank such as those due to microbubbles, biological matter, or residual thermal patches. Typically,

three sets of data were recorded with the heaters turned off, and approximately 150 samples per data set were taken at a sample rate of about 0.25 Hz. After recording these data, the heaters were turned on and allowed to warm up for 1 hour so that the turbulent mixing could reach steady state. Then an additional five sets of data, similar to those just described, were recorded with the tank heaters turned on. The water temperature was measured at the beginning and end of each data set. When the mean water temperature in the tank reached about 30° C, the heaters were turned off and the tank was allowed to cool until the following day. The reason for stopping the experiments at 30° C is that the level of amplitude fluctuations decreases as the temperature increases; thus poor 'fluctuation-to-noise' ratios usually occurred at temperatures above 30° C. We will discuss this point in more detail below.

The measurements made with heaters on and off were analyzed off-line by a PDP-11 computer, using the computer programme AFLUCT, which is listed in Appendix 5. The quantities calculated by this program are the mean, standard deviation, and coefficient of variation for the amplitude of each wave associated with the parametric receiver. A high-pass filter with cut-off frequency of 0.02 Hz is incorporated in the program to minimize the effects of slow drifts in amplifier gains and changes in received signal amplitude with temperature.⁸⁴

5.3.3 Signal Wave Amplitude Fluctuations

As an example of how amplitude fluctuations of the acoustic waves were measured and analyzed, we will consider data obtained for the 1 MHz signal wave. Data were taken over a five day period using the procedure described in Section 5.3.2. In all, 25 sets of data were taken with the heaters turned on, and 15 sets were taken with the heaters off. For all of these measurements, the separation between projector and hydrophone was $Z_g + L = 0.75$ m. Results of the measurements are shown in Table 5.2. The coefficients of

| Data Set | Temperature °C | CAV _{on} | CAV _{off} * | FNR dB | f_{μ} | CAV |
|----------|----------------|-------------------|----------------------|--------|-----------|--------|
| 1 | 23.5 | 0.0077 | 0.0030 | 8.2 | 0.7303 | 0.0052 |
| 2 | 24.2 | 0.0133 | 0.0030 | 12.9 | 0.7554 | 0.0098 |
| 3 | 25.0 | 0.0088 | 0.0030 | 8.5 | 0.7852 | 0.0058 |
| 4 | 25.7 | 0.0090 | 0.0030 | 9.5 | 0.8123 | 0.0069 |
| 5 | 26.5 | 0.0069 | 0.0030 | 7.2 | 0.8443 | 0.0052 |
| 6 | 25.6 | 0.0081 | 0.0033 | 7.8 | 0.8084 | 0.0060 |
| 7 | 26.2 | 0.0075 | 0.0033 | 7.1 | 0.8321 | 0.0056 |
| 8 | 27.2 | 0.0251 | 0.0033 | 17.6 | 0.8734 | ---- |
| 9 | 27.9 | 0.0071 | 0.0033 | 6.7 | 0.9034 | 0.0057 |
| 10 | 28.6 | 0.0072 | 0.0033 | 6.8 | 0.9345 | 0.0060 |
| 11 | 25.1 | 0.0112 | 0.0043 | 8.3 | 0.7890 | 0.0081 |
| 12 | 25.8 | 0.0111 | 0.0043 | 8.2 | 0.8162 | 0.0083 |
| 13 | 26.5 | 0.0088 | 0.0043 | 6.2 | 0.8443 | 0.0065 |
| 14 | 27.2 | 0.0077 | 0.0043 | 5.1 | 0.8734 | 0.0056 |
| 15 | 27.8 | 0.0120 | 0.0043 | 8.9 | 0.8991 | 0.0101 |
| 16 | 28.1 | 0.0089 | 0.0052 | 4.7 | 0.9122 | 0.0066 |
| 17 | 28.8 | 0.0110 | 0.0052 | 6.5 | 0.9436 | 0.0092 |
| 18 | 29.3 | 0.0094 | 0.0052 | 5.1 | 0.9667 | 0.0075 |
| 19 | 30.1 | 0.0091 | 0.0052 | 4.9 | 1.0048 | 0.0075 |
| 20 | 30.6 | 0.0103 | 0.0052 | 5.9 | 1.0294 | 0.0092 |
| 21 | 27.9 | 0.0065 | 0.0036 | 5.1 | 0.9034 | 0.0059 |
| 22 | 28.6 | 0.0060 | 0.0036 | 4.4 | 0.9345 | 0.0045 |
| 23 | 29.3 | 0.0057 | 0.0036 | 4.0 | 0.9667 | 0.0043 |
| 24 | 30.0 | 0.0052 | 0.0036 | 3.2 | 1.0000 | 0.0038 |
| 25 | 30.7 | 0.0059 | 0.0036 | 4.3 | 1.0344 | 0.0048 |

*CAV_{off} is the average of 3 data sets. Range = 0.75 m

TABLE 5.2

DATA OBTAINED FOR 1 MHz SIGNAL WAVE

amplitude variation for the 1 MHz wave for heaters on and off are labelled in the table as CAV_{on} and CAV_{off} , respectively. CAV_{on} is a measure of amplitude fluctuations in the voltage recorded by the data logging unit shown in Fig. 5.2. However, these fluctuations may be produced by a number of causes. Both thermal inhomogeneities in the medium and other inhomogeneities such as microbubbles and biological matter will produce amplitude fluctuations in a propagating pressure wave. Further amplitude fluctuations will be produced if there are gain variations in the electronic system that generate and detect a pressure wave. Therefore we can say that the measured amplitude fluctuations comprise (1) an effect which we wish to measure, a signal, which is caused by thermal inhomogeneities; and (2) extraneous effects, or noise, which is caused by nonthermal inhomogeneities and system gain variations. It is reasonable to assume that the noise is present whether the tank heaters are on or off, so CAV_{off} is a measure of the noise. If the signal and noise are uncorrelated, then they will add on a mean-squared basis, and the desired signal will have a coefficient of amplitude variation given by⁹⁵

$$CAV = \left[CAV_{on}^2 - CAV_{off}^2 \right]^{1/2} . \quad (5.3)$$

Values of CAV for the present experiment are shown in Table 5.2, and are plotted as a function of water temperature in Fig. 5.4. In making this plot, some of the data have been omitted. Specifically, data with a fluctuation-to-noise ratio (FNR) less than 4.5 dB have been omitted, where

$$FNR = 20 \log_{10} \frac{CAV_{on}}{CAV_{off}} .$$

Low values of FNR generally occur at higher values of temperature; this is demonstrated by comparing data sets 21-25 in Table 5.2 to data sets 1-5.

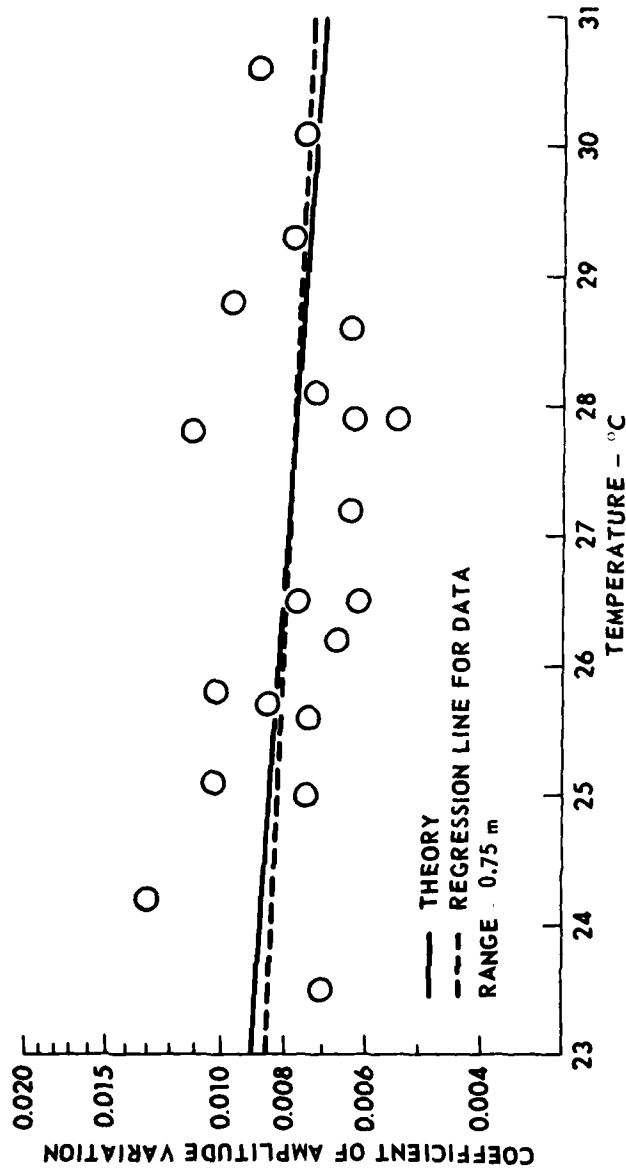


FIGURE 5.4
TEMPERATURE DEPENDENCE OF 1 MHz SIGNAL WAVE FLUCTUATIONS

A theoretical prediction for the variation of CAV with temperature may be obtained from the sum of Eqs. (3.30) and (3.32), which is:

$$\text{CAV}^2 = 0.13 C_n^2 k_s^{7/6} (Z_s + L)^{11/6} + \frac{\pi}{480} \phi_m (Z_s + L)^3 (\kappa_t^4 - \kappa_m^4). \quad (5.4)$$

It may be seen from the equations given in Table 5.1 that C_n and ϕ_m are functions of the mean-squared refractive index, which in turn is given by⁹⁵

$$\langle \mu^2 \rangle^{1/2} = \frac{1}{c} \frac{\partial c}{\partial T} \langle (\Delta T)^2 \rangle^{1/2}, \quad (5.5)$$

where

$$c = 1403 + 5T - 0.06T^2 + 0.0003T^3, \quad (5.6)$$

$$\frac{\partial c}{\partial T} = 5 - 0.12T + 0.009T^2, \quad (5.7)$$

T = mean temperature in °C, and

ΔT = deviation from mean temperature.

Substitution of Eqs. (5.5)-(5.7) into Eq. (5.4), and use of the equations defining C_n and ϕ_m in Table 5.1, gives the theoretical curve plotted in Fig. 5.4. In order to make a comparison between the experimental and measured results, a regression line for the measured data is also shown in the figure. This line is plotted using the formulae in Crow *et al.*¹⁰² and is based upon the method of least squares. It can be seen that there is good agreement in both magnitude and slope between the regression line and the theoretical curve.

The agreement between theory and experiment indicates that the temperature dependence of $\langle \mu^2 \rangle$, as expressed by Eqs. (5.5)-(5.7), is valid. By knowing this temperature dependence, we are able to compare measurements of CAV taken over a range of temperatures simply by normalizing all the measurements to the same temperature. Chotiros¹⁰⁴ has shown the factor, f_μ , for normalizing measurements to 30° C to be, approximately,

$$f_{\mu} \doteq \log_{10}^{-1} [0.021(T - 30)].$$

As an example, we calculate the coefficient of amplitude variation for the 1 MHz signal wave at the range 0.75 m as follows. For each data set in Table 5.1, a value of CAV is calculated by compensating for ambient noise with Eq. (5.3), and then normalizing the result to 30° C with multiplication by f_{μ} . Thus,

$$CAV = f_{\mu} \left[CAV_{on}^2 - CAV_{off}^2 \right]^{1/2} \quad (5.8)$$

is calculated for each data set. The mean and standard deviation of CAV is then calculated for all data sets, with the results plotted in Fig. 5.5. Similar results at other ranges are also shown in the figure, along with some curves that show the theoretical range dependence of CAV.

The nearfield theoretical curve shown in the figure is calculated from Eq. (5.4), where the range is defined to be $Z_s + L$, and values of the medium parameters at the center of the tank are taken from Table 5.1. This equation is strictly valid only for ranges much less than R_o where

$$R_o \doteq \frac{1}{\lambda_s} \left(\frac{Z\pi}{\kappa_t} \right)^2 .$$

For ranges much greater than R_o , the farfield result [Eq. (3.24)] applies. For the data in Fig. 5.5, $R_o \doteq 0.8$ m, so some of the data are in a region where the nearfield theory is only an approximation. However, as comparison between theory and experiment indicates, the nearfield approximation is in reasonable agreement with the measured results.

5.3.4. Pump Wave Amplitude Fluctuations

Measurements of the coefficient of amplitude variation for the 10 MHz

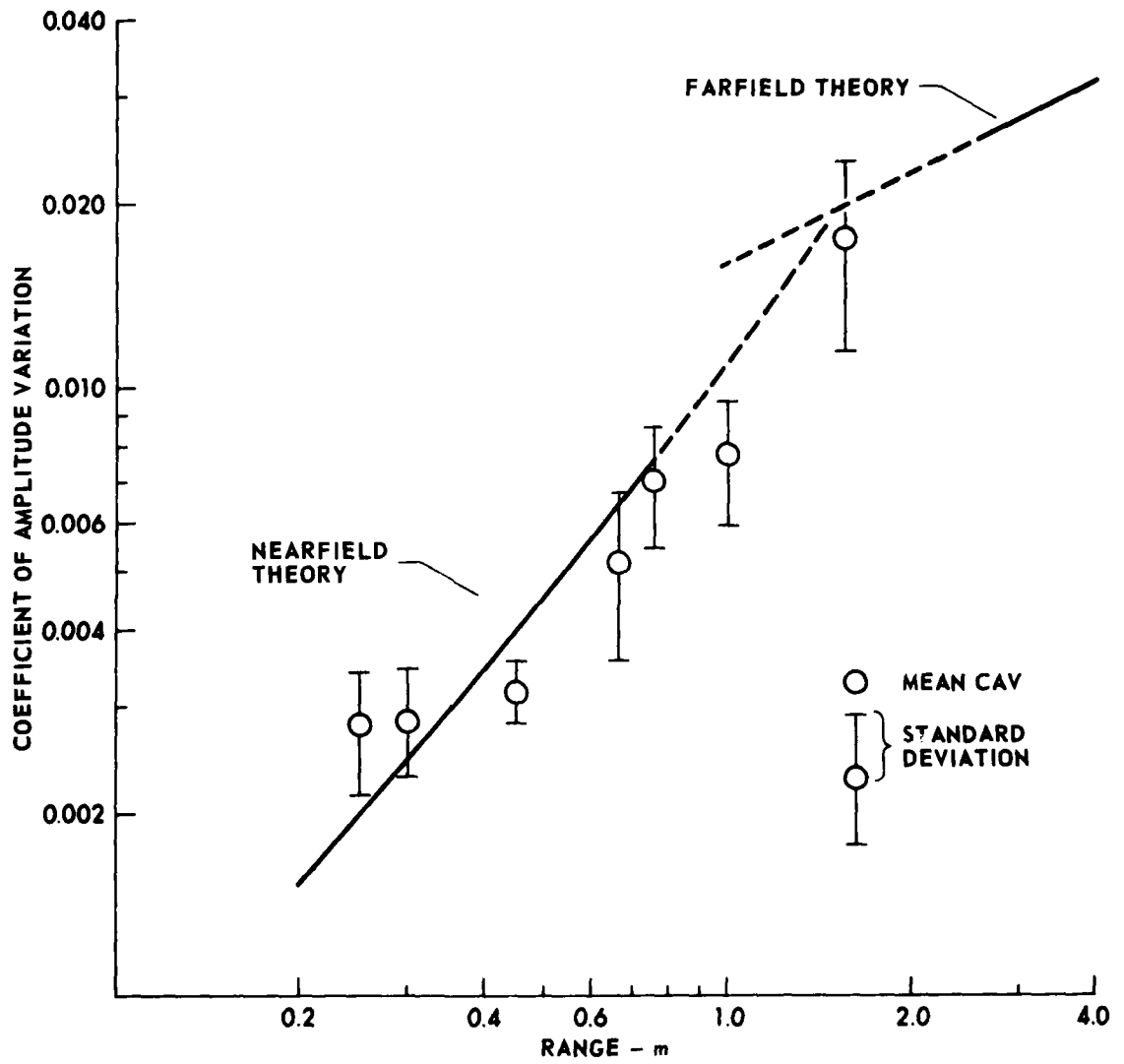


FIGURE 5.5
SIGNAL WAVE AMPLITUDE FLUCTUATIONS

pump wave (CAV_p) were made as a function of separation L between pump transducer and hydrophone. The results, shown in Fig. 5.6, were obtained using the procedure described in Section 5.3.2. The data were adjusted for ambient noise and normalized to 30° C using Eq. (5.8).

In making a theoretical prediction for CAV_p there are two factors that need to be taken into account. One is that the mean-squared temperature variations, $\langle \Delta T^2 \rangle$, near the hydrophone were measured to be different from $\langle \Delta T^2 \rangle$ in the center of the tank. This is due to the fact that the hydrophone was located near the edge of the heater array and perforated screen which produced the thermal microstructure. Because CAV_p is a function of turbulence parameters which depend upon $\langle \Delta T^2 \rangle$, this change in mean-squared temperature will affect CAV_p . Another factor that affects the value of CAV_p is due to the finite cross sectional area of the hydrophone. Chotiros¹⁰⁵ has shown that for a square transducer of dimension b on each side, a reduction occurs in the coefficient of amplitude variation of the amount

$$\frac{CAV_h^2}{CAV^2} \doteq 1 - 0.61 b (\lambda L)^{-1/2}, \quad (5.9)$$

where CAV_h and CAV are the coefficient of amplitude variation for an acoustic wave received with a square hydrophone and a point hydrophone, respectively,

λ is the acoustic wavelength, and

L is the separation between the source of the wave and the hydrophone.

Physically, this reduction in CAV is due to the lack of correlation in amplitude fluctuations across the face of the hydrophone. Thus, the hydrophone measures the average level of fluctuations across its aperture. Equation (5.9) can be taken to be the definition of an 'aperture factor', f_a ; i.e.,

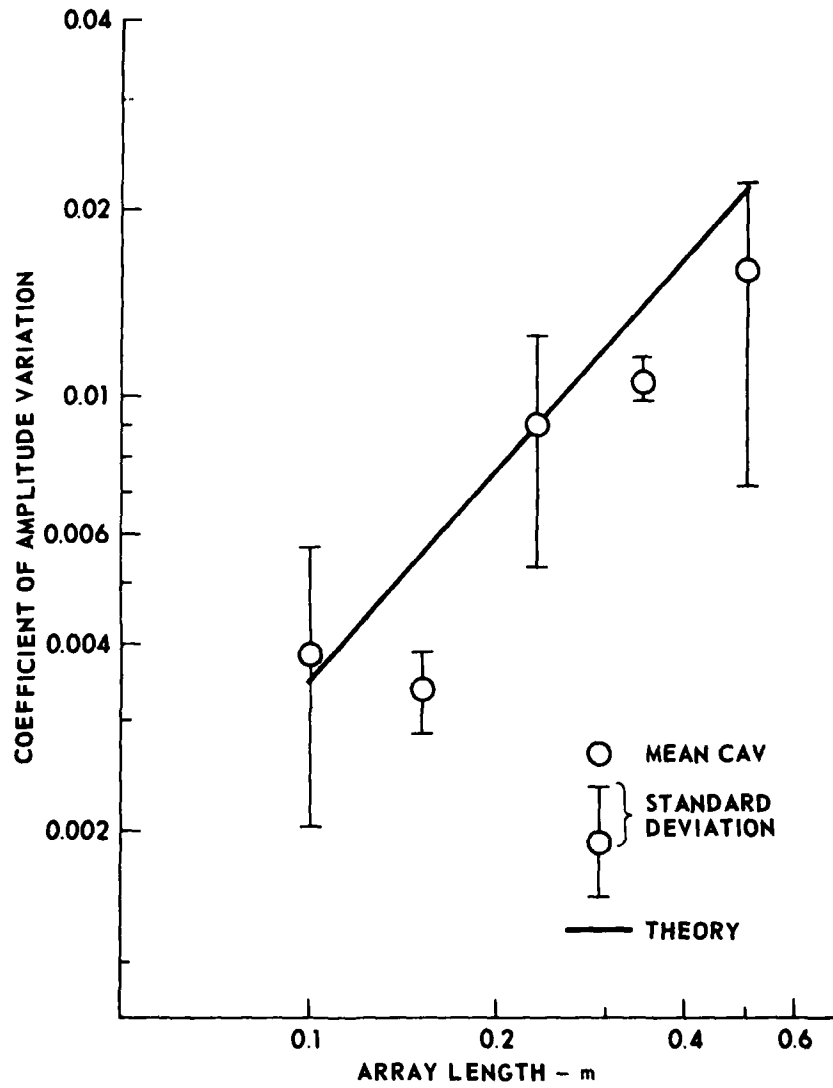


FIGURE 5.6
PUMP WAVE AMPLITUDE FLUCTUATIONS

$$f_a = 1 - 0.01 b(1L)^{-2} \quad (5.10)$$

The coefficient of amplitude variation for the pump wave can be predicted by multiplying Eq. (3.31) by Eq. (5.10), and is

$$CAV_p^2 = 0.31 f_a C_n^2 k_p^{7/6} L^{11/6} \quad (5.11)$$

The value of C_n in Eq. (5.11) is determined from the defining equations in Table 5.1, using the measured value of $\langle \Delta T^2 \rangle$ in the region between pump transducer and hydrophone. The dependence of CAV_p upon separation L , as given by Eq. (5.11), is plotted as the solid line in Fig. 5.6. It can be seen from the figure that there is reasonable agreement between theory and experiment.

5.3.5 Amplitude Fluctuations in the Upper Sideband Wave

In this section we will discuss an experimental study of the effects of medium inhomogeneities on the upper sideband wave of a nearfield parametric receiver. Three types of results were obtained in this study. First, measurements were made of the coefficient of amplitude variation for the upper sideband wave (CAV_{USB}) with the array length fixed and with variable range, $Z_s + L$. Second, measurements were made of CAV_{USB} with the range fixed and with variable array length. Third, a comparison was made between the amplitude fluctuations in the signal wave and in the upper sideband wave. All data discussed in this section were obtained by following the experimental procedure described in Section 5.3.2. Results were normalized to 30° C and adjusted for ambient noise using Eq. (5.8).

The first set of results we will consider is shown in Fig. 5.7. For this data, the array length was 0.1 m and the range, $Z_s + L$, was varied from 0.25 m to 1.55 m. As above, circles in the figure indicate mean values of

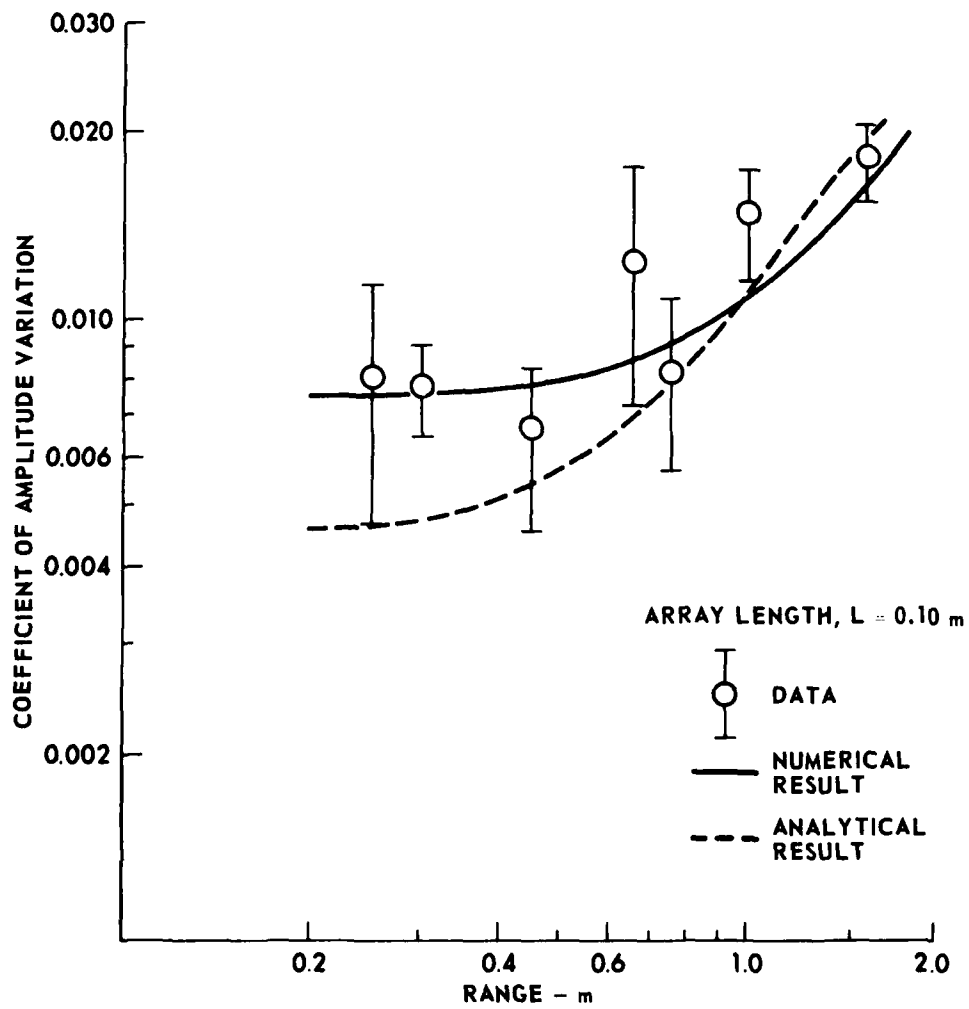


FIGURE 5.7
 CAV_{USB} FOR FIXED ARRAY LENGTH AND VARIABLE RANGE

CAV_{USB} obtained from several data sets and the vertical bars indicate the standard deviation of CAV_{USB} for the data sets. In making theoretical predictions for the experiment, two different methods were used. One prediction, shown as the dashed line in Fig. 5.7, is based on Eq. (4.49). It can be seen from the figure that Eq. (4.49) gives values of CAV_{USB} that are significantly lower than the measured values for most ranges. However, the development leading to Eq. (4.49) was based on the assumption that the pump wave can be approximated as a plane wave of infinite extent. A more accurate theoretical model, which takes into account the effects of the finite apertures of the pump transducer and hydrophone, has been developed by Chotiros.¹⁰⁶ It is shown in Appendix 6 that the coefficient of amplitude variation, CAV_{PR} , for the nearfield parametric receiver can be written as

$$\begin{aligned}
 CAV_{PR}^2 = & |v_H|^{-2} \int_0^L \int_0^L \text{Re}(K_1) \text{Re}(K_2) \langle B_1 B_2 \rangle \\
 & + \text{Im}(K_1) \text{Im}(K_2) \langle S_1 S_2 \rangle + \text{Re}(K_1) \text{Im}(K_2) \langle B_1 S_2 \rangle \\
 & + \text{Im}(K_1) \text{Re}(K_2) \langle S_1 B_2 \rangle \left\{ dz_1 dz_2 \right. , \quad (5.12)
 \end{aligned}$$

where $v_H = A_{\pm} \int_0^L \frac{1}{C_1 C_2} dz$ is the normalized voltage at the terminals of the hydrophone,

$$K = \frac{A_{\pm} e^{-j\theta}}{C_1 C_2} ,$$

$$C_1 = j \left[\frac{k_p}{2z} + \frac{k_{\pm}}{2(L-z)} \right] + \frac{k_p^2 b^2}{4z^2 \left(1 + \frac{jk_p b^2}{2z} \right)} + \frac{k_{\pm}^2 h^2}{4(L-z)^2 \left[1 + \frac{jk_{\pm} h^2}{2(L-z)} \right]} ,$$

θ is the phase angle of the second order pressure,

$$C_2 = 4z(L - z) \left(1 + \frac{jk_p b^2}{2z} \right) \left[1 - \frac{jk_+ h^2}{2(L-z)} \right] \frac{1}{h^2 b^2}, \text{ and}$$

h and b are characteristic radii of the pump transducer and hydrophone, respectively.

This result requires numerical integration for its evaluation. The program CAVNUM, listed in Appendix 5, is used to evaluate Eq. (5.12) for the experiments discussed in this section. Results obtained by the program are plotted as the solid line in Fig. 5.7. It can be seen from the figure that the numerical results based on Eq. (5.12) are generally in better agreement with the data than the analytical result, Eq. (4.49).

A similar set of results, shown in Fig. 5.8, was obtained for a fixed range of $Z_s + L = 0.75$ m, and a variable array length. In this case, there is less difference between the numerical and analytical results, although the numerical results are generally in better agreement with the data.

Another useful way of studying the parametric receiver in an inhomogeneous medium is to compare the coefficients of amplitude variation for the upper sideband (CAV_{USB}) and signal (CAV_s) waves. The ratio, CAV_{USB}/CAV_s , compares the 'noise level' of the parametric receiver in an inhomogeneous medium to the noise level of a point hydrophone in the same medium. Here 'noise level' refers to the random amplitude variations appearing at the output terminals of either the hydrophone of the parametric receiver or the point hydrophone.

Measurements of CAV_{USB} and CAV_s were made simultaneously for parametric receiver array lengths of 0.1 m and 0.5 m. The hydrophone of the parametric receiver was used to detect both upper sideband and signal waves, as shown in Fig. 5.2. A mean value, $\langle CAV_{USB}/CAV_s \rangle$, was calculated for several data sets taken at each range, with the results shown in Fig. 5.9. The theoretical curves shown in the figure are based on values of CAV_{USB} obtained

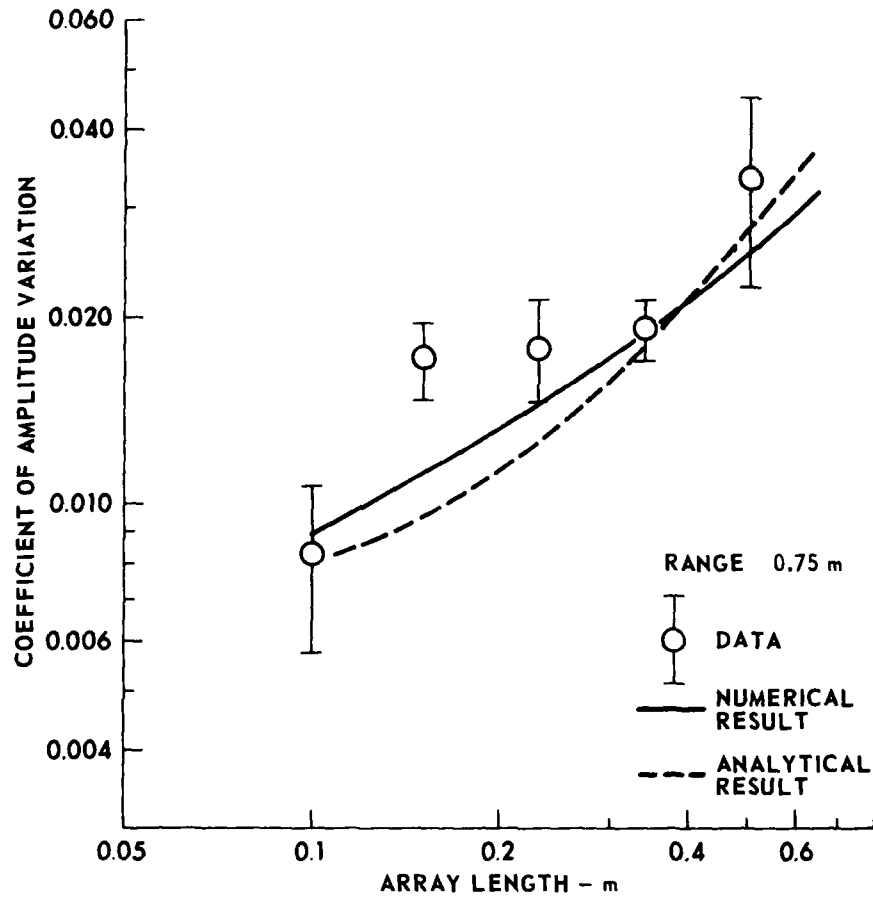


FIGURE 5.8
CAV_{USB} FOR FIXED RANGE AND VARIABLE ARRAY LENGTH

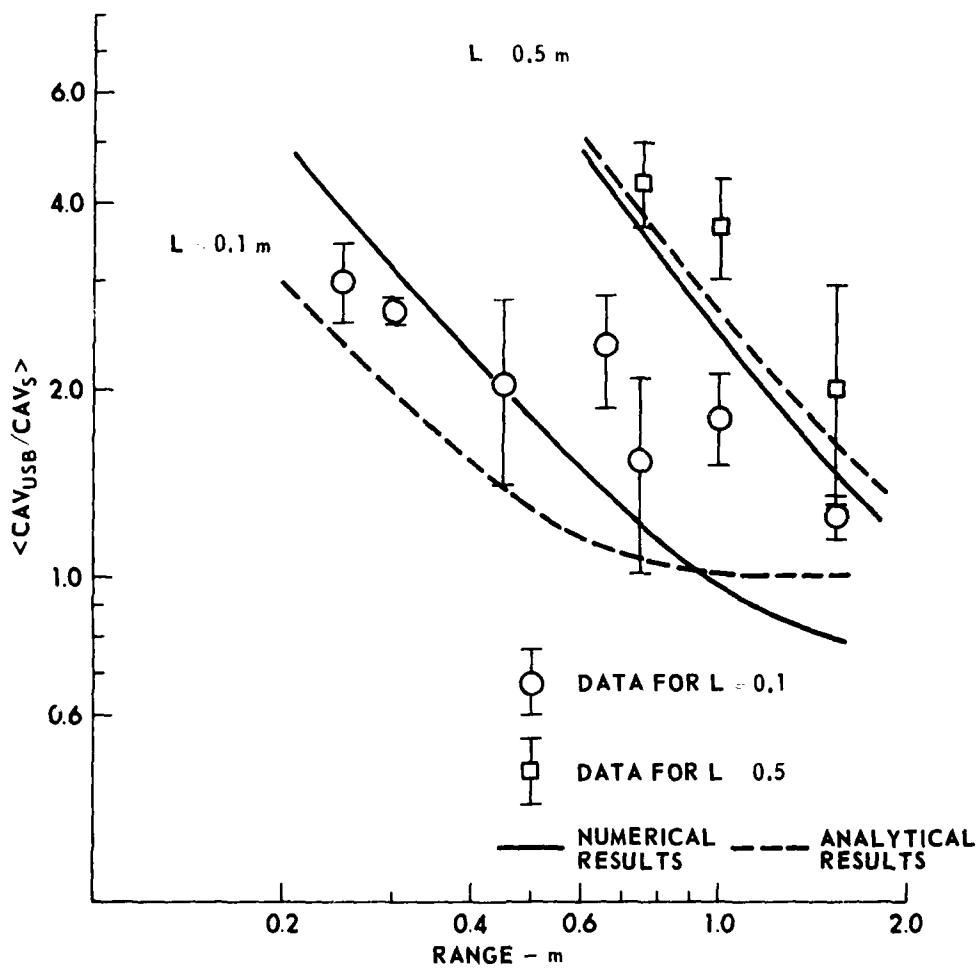


FIGURE 5.9
COMPARISON OF UPPER SIDEBAND
AND SIGNAL WAVE FLUCTUATIONS

from Eq. (4.49) [the dashed lines] or by numerical integration of Eq. (5.12), and on values of CAV_s obtained from Eq. (5.4). Discussion of the physical meaning of these results, as well as those shown in Figs. 5.6 and 5.7, will be given below.

5.3.6 Results for Spherically Spreading Pump Waves

The experiments described in the preceding section were conducted with the hydrophone placed in the nearfield of the pump transducer. Some data were also obtained with the hydrophone in the farfield of the pump, so that the pump waves were spherically spreading. The pump transducer used in the present experiment was of a smaller cross sectional area than that used in the experiments described in Sections 5.3.4 and 5.3.5 (see Appendix 3 for a description of the transducers). The experimental apparatus and the procedure used to obtain the data were similar to those described in Sections 5.2 and 5.3.2; however, amplitude fluctuations in the lower sideband wave (CAV_{LSB}) were measured rather than those in the upper sideband wave. Details of the electronic receiving system used for this experiment are given in Appendix 4.

Measurements of CAV_{LSB} were made for a fixed range, $Z_s + L = 1.4$ m, and a variable array length. Data from the experiment are plotted in Fig. 5.10. Each open dot in the figure represents a mean value of CAV_{LSB} obtained for a set of approximately 150 samples. These experimental values of CAV_{LSB} have been compensated for temperature and ambient noise using Eq. (5.9). The theoretical curve shown in the figure is obtained from Eq. (4.44), which for the present experiment can be written as

$$CAV_{LSB}^2 \doteq \frac{1}{L^2} \int_0^L \int_0^L \left(\langle B_{s1} B_{s2} \rangle + \langle B_{p1} B_{p2} \rangle + \langle B_{p1} B_{+2} \rangle + \langle B_{+1} B_{p2} \rangle + \langle B_{+1} B_{+2} \rangle \right) dz_1 dz_2, \quad (5.13)$$

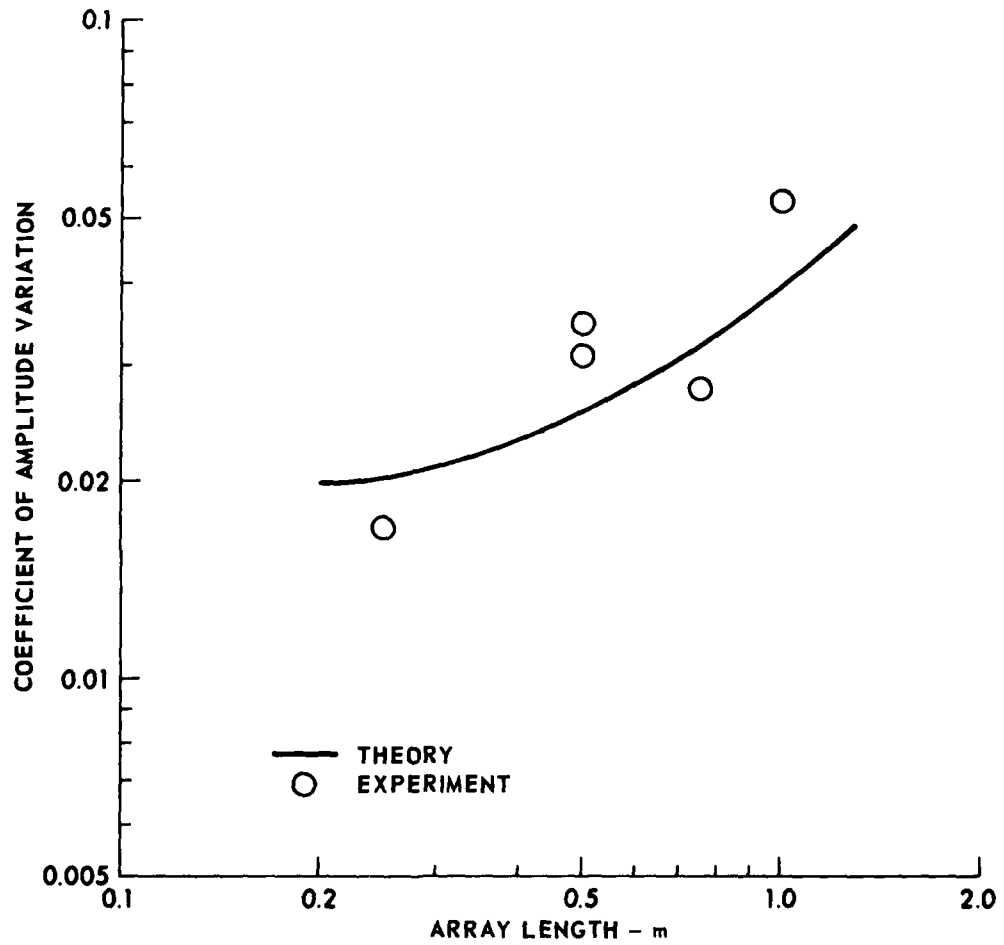


FIGURE 5.10
CAV FOR SPHERICAL PUMP WAVES

where

$$\begin{aligned} \langle B_{s1} B_{s2} \rangle = & \left[0.13 C_{n_s}^2 k_s^{7/6} (z_s + z_1)^{11/6} + \frac{\pi}{480} \phi_m (z_s + z_1)^3 (\kappa_t^4 - \kappa_m^4) \right]^{1/2} \\ & + \left[0.13 C_{n_s}^2 k_s^{7/6} (z_s + z_2)^{11/6} + \frac{\pi}{480} \phi_m (z_s + z_2)^3 (\kappa_t^4 - \kappa_m^4) \right]^{1/2}, \end{aligned}$$

$$\langle B_{p1} B_{p2} \rangle = 0.13 C_n^2 k_p^{7/6} (z_1 z_2)^{11/12},$$

$$\langle B_{p1} B_{+2} \rangle \doteq 0.13 C_n^2 k_p^{7/6} z_1^{11/12} (L - z_2)^{11/12},$$

$$\langle B_{+1} B_{p2} \rangle \doteq 0.13 C_n^2 k_p^{7/6} (L - z_1)^{11/12} z_2^{11/12}, \text{ and}$$

$$\langle B_{+1} B_{+2} \rangle \doteq 0.13 C_n^2 k_p^{7/6} (L - z_1)^{11/12} (L - z_2)^{11/12}.$$

Integration of Eq. (5.13) gives

$$\begin{aligned} \text{CAV}_{\text{LSB}} \doteq & 0.1415 C_n^2 k_p^{7/6} L^{11/6} \\ & + \frac{1}{L} \frac{4}{ab^2} \left[(a + bL)^{3/2} - a^{3/2} \right]^2, \end{aligned} \quad (5.14)$$

where

$$a = 0.13 C_n^2 k_s^{7/6} z_s^{11/6} + \frac{3\pi}{480} \phi_m (\kappa_t^4 - \kappa_m^4) z_s^3, \text{ and}$$

$$b = \frac{11}{6} (0.13 C_n^2 k_s^{7/6}) z_s^{5/6} + \frac{3\pi}{480} \phi_m (\kappa_t^4 - \kappa_m^4) z_s^2.$$

It can be seen from Fig. 5.10 that values of CAV_{LSB} predicted by Eq. (5.14) are in reasonable agreement with the data.

5.4 Discussion

There are a few simple, but useful, conclusions that can be drawn from the results presented in Figs. 5.4-5.10.

Theoretical values of the coefficient of amplitude variation for the linear waves are in fairly good agreement with measured values (Figs. 5.4-5.6). This agreement between theory and experiment allows us to conclude that the theoretical model for the acoustic medium discussed in Section 5.1 is a reasonable one.

Examination of Figs. 5.7, 5.8, and 5.10 shows that CAV_{USB} tends to increase with either increasing array length or increasing range. This result seems reasonable if we recall the physical considerations discussed in Section 4.6. It was noted there that the coefficient of amplitude variation for both nearfield and farfield parametric receivers depends upon two contributions: one from the high frequency waves in the interaction region and a second from the signal wave. As the range between signal source and parametric receiver is increased, the contribution to CAV_{USB} from the signal wave is increased. This is simply because more scatterers are present in the propagation path of the signal wave as the range is increased. Similarly, as the array length increases, there is an increase in the contribution to CAV_{USB} due to the pump and upper sideband waves, because they propagate through an increased volume of scatterers.

Similar considerations apply to the results shown in Fig. 5.9. It can be seen in the figure that, for an array length of 0.1 m, the amplitude fluctuations in the upper sideband wave and in the signal wave are approximately equal; i.e., $CAV_{USB}/CAV_s \doteq 1$ for long ranges. It can be shown theoretically that this is also true for the 0.5 m array length, although CAV_{USB} and CAV_s become approximately equal at larger ranges for the 0.5 m long array than for the 0.1 m long array. This result is reasonable, because as the range of the signal source is increased, the fluctuations in

the signal wave will increase while the high frequency fluctuations in the interaction region will remain constant. At sufficiently long ranges, the contribution to CAV_{USB} due to scatterers in the interaction region will become negligible, and only scattering of the signal wave will contribute significantly to CAV_{USB} . For array lengths greater than the spatial correlation distance of the signal wave fluctuations, it may be expected that CAV_{USB} would become less than CAV_s at sufficiently long ranges. This effect would occur if the parametric receiver summed uncorrelated 'noise' throughout the interaction volume, thus 'averaging out' some of the fluctuations. The size limitation of the model tank and choice of signal frequency prevented a demonstration of this effect; it would be an interesting point to pursue in future research.

5.5 Summary

The experimental study described in this chapter investigated some effects of medium inhomogeneities on the parametric receiver. The experiments were conducted in a model tank in which an array of immersion heaters and a perforated screen produced a thermal microstructure. Measurements were made of the coefficient of amplitude variation for the signal, pump, and upper sideband waves associated with a nearfield parametric receiver, the measurements being made as functions of array length and of range from signal source to hydrophone. It was found that the amplitude fluctuations in the signal and pump waves were reasonably well predicted by the theoretical work reviewed in Chapter 3. It was found that predictions of amplitude fluctuations in the upper sideband wave required a theory which takes into account the phase variations of the pump radiation in the nearfield of the pump transducer. Some simple conclusions were drawn from the experimental results and from physical considerations: CAV_{USB} increases with range and with array length; and for sufficiently large ranges, signal

wave fluctuations measured by a point hydrophone will approximately equal the sideband fluctuations measured by the parametric receiver.

6.1 Summary of the Thesis

The aim of the investigation reported in this thesis was to determine the effects that medium inhomogeneities have on the performance of a parametric receiver. An introduction to the study was given in Chapter 1, where the topics of nonlinear acoustics and wave propagation in an inhomogeneous medium were briefly discussed.

In Chapter 2, the basic principles of parametric receiving arrays were reviewed. It was shown that nonlinear interaction between an incoming 'signal' wave and a locally generated 'pump' wave produces an array of virtual sources in the region in front of the pump transducer. For a homogeneous acoustic medium, this array has the same directivity characteristics as a conventional end-fire array realized from elements operating at the frequency of the wave to be detected. Expressions were given which describe the interaction frequency pressure field when the hydrophone of the parametric receiver is placed in the nearfield and in the farfield of the pump transducer. Practical considerations regarding processing of the difference frequency signal, shadowing, and finite amplitude attenuation were discussed briefly.

A discussion of acoustic wave propagation in an inhomogeneous medium was given in Chapter 3. Brief consideration was given to the historical development of the subject. It was seen that acoustic scattering in the ocean is primarily due to the thermal microstructure, which produces random variations in the refractive index of the acoustic medium. Two functions were discussed that can be used to describe an inhomogeneous medium: the spatial correlation function, and the spatial wavenumber spectral density. Because the spectral composition of an inhomogeneous medium may be determined by turbulence, some basic concepts from turbulence theory were

presented. A summary of expressions was given for amplitude and phase fluctuations and their correlation.

In Chapter 4, the analytical methods discussed in the two previous chapters were used to develop a theory predicting fluctuations in the interaction frequency pressure wave for both nearfield and farfield parametric receivers. It was assumed in developing the analysis that (1) the medium is weakly inhomogeneous, so that the amplitude and phase fluctuations are small compared to unity; (2) there is complete transverse correlation of amplitude and phase fluctuations in the interaction region of the array; and (3) the signal source is located on the main beam of the parametric receiver. By approximating the pump wave as being planar and collimated, it was shown in Eq. (4.22) that mean-squared amplitude fluctuations for the nearfield parametric receiver may be written as

$$\langle B_{PR}^2 \rangle = \frac{1}{L^2} \int_0^L \int_0^L \langle B_1 B_2 \rangle dz_1 dz_2 \quad , \quad (6.1)$$

where $\langle B_1 B_2 \rangle$ is a convenient notation for the nine correlation terms specified by Eq. (4.30). A similar expression was derived for the farfield parametric receiver [see Eq. (4.29)]. These integral expressions, Eqs. (4.22) and (4.29), were evaluated by making a number of assumptions regarding the spatial correlation of the various amplitude fluctuations. The following results were obtained. For the nearfield parametric receiver, the coefficient of amplitude variation is given by Eq. (4.49), which is

$$CAV_{PR}^2 \doteq 0.3375 C_n^2 k_p^{7/6} L^{11/6} + \frac{1}{L^2} \frac{4}{9b^2} \left[(a + bL)^{3/2} - a^{3/2} \right]^2 \quad , \quad (6.2)$$

$$\text{where } a = 0.13 C_n^2 k_s^{7/6} Z_s^{11/5} + \frac{3\pi}{480} \Phi_m(\kappa_t^4 - \kappa_m^4) Z_s^3,$$

$$\text{and } b = \frac{11}{6} (0.13 C_n^2 k_s^{7/6}) Z_s^{5/6} + \frac{3\pi}{480} \Phi_m(\kappa_t^4 - \kappa_m^4) Z_s^2.$$

For the farfield receiver, the result is [Eq. (4.51)]

$$\text{CAV}_{PR}^2 \doteq \frac{\sqrt{\pi}}{2L} k_s^3 a^3 \langle \mu^2 \rangle Z_s \tan^{-1} \left(\frac{2L}{k_s a^2} \right) + 0.1415 C_n^2 k_p^{7/6} L^{11/6}, \quad (6.3)$$

where a is the correlation distance of the refractive index variations.

The experiments discussed in Chapter 5 were conducted in a model tank in which an array of immersion heaters and a perforated screen produced a thermal microstructure. Measurements were made of the coefficient of amplitude variation for the pump, signal, and upper sideband waves associated with a nearfield parametric receiver. It was found that the amplitude fluctuations in the signal and pump waves were reasonably well predicted by the theoretical results reviewed in Chapter 3. Amplitude fluctuations in the upper sideband wave were compared to theoretical predictions based on the analysis of Chapter 4, and to numerical results based on a theory which uses a more exact model for the pump radiation than that of Chapter 4. Both theoretical models gave predictions which were in reasonably good agreement with the experimental results, although the numerical results were generally in better agreement.

6.2 Discussion of Results

The coefficients of amplitude variation for the nearfield and farfield parametric receiver each contain a high frequency component due to scattering of the pump and interaction frequency waves, and a low frequency component due to scattering of the signal wave.

If the array is sufficiently long, and if the pump frequency is much higher than the signal frequency, then the low frequency contribution will

be negligible, and the coefficients of amplitude variation for the parametric receivers will be approximately equal to their high frequency components. This point is demonstrated by the experimental results shown in Fig. 5.7, where, at shorter array lengths, CAV_{PR} tends to 'level out' at a value determined by the high frequency contribution. Also, it can be seen from Fig. 5.8 that CAV_{PR} tends to increase with increasing array length. In the numerical example for the farfield receiver (see Fig. 4.6), it was seen that, for longer array lengths, the high frequency contributions were dominant.

If the array length is sufficiently short, and if the range of the signal source is large, then the high frequency contribution to CAV_{PR} will be of the form

$$CAV_{PR}^2 \doteq \frac{1}{L^2} \int_0^L \int_0^L \langle B_s(z_1) B_s(z_2) \rangle dz_1 dz_2 \quad ,$$

which is identical to the coefficient of amplitude variation for a continuous end-fire array of length L . Therefore, it is only when the low frequency component of the fluctuations is dominant that the parametric receiver performs like an end-fire array in an inhomogeneous medium. Otherwise the value of CAV is greater for the parametric receiver than that for the end-fire array by an amount determined by the scattering of the high frequency waves in the interaction region. For very short array lengths, the parametric receiver and the end-fire array will behave like point hydrophones, so that

$$CAV_{PR}^2 \doteq CAV_{EF}^2 \doteq \langle B_s^2 \rangle \quad (L \doteq 0) \quad .$$

This conclusion is supported by the experimental results shown in Fig. 5.9, where it is shown that the coefficients of amplitude variation for the parametric receiver and for the 'point' hydrophone tend to become equal at longer ranges.

For array lengths greater than the spatial correlation distance of the sideband wave fluctuations, but still sufficiently short that the high frequency fluctuations are negligible, it may be expected that CAV_{PR}^2 would become less than πB_s^2 . This effect would occur if the parametric receiver summed uncorrelated 'noise' throughout the interaction volume, thus 'averaging out' some of the fluctuations. In this way the parametric receiver would exhibit the array gain of a conventional end-fire array having an array length greater than the correlation distance of the signal wave fluctuations. This effect was not demonstrated in the experimental study, due to the size limitations of the model tank and the choice of signal frequency; it would be an interesting topic for future research.

6.3 Conclusions

The purpose of the investigation reported in this thesis has been achieved, that purpose being to determine the effects that thermal inhomogeneities have upon the performance of the parametric receiver. It was determined both theoretically and experimentally that the thermal microstructure generated in a model tank produced a negligibly small level of fluctuations in the sideband waves of both nearfield and farfield parametric receivers. The maximum level of sideband fluctuations measured was 0.05, or five percent. It was shown theoretically that the effects of a typically encountered thermal microstructure in an ocean application are also likely to be small. Only at array lengths greater than about 125 m (for a 100 kHz pump frequency) are the fluctuations in sideband pressure likely to exceed 0.1, or ten percent. The main conclusion of this work, therefore, is that the thermal microstructure will generally have a negligible effect upon parametric reception.

There are several other conclusions that can be drawn from the study. The reconciliation of experimental and theoretical results provides evidence that the spectral description of the medium, as formulated by Chotiros and Smith,⁸⁴

is correct. Furthermore, as this spectral description is based upon Pao's⁸⁵ model of the dissipative subrange, the present results provide further evidence to support Pao's model.

In comparing results for the nearfield and farfield parametric receivers, it may be concluded that the thermal microstructure will, with all other conditions being the same, have less effect on the farfield receiver than the nearfield one. This assumes that the condition $L_0 \gg \sqrt{\lambda_p} L$ is satisfied, so that the results in sections 4.5.1 and 4.5.2 apply.

It was determined that varying the array length of a parametric receiver has two effects upon its performance in an inhomogeneous medium. Firstly, if the array is long compared to the correlation distance of the signal wave that is to be detected, then the array will tend to reduce the level of the signal wave fluctuations by 'averaging them out' over the array. In this regard, the parametric receiver performs like a conventional end-fire array of the same length. Secondly, the fluctuations of the pump and interaction frequency waves increase with array length, so the performance of the parametric receiver will be degraded in comparison to that of the end-fire array at very long array lengths. If the randomizing effect of the medium on the incoming signal has already been large by the time the signal reaches the parametric receiver, then the signal wave fluctuations will dominate the medium effects, and there will be little difference between the performance of the parametric receiver and the end-fire array.

APPENDIX 1. DERIVATION OF EQUATIONS (4.20) and (4.21)

The integral we wish to evaluate is the transverse component of the second order pressure in the interaction region and is given by

$$I = \int_{-b}^b \int_{-b}^b \frac{1}{r} \exp(-jk_{\pm} r) dx dy, \quad (\text{A1.1})$$

where $r = [(L - z)^2 + x^2 + y^2]^{1/2}$.

Using a procedure developed by Berktaf,¹⁰⁷ we will find an approximate expression for I, cast that expression into the form of Fresnel integrals, and then use asymptotic values of the Fresnel integrals to obtain a final result.

In Eq. (A1.1) make the following approximations: in the $1/r$ term, use $r \doteq L - z$; and in the argument of the exponential term, use

$$r \doteq L - z + \frac{1}{2} \frac{x^2 + y^2}{L - z}.$$

Making use of the symmetry in x and y, Eq. (A1.1) can then be written as

$$I = \frac{2e^{-jk_{\pm}(L-z)}}{L-z} \int_0^b \exp[-jk_{\pm} x^2 / (L-z)] dx \int_0^b \exp[-jk_{\pm} y^2 / (L-z)] dy. \quad (\text{A1.2})$$

This expression contains two integrals of the form

$$F = \int_0^b \exp[-jk_{\pm} u^2 / (L-z)] du. \quad (\text{A1.3})$$

Making the change of variable,

$$u = v \sqrt{\frac{\pi(L-z)}{k_{\pm}}}$$

Eq. (A1.3) becomes

$$F = \sqrt{\frac{\pi(L-z)}{k_{\pm}}} \int_0^{b'} \exp[-j\frac{\pi}{2} v^2] dv, \quad (\text{A1.4})$$

where $b' = b \left[\frac{k_{\pm}}{\pi(L-z)} \right]^{1/2}$. The integral in Eq. (A1.4) is the Fresnel integral and in the nearfield of the pump transducer the following asymptotic value may be used^{93,47}

$$\lim_{b' \rightarrow \infty} \int_0^{b'} \exp[-j\frac{\pi}{2} v^2] dv = \frac{1}{2}(1-j). \quad (\text{A1.5})$$

Substitution of Eq. (A1.5) into Eq. (A1.4) and using the result in Eq. (A1.2) gives

$$I \doteq \frac{2e^{-jk_{\pm}(L-z)}}{(L-z)} \left[\frac{1}{2}(1-j) \sqrt{\frac{\pi(L-z)}{k_{\pm}}} \right]^2,$$

or

$$I = \frac{-j\pi}{k_{\pm}} e^{-jk_{\pm}(L-z)}. \quad (\text{A1.6})$$

This appears in the text as Eq. (4.20). A similar result can be obtained for the normalized homogeneous component, H, of the observed pressure. The definition of H is given in Eq. (4.16) and is

$$H = \int_V e^{-jk_{\pm}(z+r')} \frac{1}{r'} dv.$$

This can be written in terms of I as

$$H = \int_0^L e^{-jk_{\pm}z} I dz. \quad (\text{A1.7})$$

Substitution of Eq. (A1.6) for I gives

$$H \doteq \frac{-j\pi L}{k_{\pm}} e^{-jk_{\pm}L},$$

which appears in the text as Eq. (4.21).

APPENDIX 2. TRANSVERSE CORRELATION OF FLUCTUATIONS

One of the assumptions made in the theoretical analysis of Chapter 4 was that there is complete transverse correlation of amplitude and phase fluctuations in the interaction region of the parametric receiver. We will discuss this assumption for both the nearfield and farfield parametric receiver in this appendix.

A2.1 Transverse Correlation for the Nearfield Case

For a plane wave, the volume of inhomogeneities that contribute to the scattered pressure is a cone with its vertex at the observation point and an aperture angle of $1/ka$ radians, where a is the radius of the inhomogeneities.¹⁸ If the medium contains a distribution of various sizes of inhomogeneities, there is a cone associated with each size, the largest cone being associated with the smallest inhomogeneities. At each point in the interaction region of a nearfield parametric receiver, therefore, only the scatterers contained within their associated cone contribute to the observed scattered pressure. Furthermore, only scatterers insonified by the collimated pump beam contribute to the observed pressure. The volume over which the fluctuations are assumed to be transversely correlated is the intersection of the cone and the insonified region, as shown by the diagonal lines in Fig. A2.1.

As an example, for the model tank used in the present study, most patches contributing to the acoustic fluctuations will be larger than $a = 2\pi/\kappa_0 = 4.19 \times 10^{-3}$ m. This means that the largest cone will have, for pump waves of 10 MHz, an aperture angle of 5.7×10^{-3} rad. For an array length of $L = 0.5$ m, it can be shown that the width of the significant scattering volume in the middle of the array (at $z = 0.25$ m) is 1.43×10^{-3} m. It can be found from Tatarski's results (Fig. 13 of Ref. 19) that the correlation coefficient for the maximum transverse separation, 1.43 mm, is

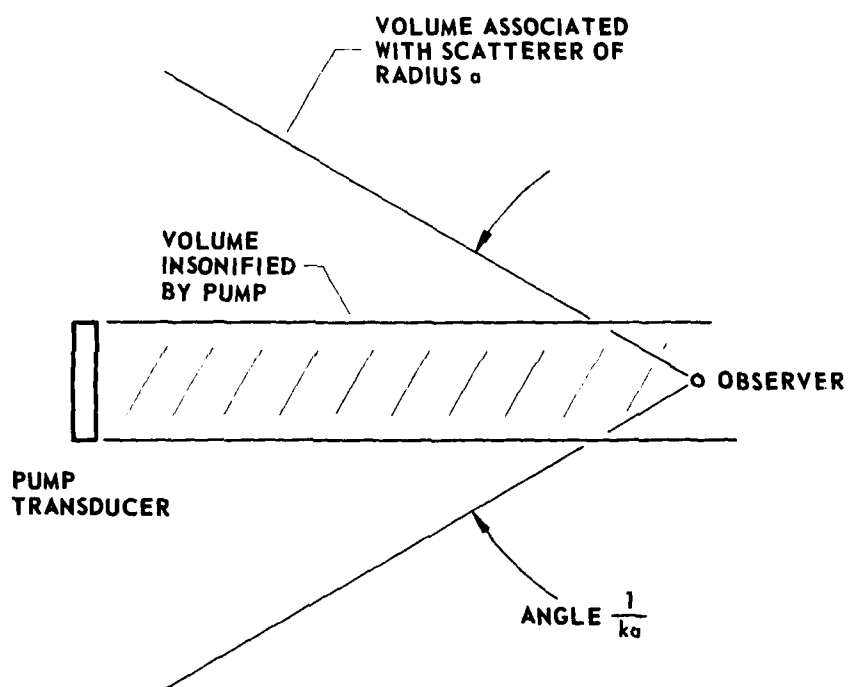


FIGURE A2.1
SIGNIFICANT SCATTERING VOLUMES
IN NEARFIELD OF PUMP

$R_B^T \doteq 0.65$. The transverse correlation coefficient for a 9 MHz plane wave at a range 0.255 was measured in the model tank to be⁸⁴ $R_B^T \doteq 0.7$ at a separation of 1.4 mm. These results indicate that the assumption of complete transverse correlation of the pump amplitude fluctuations is reasonable for array lengths $L \leq 0.5$ m. A comparison of the correlation coefficients R_B^T and R_S^T [see Eqs. (3.38) and (3.39) or their plot in Fig. 3.3.1 of Ref. 91] indicates that, for $0 < (\Delta\rho/a) < z$, $R_S^T \geq R_B^T$. This means the phase fluctuations will be correlated over a larger volume than the amplitude fluctuations.

A.2.2 Transverse Correlation for the Farfield Case

For a spherical wave, the significant scattering volume is an ellipsoid with foci at the points where the source and receiver are located.⁶⁸ The maximum transverse dimension of the significant scattering volume for a scatterer of radius a is given by Aiken¹⁰⁸ to be equal to $L \tan[(4\kappa a)^{-1}]$. For a point source, the condition of having complete transverse correlation of fluctuations is therefore approximately given by

$$L \tan \left[\frac{\kappa_0}{8\pi k} \right] < l_t \quad ,$$

where l_t is the correlation distance of the fluctuations; i.e., the separation at which R_B^T equals $1/e$.

For a source having a finite aperture and, hence, directivity, the volume of scatterers which contribute to acoustic fluctuations is the intersection of the significant scattering volume and the volume insonified by the source beam.

The transducers used in the experimental study are described in this appendix.

A.3.1 Signal Source

The signal source transducer consisted of a 2.0 cm square ceramic plate mounted on a backing made from a mixture of flyash and epoxy resin. The transducer was operated at its resonant frequency of 1 MHz. Its efficiency was measured with a radiation balance, and found to be 37%. The 3 dB beam-width was measured as 3.2°.

A.3.2 Pump Transducer for the Nearfield Receiver

The pump transducer used with the nearfield parametric receiver consisted of an air-backed 1 cm circular ceramic plate, resonant at 10 MHz, and mounted in a brass housing. The diameter of the housing was 2.0 cm. A radiation balance was used to measure the transducer efficiency, which was found to be 3.4%. Excess attenuation of the pump wave at ranges of 10 cm and 50 cm was shown to be negligible by demonstrating that the pump pressure increased linearly as a function of driving voltage applied to the pump transducer. The 3 dB width of the pump column was measured to be 0.38 cm at 10 cm range, and 0.75 cm at 50 cm range.

A.3.3 Pump Transducer for the Farfield Receiver

For the farfield parametric receiver, the pump transducer was a 0.5 cm square ceramic plate backed by epoxy resin. The efficiency was determined from admittance measurements made in air and water, and was measured to be 3%.

A.3.4 Hydrophone

The hydrophone used in the experiments was a 2 mm square ceramic plate backed with epoxy resin. Its sensitivity at the frequencies of interest are

given in Table A1.1. The sensitivity was determined by placing the hydrophone in a pressure field of known amplitude and measuring the voltage appearing at the hydrophone terminals.

| f MHz | S mV/Pa |
|----------|-----------------------|
| 1 | 8.37×10^{-5} |
| 9 | 3.7×10^{-3} |
| 10 | 1.31×10^{-3} |
| 11 | 1.15×10^{-3} |

f = frequency

S = receiving sensitivity

TABLE A1.1

HYDROPHONE SENSITIVITY

A block diagram of the electronic receiving system used with the nearfield parametric receiver is shown in Fig. A4.1. The hydrophone is transformer coupled to the filters and tuned amplifiers that are used to separate the various signals.

A single channel of the signal processing unit is sketched in block form in Fig. A4.2. For the 'upper sideband' (USB) and 1 MHz 'signal' channels, a peak detector based on Knott's design¹⁰⁹ was used. For these two channels, a sample and hold circuit was constructed that uses a National Semiconductor LF398 integrated circuit. The peak detector and sample and hold circuits used for the 'pump' channel had been used in previous studies and are described in Ref. 110. The data logger was a commercial unit made by Solartron.

The gain of each channel at the frequencies of interest is shown in Table A4.1. The voltage transfer characteristic of the receiving system was determined by replacing the hydrophone with a voltage source and measuring the output voltage for each channel of the signal processing unit as a function of input voltage. Each channel was determined to be linear over the voltage ranges used in the experiments.

A block diagram of the receiving system used with the farfield parametric receiver is shown in Fig. A4.3. An inductor L_0 was placed in parallel with the hydrophone to tune out the static capacitance of the ceramic plate at the lower sideband frequency, 9 MHz. The low-pass filter shown in the figure attenuated the pump frequency voltage by approximately 40 dB, and attenuated the 9 MHz voltage by about 11 dB. The variable-gain tuned amplifier was operated typically at a gain of 50 dB, with a bandwidth of approximately 70 kHz, centered about 9 MHz. The signal processing unit was that described in Ref. 110. It selected a 10 to 35 μ sec section of the received pulse, the section being sampled about 40 μ sec after the beginning

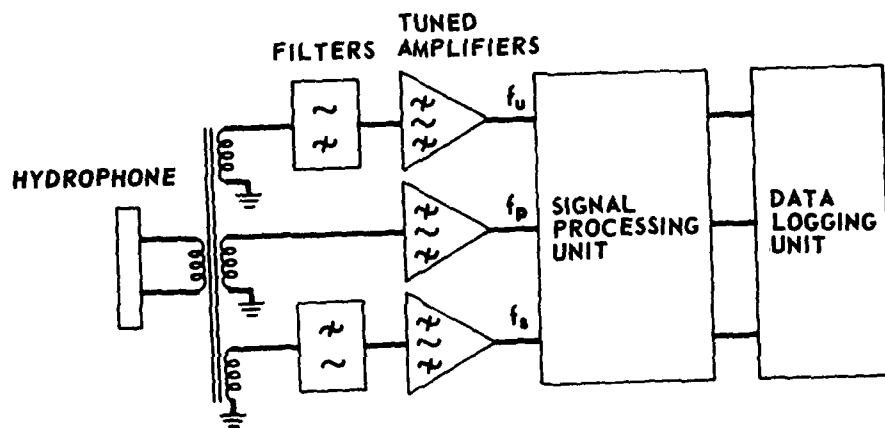


FIGURE A4.1
ELECTRONIC RECEIVING SYSTEM

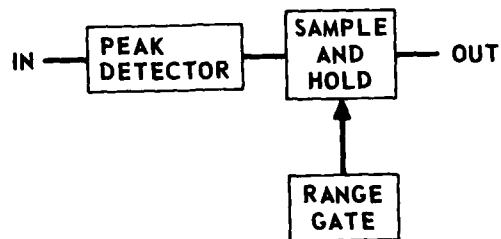


FIGURE A4.2
ONE CHANNEL OF SIGNAL PROCESSING UNIT

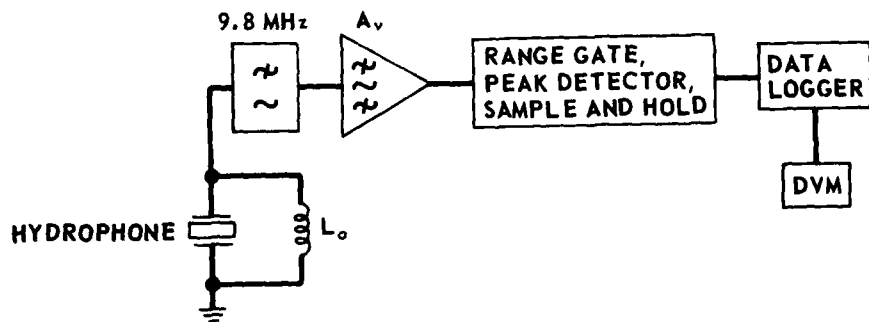


FIGURE A4.3
RECEIVING SYSTEM FOR FARFIELD RECEIVER

of the pulse. The sampled pulse was peak-detected and converted to digital form by the data logger.

| Channel | Frequency MHz | Gain dB |
|-----------------|------------------|------------|
| 1 MHz Signal | 1 | + 48 |
| | 10 | - 48 |
| | 11 | - 45 |
| 10 MHz Pump | 1 | - 32 |
| | 10 | + 11 |
| | 11 | - 12 |
| 11 MHz USB | 1 | - 60 |
| | 10 | - 49 |
| | 11 | + 24 |

TABLE A4.1

FREQUENCY RESPONSE OF SIGNAL PROCESSING UNIT

APPENDIX 5. COMPUTER PROGRAMS

This appendix contains listings of the computer programs used in this study. All programs are written in the FORTRAN language. The program AFLUCT was written for a PDP 11 computer. Program CAVANA and CANVUM were written for a CDC Cyber 171 computer.

```

C*****
C      PROGRAM AFLUC1
C*****
C      THIS PROGRAM CALCULATES THE MEAN, STANDARD DEVIATION,
C      COEFFICIENT OF AMPLITUDE VARIATION, AND
C      AUTOCORRELATION FOR DATA READ FROM PAPER TAPE.
C      PROVISION IS MADE FOR 1 - 5 CHANNELS OF DATA.
C      A HIGH PASS FILTER WITH VARIABLE CUTOFF FREQUENCY
C      IS PROVIDED.
C
C      SET UP ARRAYS.
C          DIMENSION RLABEL(5),ILABEL(4),AD1(3),AD2(3)
C          DIMENSION DATA(5,5),CROS(5),CPRU(5,5),COV(5,5),IX(5)
C          DIMENSION RMEAN(5,5),SDS(5),CVS(5),RMX(5)
C          DIMENSION SDX(5),CVX(5),STD(5)
C
C      ENTER DATA INTO ARRAYS.
C          DATA RLABEL/#MEAN#,#SDVN#,#COVA#,#AUCC#,#PRCO#/
C          DATA ILABEL/# #,#F #,#S #,#RF#/
C          DATA AD1/#1#1 #,#1#2 #,#1#3 #/
C          DATA AD2/#1#2 #,#2#3 #,#3#1 #/
C
C      START HERE AT BEGINNING OF EACH TAPE.
1      CONTINUE
      REWIND 5
C
C      READ IN FILTER CONSTANT
      WRITE (6,300)
300     FORMAT (//# NUMBER POINTS IN FILTER#/)
      READ (6,3,1) IFLTR
301     FORMAT (I1)
      IFL1=IFLTR-1
C
C      READ IN NUMBER OF CHANNELS WITH DATA
      WRITE (6,302)
302     FORMAT (//#NUMBER OF CHANNELS WITH DATA#/)
      READ (6,3,3) NCH
303     FORMAT (I1)
C
C      SET ARRAY ELEMENTS = 0
      DO 3 I=1,NCH
          SDS(I)= .
          CVS(I)= -.
          CROS(I)=0.
          DO 3 J=1,IFLTR
              DATA(I,J)=0.0
              RMEAN(I,J)=.
3          COV(I,J)=0.
          EN=0.
          N=0
          ENF=IFLTR
C
C      READ IN TAPE ID AND NUMBER OF POINTS TO BE ANALYZED
C
      WRITE (6,7)
70     FORMAT (//# ID #/)
      READ (6,8)
80     FORMAT (X)
4      WRITE (6,71)
71     FORMAT (//# NUMBER OF POINTS (USE I3)#/)
      READ (6,81) INSP
81     FORMAT (I3)

```

```

C
C   SHIFT DATA THROUGH ARRAY. READ IN NEW DATA
C
5   CONTINUE
    DO 7 I=1,NCH
      DO 7 J=1,IFLT1
        K=IFLTR-J
7     DATA(I,K+1)=DATA(I,K)
      READ(5,101,END=19,ERR=19) (DATA(I,1),IX(1),DATA(2,1),
2     X(2),DATA(3,1),IX(3),DATA(4,1),IX(4),DATA(5,1),IX(5)
101  FORMAT(F5.0,I3,F7.3,I3,F7.3,I3,F7.3,I3)
C
C   TEST FOR END OF TAPE.
6     DO 8 I=1,NCH
      IF(DATA(I,1).EQ.0.) GO TO 13
C   TEST FOR BAD DATA
      IF(IX(1).NE.4.) GO TO 50
      IF(DATA(I,1).GT.1.98) GO TO 50
      IF(DATA(I,1).LT.0.065) GO TO 50
8     CONTINUE
      IF(N.GT.0) GO TO 16
C   PRINT FIRST DATA
      WRITE(6,100) (DATA(I,1),I=1,NCH)
100  FORMAT(11H FIRST DATA,I3,5F7.3)
16    N=N+1
      IF(N.LE.IFLT1) GO TO 5
C
C   COLLECT DATA INTO SUMS AND SUMS OF SQUARES AND PRODUCTS
C
      EN=EN+1
      DO 15 I=1,NCH
        RMX(I)=0.
        SDX(I)=0.
        DO 14 J=1,IFLTR
          RMEAN(I,J)=RMEAN(I,J)+DATA(I,J)
          SDX(I)=SDX(I)+(DATA(I,J)**2)
          RMX(I)=RMX(I)+DATA(I,J)
          COV(I,J)=COV(I,J)+(DATA(I,1)*DATA(I,J))
          CPRO(1,J)=CPRO(1,J)+DATA(1,J)*DATA(2,J)
          CPRO(2,J)=CPRO(2,J)+DATA(2,J)*DATA(3,J)
          CPRO(3,J)=CPRO(3,J)+DATA(3,J)*DATA(1,J)
14     CONTINUE
          RMX(I)=RMX(I)/ENF
          RMS=RMX(I)**2
          SDX(I)=SDX(I)/ENF
          SDX(I)=SDX(I)-RMS
          SDS(I)=SDS(I)+SDX(I)
          IF(RMS.EQ.0.) GO TO 15
          CVS(I)=CVS(I)+(SDX(I)/RMS)
15     CONTINUE
          IF(N.LT.INSP) GO TO 5
          GO TO 2
19    INSP=0

```

```

C   PROCESS DATA
20  CONTINUE
    WRITE(6,1) 200
102  FORMAT(1X,15,0H SAMPLES//)
    DO 23, I=0H
C   CALCULATE THE MEAN OF ALL BUT THE FIRST TWO DATA POINTS
    DO 30 J=1,IFLTR
      RMEAN(I,J)=RMEAN(I,J)/EN
30  CONTINUE
C   CALCULATE STANDARD DEVIATION FOR ALL BUT
C   THE FIRST FOUR DATA POINTS
      STD(I)=(COV(I,1)/EN)-(RMEAN(I,1)**2)
      STD(I)=SQRT(STD(I))
C   CALCULATE COEFFICIENT OF VAR. W/O FILTER FOR
C   ALL BUT FIRST FOUR POINTS
      RMX(I)=STD(I)/RMEAN(I,1)
C   FILTERED STANDARD DEVIATION
      SDX(I)=SQRT(SHS(I)/E)
C   FILTERED COEFFICIENT OF VARIATION
23  CVX(I)=SQRT(CVS(I)/EN)
    WRITE(6,104)
104  FORMAT(6H CHANNEL,6X,2H 1,8X,2H 2,8X,2H 3,8X,
2     2H 4,8X,2H 5/)
    WRITE(6,103) RLABEL(1),ILABEL(1),(RMEAN(I,1),I=1,NCH)
    WRITE(6,103) RLABEL(2),ILABEL(1),(STD(I),I=1,NCH)
    WRITE(6,103) RLABEL(3),ILABEL(3),(RMX(I),I=1,NCH)
    WRITE(6,103) RLABEL(2),ILABEL(2),(SDX(I),I=1,NCH)
    WRITE(6,103) RLABEL(3),ILABEL(4),(CVX(I),I=1,NCH)
103  FORMAT(1X,A5,A2,5F10.4)
C   CALCULATE AUTOCORRELATION FUNCTION  $X(I,1)*X(I,1)$ 
    DO 24 J=1,IFLTR
      DO 25 I=1,NCH
        RMX(I)=((COV(I,J)/EN)-(RMEAN(I,1)*RMEAN(I,J)))
2         /(STD(I)**2)
25  CONTINUE
    WRITE(6,103) RLABEL(4),ILABEL(3),(RMX(I=NC))
    CONTINUE
    IF(INSP.EQ.0) GO TO 1
    GO TO 4
C   IF ERRORS ARE PRESENT IN DATA, CONTROL COMES HERE
50  WRITE(6,201)N
    WRITE(6,99)DATA(1,1),IX(1),DATA(2,1),IX(2),DATA(3,1)
2    ,IX(3),DATA(4,1),IX(4),DATA(5,1),IX(5)
    READ(6,202)DATA(1,1),IX(1),DATA(2,1),IX(2),DATA(3,1)
2    ,IX(3),DATA(4,1),IX(4),DATA(5,1),IX(5)
    GO TO 6
99  FORMAT(1X,F5.3,I3,F7.3,I3,F7.3,I3,F7.3,I3,F7.3,I3/)
202  FORMAT(F5.3,I3,F7.3,I3,F7.3,I3,F7.3,I3,F7.3,I3)
201  FORMAT(6H ERROR,I5)
    END

```

```

*****
PROGRAM CAVANA (INPUT,OUTPUT)
*****
C
      REAL KP,KS,PHI,KT,KM,L,LF,MUP,MUS
      COMMON/A/ KP,KS,PHI,KT,KM,L,LF,MUP,MUS,ZS,RNG,PI
      COMMON/B/ CAV,CSIG,CPUMP
      KP=4.1691E4
      KS=4.1691E3
      DATA PHI,KT,KM /2.8E-12,179.0,22.9/
      PI = 3.14159265
C
C      THIS PROGRAM CALCULATES THE COEFFICIENT OF AMPLITUDE
C      VARIATION FOR SIGNAL,PUMP, AND USB WAVES USING ANALYTICAL
C      EXPRESSIONS DISCUSSED IN CHAPTERS 3 AND 4.
C      THE TURBULENCE PARAMETERS ARE VARIED WITH
C      POSITION IN THE TANK.
C      AN APERTURE CORRECTION FACTOR IS USED TO COM-
C      PENSATE FOR THE FINITE SIZE OF THE HYDROPHONE.
C
C      SET RANGE AT RNG=0.75M AND VARY THE ARRAY LENGTH.
C
      RNG=0.75
C      PRINT HEADING FOR RESULTS OBTAINED WITH FIXED RANGE.
      PRINT 1)
10      FORMAT (/,16X, #THE FOLLOWING ARE FOR RANGE=0.75 M#)
      PRINT 2)
20      FORMAT (/,22X, #L#,10X, #CPUMP#,10X, #CAVUSB#)
C      VARY ARRAY LENGTH IN INCREMENTS OF 0.05M.
      DO 30 I=1,14
      RI = I
      L = RI* 0.05
      ZS = RNG-L
C      CALCULATE CAV FOR PUMP,USB,AND SIGNAL WAVES.
      CALL CAVSUB
      PRINT 21,L,CPUMP,CAV
21      FORMAT (/,16X,F8.2,2F15.6)
30      CONTINUE
C
C      SET ARRAY LENGTH AT L=0.1M AND VARY RANGE.
C
      PRINT 11
11      FORMAT (////, # THE FOLLOWING ARE FOR L = 0.1 M#)
C      PRINT HEADINGS FOR THESE RESULTS.
      PRINT 25
25      FORMAT (/,20X, #RANGE#,8X, #CSIG#,12X, #CAV#)
      L = 0.1
C      VARY RANGE IN INCREMENTS OF 0.1M.
      DO 31 I=1,24
      RI = I
      RNG= RI* 0.1+0.1
      ZS = RNG-L
C      CALCULATE CAV FOR PUMP,USB,AND SIGNAL WAVES.
      CALL CAVSUB
      PRINT 21,RNG,CSIG,CAV
21      CONTINUE
31      CONTINUE
C      SET ARRAY LENGTH AT L=0.5M AND VARY RANGE.

```

```

C
      PRINT 111
111      FORMAT (////, ' THE FOLLOWING ARE FOR L = 0.5 M')
C PRINT HEADINGS FOR THESE RESULTS.
      PRINT 125
125      FORMAT (/,'20X,'RANGE',BX,'CSIG',12X,'CAV')
      L = 0.5
C VARY RANGE IN INCREMENTS OF 0.1M.
      DO 131 I=1,20
      RI = I
      RNG= RI* 0.1+0.5
      ZS = RNG-L
C CALCULATE CAV FOR PUMP,USB,AND SIGNAL WAVES.
      CALL CAVSUB
      PRINT 21,RNG,CSIG,CAV
131      CONTINUE
      END

```

```

C*****
      SUBROUTINE CAVSUB
C*****
C
C THIS SUBROUTINE CALCULATES THE COEFFICIENT OF AMPLITUDE
C VARIATION FOR PUMP,SIGNAL,AND USB WAVES, AND RETURNS
C THEIR VALUES TO PROGRAM CAVANA.
C
      REAL KP,KS,PHI,KT,KM,L,LF,MUP,MUS
      COMMON/A/ KP,KS,PHI,KT,KM,L,LF,MUP,MUS,ZS,RNG,PI
      COMMON/B/ CAV,CSIG,CPUMP
C VARY TURBULENCE PARAMETERS WITH POSITION IN TANK.
C AUXP1,AUXP2,AUXP3 ARE BOOK-KEEPING VARIABLES, KM
C AND KT ARE SPATIAL WAVENUMBERS. PHI IS A TURBULENCE
C PARAMETER, AS ARE CNS AND CNP, WHICH ARE FOR SIGNAL
C AND PUMP WAVES, RESPECTIVELY.
C
C VARY MU WITH POSITION IN TANK
      MUP=(1.5249*(L/2.+0.1)+0.8323)*2.1E-5
      MUS=(1.5249*((ZS+L)/2.+0.1)+0.8323)*2.1E-5
      AUXP1=0.105+(RNG/2.)
      AUXP2=1.695-(RNG/2.)
      AUXP3=(12.44+(1./AUXP1)+(1./AUXP2))
      KM=(PI/2.)*AUXP3
      PHI1=PHI*(4.7854)*KM**(-0.5)
      KT1=KT*SQRT(KM/22.9)
      CNS=MUS/SQRT(.33*PI*KT1**(-2./3.))
      AUXP1=0.105+(L/2.)
      AUXP2=1.695-(L/2.)
      AUXP3=(12.44+(1./AUXP1)+(1./AUXP2))
      KM=(PI/2.)*AUXP3
      KT1=KT*SQRT(KM/22.9)
      CNP=MUP/SQRT(.33*PI*KT1**(-2./3.))
C CALCULATE COEFFICENTS FOR FLUCTUATION TERMS.
      A1 = 0.31*CNP**2.*KP**(7./6.)
      A2 = 0.13*CNS**2.*KS**(7./6.)
      A3 = (PI/480.)*PHI1*(KT1**4.-KM**4.)
C CALCULATE THE LOW FREQ COMPONENT, LF, OF THE

```

```

C  AMPLITUDE FLUCTUATIONS IN THE USR WAVE.
  T1=A2*ZS**(11./6.)
  T2=3.*A3*ZS**3.
  A=T1+T2
  T3=(11./6.)*A2*ZS**(5./6.)
  T4=3.*A3*ZS**2.
  B=T3+T4
  T5=(A+B*L)**(3./2.)-A**(3./7.)
  LF=(1./L**2.)*(4./(9.*B**2.))*T5**2.
C  CALCULATE CAV FOR THE PUMP WAVE.  AN APERTURE FACTOR
C  IS USED TO ACCOUNT FOR FINITE SIZE OF HYDROPHONE.
  CPUMP = 0.31*CNP**2.*KP**(7./6.)*L**(11./4.)
  HF=(0.4922/0.31)*CPUMP
  CAVSQ = LF + HF
  APFAC1 = 1. - (9.9613E-2/SQRT(L))
  APFAC2 = 1. - (1.0447E-1/SQRT(L))

  CAV = SQRT(CAVSQ*APFAC2)
  CPUMP = SQRT(CPUMP*APFAC1)
  CSIG = 0.13*CNS**2.*KS**(7./6.)*RNG**(11./6.)
  CSIG = CSIG+((PI/480.)*PHI1*(KT1**4.-KM**4.)
  2      *RNG**3.)
  CSIG = SQRT(CSIG)
  RETURN
  END

```

```

C*****
C          PROGRAM CAVNUM (INPUT,OUTPUT)
C*****
C
C   THIS PROGRAM CALCULATES THE MEAN SQUARE AMPLITUDE
C   FLUCTUATIONS IN THE SIDEBAND PRESSURE FOR A PARAMETRIC
C   RECEIVER, WHERE THE HYDROPHONE IS IN THE NEARFIELD OF
C   THE PUMP TRANSDUCER.  A NUMERICAL INTEGRATION IS USED.
C
C   THIS VERSION OF THE PROGRAM IS USED TO COMPUTE CAVPR
C   FOR AN ARRAY LENGTH L=0.1M AND VARIABLE RANGE.  SIMILAR
C   VERSIONS OF CAVNUM ARE USED FOR L=0.5M AND VARIABLE
C   RANGE, AND FOR FIXED RANGE AND VARIABLE ARRAY LENGTH.
C
C   SET UP INITIAL VALUES AND CONSTANTS.  KS,KP,AND KUSB ARE
C   SIGNAL,PUMP, AND USB WAVENUMBERS.  AL IS ARRAY LENGTH.
C   CNP AND MUP ARE TURBULENCE PARAMETERS IN THE INTERACTION
C   REGION.  CNS,MU,KM,KT, AND PHI ARE TURBULENCE PARAMETERS
C   IN THE CENTRE OF THE TANK.
C
      REAL L,KS,KP,KUSB,KM,KT,MU,MUP
      REAL IMKI1,IMKI2
      COMPLEX C1,C2,VUSB,KZ,AUX1,AUX2,AUX3,RINT
      COMMON/A/AL(2),Z1(1),Z2(1)
      COMMON/B/CNP,KP,CNS,KS,PHI,KT,KM,PI,MU,ZS,A,AP
      COMMON/C/KT1,PHI1,A1,A2,A3,A4,A5,L,I,J,K,M,N,MUP,RBL
      COMMON/D/KUSB,A11,AUSB,AS,A44,B1B2,S1S2,H1S2,S1B2
      DIMENSION Y1(10),SUMZ1(10),SUMR1(10),SRL(10),SIM(10)
      DIMENSION Z(1),RNG(1)
      DATA CNP,KP /1.162E-4,4.169E4/
      DATA CNS,KS /1.9594E-4,4.1691E3/
      DATA PHI,KT,KM /2.8E-12,179.0,22.9/
      PI = 3.14159265
      KUSB=4.586E4
C   FILL ARRAYS WITH ZEROS AS INITIAL VALUES.
      DATA SUMR1,AL,Z /30*0.0/
      DATA Z1,Z2,Y1,SUMZ1 /4 *0./
C   AR AND HR ARE THE CHARACTERISTIC RADII OF THE PUMP
C   TRANSDUCER AND HYDROPHONE, RESPECTIVELY.
      AR=0.005
      HR=1.128E-3
C   L-RLIM IS THE UPPER LIMIT OF INTEGRATION.
      RLIM=0.001
C   AP IS THE EFFECTIVE PATCH SIZE.
      AP=1.41E-2
C   Z(1),Z1(1),Z2(1) ARE LOWER LIMITS OF INTEGRATION.
      Z(1)=1.E-8
      Z1(1)=1.E-8
      Z2(1)=1.E-8
C   PRINT HEADING FOR RESULTS.
      PRINT 30
30      FORMAT(/,5X,#CPR#,12X,#RANGE#,15X,#ZS#,15X,#L#)
C
C   VARY RANGE WITH ARRAY LENGTH CONSTANT AT 0.1M:

```

```

C
      DRNG=0.2
      AL(1)=0.1
      RNG(1)=.2
      DO 97 N=1,10
C
C   CALCULATE HOMOGENEOUS USB SIGNAL, VUSB, AT THE
C   HYDROPHONE OUTPUT.
C
      H=(AL(1)-RLIM)/8.
      L=AL(1)
      ZS=RNG(N)-L
C   VARY TURBULENCE PARAMETERS WITH POSITION IN TANK
      MU=(1.5249*((ZS+L)/2.+0.1)+0.8323)*2.1E-5
      MUP=(1.5249*(L/2.+0.1)+0.8323)*2.1E-5
      AUXP1=0.105+(ZS+L)/2.
      AUXP2=1.695-(ZS+L)/2.
      AUXP3=(12.44+1./AUXP1+1./AUXP2)
      KM=(PI/2.)*AUXP3
      PHI1=PHI*(4.7854)*KM**(-0.5)
      KT1=KT*SQRT(KM/22.9)
      CNS=MU/SQRT(0.33*PI*KT1**(-2./3.))
      AUXP1=0.105+L/2.
      AUXP2=1.695-L/2.
      AUXP3=(12.44+1./AUXP1+1./AUXP2)
      KM=(PI/2.)*AUXP3
      KT1=KT*SQRT(KM/22.9)
      CNP=MUP/SQRT(0.33*PI*KT1**(-2./3.))
C   CALCULATE COEFFICIENTS FOR FLUCTUATION TERMS.
      A1 = 0.31*CNP**2.*KP**(7./6.)
      A2 = 0.13*CNS**2.*KS**(7./6.)
      A3 = (PI/480.)*PHI1*(KT1**4.-KM**4.)
      A4=2.5E-2*KP**2*MUP**2
      A5=1.25E-2*KS**2*MU**2
C   INTEGRATE HOMOGENEOUS PRESSURE USING SIMPSON'S RULE.
      DO 50 I=1,9
C
C   CALCULATE C1 AND C2. AX,AUX ARE AUXILARY VARIABLES.
      AX1=(KP*(AR**2.))/(2.*Z(I))
      AUX1=CMPLX(1.0,AX1)
      AX2=(KUSB*(HR**2.))/(2.*(L-Z(I)))
      AUX2=CMPLX(1.0,AX2)
      AX3=(4.*Z(I)*(L-Z(I)))/((HR**2.)*(AR**2.))
      C2=AX3*AUX1*AUX2
      AX1=((KP**2.)*(AR**2.))/(4.*(Z(I)**2.))
      AUX1=AX1/AUX1
      AX2=((KUSB**2.)*(HR**2.))/(4.*(L-Z(I))**2.)
      AUX2=AX2/AUX2
      AX3=(KP/(2.*Z(I)))+(KUSB/(2.*(L-Z(I))))
      AUX3=CMPLX(0.,AX3)
      C1=AUX3+AUX1+AUX2
C   CALCULATE REAL AND IMAGINARY PARTS OF INTEGRAND. RINT
      RINT=1./(C1*C2)
      SRL(I)=REAL(RINT)
      SIM(I)=AIMAG(RINT)
C   INCREMENT Z(I) BY H.
      Z(I+1)=Z(I)+H
50   CONTINUE

```

```

C PERFORM INTEGRATION. CALCULATE REAL AND IMAGINARY PARTS
C SEPARATELY.
      I      *SRL(4)*.4.*SRL(5)*.4.*SRL(6)*.4.*SRL(7)*.4.*SRL(8)*SRL(9)
      I      *SRL(15)*.4.*SRL(16)*.4.*SRL(17)*.4.*SRL(18)*SRL(19)
      VUSH=CMPLX(RI,RT)
C
C DETERMINE MAGNITUDE, RMAG, AND PHASE OF VUSB.
      RMAG=CABS(VUSB)
      PHASE=ATAN2(AIMAG(VUSB),REAL(VUSB))
C
C
C INTEGRATE OVER THE ARRAY; Z1,Z2=N TO Z1,Z2=(L-RLIM)
C IN STEPS OF H.
      DO 100 J=1,9
      DO 101 I=1,9
C
C
C CALCULATE ARGUMENT, K(Z), OF HOMOGENEOUS PRESSURE
C
C CALCULATE C1,C2 FOR Z1.
      AX1=(KP*(AR**2.))/(2.*Z1(I))
      AUX1=CMPLX(1.,AX1)
      AX2=(KUSB*(HR**2.))/(2.*(L-Z1(I)))
      AUX2=CMPLX(1.,AX2)
      AX3=(4.*Z1(I)*(L-Z1(I)))/((HR**2.)*(AR**2.))
      C2=AX3*AUX1*AUX2
      AX1=(KP**2.)*(AR**2.)/(4.*(Z1(I)**2.))
      AUX1=AX1/AUX1
      AX2=((KUSB**2.)*(HR**2.))/(4.*(L-Z1(I))**2.)
      AUX2=AX2/AUX2
      AX3=(KP/(2.*Z1(I)))+(KUSB/(2.*(L-Z1(I))))
      AUX3=CMPLX(0.,AX3)
      C1=AUX3+AUX1+AUX2
C CALCULATE K(Z) FOR Z1.
      KZ=CMPLX(COS(PHASE),-SIN(PHASE))
      KZ=KZ/(C1*C2)
      REK1=REAL(KZ)
      IMK1=AIMAG(KZ)
C CALCULATE C1,C2 FOR Z2.
      AX1=(KP*(AR**2.))/(2.*Z2(J))
      AUX1=CMPLX(1.,AX1)
      AX2=(KUSB*(HR**2.))/(2.*(L-Z2(J)))
      AUX2=CMPLX(1.,AX2)
      AX3=(4.*Z2(J)*(L-Z2(J)))/((HR**2.)*(AR**2.))
      C2=AX3*AUX1*AUX2
      AX1=(KP**2.)*(AR**2.)/(4.*(Z2(J)**2.))
      AUX1=AX1/AUX1
      AX2=((KUSB**2.)*(HR**2.))/(4.*(L-Z2(J))**2.)
      AUX2=AX2/AUX2
      AX3=(KP/(2.*Z2(J)))+(KUSB/(2.*(L-Z2(J))))
      AUX3=CMPLX(0.,AX3)
      C1=AUX3+AUX1+AUX2

```

```

C  CALCULATE K(Z) FOR Z2.
      KZ=CMPLX(COS(PHASE),-SIN(PHASE))
      KZ=(KZ)/(C1*C2)
      REKI2=REAL(KZ)
      IMKI2=AIMAG(KZ)

C
C
C  CALCULATE CONTRIBUTION OF AMPLITUDE FLUCTS
      CALL B1B2SR
      BB=B1B2*REKI1*REKI2

C
C  CALCULATE CONTRIBUTION OF PHASE FLUCTS
      CALL S1S2SR
      SS=S1S2*IMKI1*IMKI2

C
C  CALCULATE CONTRIBUTION OF AMP-PHASE CORR
      CALL B1S2SR
      BS=REKI1*IMKI2*B1S2

C
C  CALCULATE CONTRIBUTION OF PHASE-AMP CROSS CORR
      CALL S1B2SR
      SB=REKI2*IMKI1*S1B2
C  COMPUTE INTEGRAND.
      Y1(I)=BB+BS+SB+SS

C
C  INCREMENT Z1 BY H.
103   CONTINUE
      Z1(I+1) = Z1(I) + H
101   CONTINUE

C
C  INCREMENT Z2.
      1   +Y1(5)*2.+4.*Y1(6)+2.*Y1(7)+4.*Y1(8)+1(9))
      Z2(J+1)=Z2(J) + H
100   CONTINUE

C
C  INTEGRATE OVER VARIABLE Z2.STORE RESULT IN SUMZ2.
      SUMZ2=(H/3)*(SUMZ1(1)+4*SUMZ1(2)+2*SUMZ1(3)+4*SUMZ1(4)+
1      +4.*SUMZ1(8)+SUMZ1(9))

C
C  CALCULATE RESULT OF NUMERICAL INTEGRATION
      SUMZ2=SUMZ2/RMAG**2.

C
C  CALCULATE THE CONTRIBUTION OF SOURCE WAFERS FROM
C  Z=(L-RLIM) TO Z=L. THE HYDROPHONE IS IN THE EXTREME
C  NEARFIELD OF THESE WAFERS, SO THEIR RADIATION IS APPROX-
C  IMATED BY PLANE WAVES OF INFINITE EXTENT.
      T1=A2*(ZS+L)**(11./6.)
      T2=A3*(ZS+L)**3.
      B1=(RLIM**2./L**2)*(T1+T2)
      T3=L**(23./12.)-(L-RLIM)**(23./12.)

```

```

T4=0.2722*T3**2.+0.2722*RL1M**23./6)
T4=T4+2*0.2722*RL1M**23./12.)*T3**2.
B2=(A1/L**2.)*T4
BSQ=B1+B2
C SUM THE NUMERICAL AND ANALYTICAL RESULTS.
CPRSQ=SUMZ2+BSQ
C
C CORRECT FOR THE EFFECT OF FINITE APERTURE AT THE HYROPHONE.
C
APFAC =1.-(0.10423/SQRT(L/2.))
CPRSQ=CPRSQ*APFAC
C
C CALCULATE THE MEAN-SQ AMPLITUDE FLUCTS,CPR,IN THE
C SIDEBAND PRESSURE AT Z=L. PRINT THE RESULT.
C
CPR=SQRT(CPRSQ)
PRINT 31, CPR,RNG(N),ZS,L
FORMAT(/,E12.4,F14.4,7X,F16.4,F16.4)
31 INCREMENT THE RANGE.
79 CONTINUE
RNG(N+1)=RNG(N)+DRNG
97 CONTINUE
END
C
C
C*****
C END OF MAIN PROGRAM
C*****
C
C
C CONTRIBUTIONS FROM THE CORRELATION TERMS B1B2,B1S2,S1B2,S1S2.
C
C*****
SUBROUTINE B1B2SR
C*****
C
C CALCULATE B1B2,THE AMPLITUDE FLUCT CORR TERM.
C
REAL L,KS,KP,KUSB,KM,KT,MU,MUP
REAL LCOR1,LCOR2,LCOR3,LCOR4
COMMON/A/AL(20),Z1(10),Z2(10)
COMMON/B/CNP,KP,CNS,KS,PHI,KT,KM,PI,MU,ZS,A,AP
COMMON/C/KT1,PHI1,A1,A2,A3,A4,A5,L,I,J,K,M,N,MUP,RBL
COMMON/D/KUSB,A11,AUSB,AS,A44,B1B2,S1S2,B1S2,S1B2
A1 = 0.31*CNP**2.*KP**(7./6.)
AUSB=0.31*CNP**2.*KUSB**(7./6.)
A11=SQRT(A1*AUSB)
T1 = (Z1(I)*(AL(1)-Z2(J)))*(11./12.)
T2 = (Z2(J)*(AL(1)-Z1(I)))*(11./12.)
T3 = (Z1(I)*Z2(J))*(11./12.)
T4 = ((AL(1)-Z1(I))*(AL(1)-Z2(J)))*(11./12.)

```

C
C
C
C
C
C

ACCOUNT FOR LONGITUDINAL CORRELATION OF HIGH FREQ FLUCTS
THERE ARE FOUR SEPARATE TERMS FOR THE DIFFERENT
GEOMETRIES. ALSO THERE ARE TWO VERSIONS OF EACH
TERM FOR Z1 GT Z2 OR Z2 GT Z1.

```

      IF (Z2(J).GT.Z1(I)) GO TO 201
      DELZ1=Z1(I)-Z2(J)
      LCOR1=(1.+3.*DELZ1)/(2.*Z2(J))
      LCOR1=LCOR1/((1.+DELZ1/Z2(J))**(3./2.))
      DELZ2=AL(I)-Z2(J)
      LCOR2=(1.+3.*DELZ2)/(2.*Z2(J))
      LCOR2=LCOR2/((1.+DELZ2/Z2(J))**(3./2.))
      DELZ3=Z1(I)-Z2(J)
      LCOR3=(1.+3.*DELZ3)/(2.*(AL(I)-Z1(I)))
      LCOR3=LCOR3/((1.+DELZ3/(AL(I)-Z1(I)))*(3./2.))
      DELZ4=AL(I)-Z1(I)
      LCOR4=(1.+3.*DELZ4)/(2.*Z1(I))
      LCOR4=LCOR4/((1.+DELZ4/Z1(I))**(3./2.))
      GO TO 2 2
201  CONTINUE
      DELZ1=Z2(J)-Z1(I)
      LCOR1=(1.+3.*DELZ1)/(2.*Z1(I))
      LCOR1=LCOR1/((1.+DELZ1/Z1(I))**(3./2.))
      DELZ2=AL(I)-Z1(I)
      LCOR2=(1.+3.*DELZ2)/(2.*Z1(I))
      LCOR2=LCOR2/((1.+DELZ2/Z1(I))**(3./2.))
      DELZ3=Z2(J)-Z1(I)
      LCOR3=(1.+3.*DELZ3)/(2.*(AL(I)-Z2(J)))
      LCOR3=LCOR3/((1.+DELZ3/(AL(I)-Z2(J)))*(3./2.))
      DELZ4=AL(I)-Z2(J)
      LCOR4=(1.+3.*DELZ4)/(2.*Z2(J))
      LCOR4=LCOR4/((1.+DELZ4/Z2(J))**(3./2.))
202  CONTINUE
      DELZ=ABS(Z1(I)-Z2(J))
      RBL=1./((1.+((2.*DELZ)/(KS*AP**2.))**2.))
      TB1=A11*(T1*LCOR2+T2*LCOR4)+A11*T3*LCOR1+A11SB*T4*LCOR3
C    CALCULATE LOW FREQ AMP FLUCTS
      A2 = 0.13*CNS**2.*KS**(7./6.)
      A3 = (PI/480.)*PHI1*(KT1**4.-KM**4.)
      T1 = A2*(ZS+Z1(I))**(11./6.)
      T2 = A3*(ZS+Z1(I))**3.
      T3 = A2*(ZS+Z2(J))**(11./6.)
      T4 = A3*(ZS+Z2(J))**3.
      TB2 = SQRT((T1+T2)*(T3+T4))
      TB2=TB2*RBL
      B1B2=TB1+TB2
      RETURN
      END

```

C
C

```

C*****
SUBROUTINE SIS2SR
C*****
C
C CALCULATE SIS2, THE PHASE FLUCTUATION CORR. TERM.
C
REAL L,KS,KP,KUSB,KM,KT,MU,MUP
REAL LCOR1,LCOR2,LCOR3,LCOR4
COMMON/A/AL(20),Z1(10),Z2(10)
COMMON/B/CNP,KP,CNS,KS,PHI,KT,KM,PI,MU,ZS,A,AP
COMMON/C/KT1,PHI1,A1,A2,A3,A4,A5,L,I,J,K,M,N,MUP,RBL
COMMON/D/KUSH,A11,A13B,AS,A44,B1B2,S1S2,B1S2,S1B2
A4=2.5E-2*KP**2*MUP**2
AS=2.5E-2*KUSB**2.*MUP**2.
A44=SQRT(A4*AS)
T1=SQRT(Z1(I)*(L-Z2(J)))
T2=SQRT(Z2(J)*(L-Z1(I)))
T3=SQRT(Z1(I)*Z2(J))
T4=SQRT((L-Z1(I))*(L-Z2(J)))
C ACCOUNT FOR LONGITUDINAL CORRELATION OF HIGH FREQ FLUCTS
IF(Z2(J).GT.Z1(I))GO TO 203
DELZ1=Z1(I)-Z2(J)
LCOR1=1.+((2.*DELZ1)/(KP*AP**2))**2
LCOR1= 1./((LCOR1*SQRT(1.+DELZ1/Z2(J)))
DELZ2=L-Z2(J)
LCOR2=1.+((2.*DELZ2)/(KP*AP**2))**2
LCOR2= 1./((LCOR2*SQRT(1.+DELZ2/Z2(J)))
DELZ3=Z1(I)-Z2(J)
LCOR3=1.+((2.*DELZ3)/(KP*AP**2))**2
LCOR3= 1./((LCOR3*SQRT(1.+DELZ3/(L-Z1(I))))
DELZ4=L-Z1(I)
LCOR4=1.+((2.*DELZ4)/(KP*AP**2))**2
LCOR4= 1./((LCOR4*SQRT(1.+DELZ4/Z1(I)))
GO TO 204
203 CONTINUE
DELZ1=Z2(J)-Z1(I)
LCOR1=1.+((2.*DELZ1)/(KP*AP**2))**2
LCOR1= 1./((LCOR1*SQRT(1.+DELZ1/Z1(I)))
DELZ2=L-Z1(I)
LCOR2=1.+((2.*DELZ2)/(KP*AP**2))**2
LCOR2= 1./((LCOR2*SQRT(1.+DELZ2/Z1(I)))
DELZ3=Z2(J)-Z1(I)
LCOR3=1.+((2.*DELZ3)/(KP*AP**2))**2
LCOR3= 1./((LCOR3*SQRT(1.+DELZ3/(L-Z2(J))))
DELZ4=L-Z2(J)
LCOR4=1.+((2.*DELZ4)/(KP*AP**2))**2
LCOR4= 1./((LCOR4*SQRT(1.+DELZ4/Z2(J)))
204 CONTINUE
SSHI=A44*(T1*LCOR2+T2*LCOR4)+A4*T3*LCOR1
+ A4*T3*LCOR1
C CALCULATE LOW FREQ PHASE FLUCTS
A5=1.25E-2*KS**2*MU**2
T5=A5*SQRT((ZS+Z1(I))*(ZS+Z2(J)))
T5=T5*RBL
D1=(4.*ZS+Z1(I))/(KS*AP**2.)
D2=(4.*ZS+Z2(J))/(KS*AP**2.)

```

```

T5=SQRT((1.+D1*ATAN(D1))*(1.+D2*ATAN(D2)))*T5
S1S2=SS*J+T5
RETURN
END

```

C
C

```

C*****
SUBROUTINE B1S2SR
C*****
C
C CALCULATE B1S2, THE AMPLITUDE-PHASE FLUCT CROSS-CORR
C
REAL L,KS,KP,KUSB,KM,KT,MII,MUP
COMMON/A/AL(20),Z1(10),Z2(10)
COMMON/B/CNP,KP,CNS,KS,PHI,KT,KM,PI,KU,ZS,A,AP
COMMON/C/KT1,PHI1,A1,A2,A3,A4,A5,L,I,J,K,M,N,MUP,RBL
COMMON/D/KUSB,A11,AUSH,AS,A44,B1B2,S1S2,H1S2,S1B2
TB1=SQRT(A2*(ZS+Z1(I))**(11./6.))*A3*(ZS+Z1(I))**3.)
TS1=SQRT(A5*(ZS+Z2(J)))
D2=(4.*ZS+Z2(J))/(KS*AP**2.)
TS1=TS1*SQRT(1.+D2*ATAN(D2))
T1=TB1*TS1
TB2=SQRT(A1*Z1(I))**(11./6.)
TS2=SQRT(A4*Z2(J))
T2=TB2*TS2
TB3=SQRT(A1*Z1(I))**(11./6.)
TS3=SQRT(AS*(L-Z2(J)))
T3=TB3*TS3
TB4=SQRT(AUSB*(L-Z1(I))**(11./6.))
TS4=SQRT(A4*Z2(J))
T4=TB4*TS4
TB5=SQRT(AUSB*(L-Z1(I))**(11./6.))
TS5=SQRT(AS*(L-Z2(J)))
T5=TB5*TS5
B1S2=T1+T2+T3+T4+T5
C ACCOUNT FOR LONGITUDINAL CORRELATION OF FLUCTS
B1S2=B1S2*0.6
RETURN
END

```

C
C

```

C*****
SUBROUTINE S1B2SR
C*****
C
C CALCULATE S1B2, THE AMPLITUDE-PHASE FLUCT CROSS-CORR
C
REAL L,KS,KP,KUSB,KM,KT,MII,MUP
COMMON/A/AL(20),Z1(10),Z2(10)

```

```

COMMON/HZ,CNP,KP,CNS,KS,PHI,PI,KM,PI,MD,ZS,A,AP
COMMON/CZ,FI,PHI1,A1,AP,AB,AC,AD,AE,AF,AG,AH,AI,AM,AN,AO,AP,AQ,AR,AS,AT,
COMMON/D,K,LSB,A11,AUSH,AL,AM,AN,AO,AP,AQ,AR,AS,AT,AV,AW,AX,AY,AZ,
TB1=SQRT(A2*(ZS+Z1(I))**2+(A1**2)*Z1(I)**3.)
TS1=SQRT(A5*(ZS+Z1(I)))
DI=(4.*ZS+Z1(I))/(KS*AP**2.)
TS1=TS1*SQRT(1.+DI*ATAN(DI))
T1=TB1*TS1
TB2=SQRT(A1*Z2(I)**(11./6.))
TS2=SQRT(A4*Z1(I))
T2=TB1*TB2
TB3=SQRT(AUSH*(L-Z2(I))**(.11./21.))
TS3=SQRT(A4*Z1(I))
T3=TB3*TS3
TB4=SQRT(A1*Z2(I)**(11./6.))
TS4=SQRT(A5*(L-Z1(I)))
T4=TB4*TS4
TB5=SQRT(AUSH*(L-Z2(I))**(.11./21.))
TS5=SQRT(A5*(L-Z1(I)))
T5=TB5*TS5
SIB2=T1+T2+T3+T4+T5
C ACCOUNT FOR LONGITUDINAL CORRELATION OF RESULTS
SIB2=SIB2*0.6
RETURN
END

```

APPENDIX 6. ANALYSIS OF THE NEARFIELD PARAMETRIC RECEIVER

In developing a theoretical analysis for the nearfield parametric receiver, it was assumed in Section 4.2 that the pump wave could be approximated as a collimated plane wave. In evaluating the integrals arising from this assumption (see Appendix 2), no account was made of the effect of the finite radius of the pump transducer. Consequently, the phase of the integrand of Eq. (4.19) was such that only the amplitude correlation term $\langle B_1 B_2 \rangle$ contributed to the amplitude fluctuations $\langle B_{PR}^2 \rangle$ of the second-order pressure wave, as shown in Eq. (4.20). A more detailed analysis, based on the work of Chotiros,¹⁰⁶ is presented in this appendix. It will be shown that there are additional contributions to $\langle B_{PR}^2 \rangle$ when the finite radius of the pump transducer is taken into account.

A6.1 Second-Order Solution for a Homogeneous Medium

The geometry for this analysis is shown in Fig. A6.1. As in the analysis of Chapter 4, the source of the signal to be detected by the parametric receiver is located at $z = -Z_s$. The signal source is situated sufficiently far from the pump that the signal pressure wave, p_s , is assumed to be planar in the vicinity of the parametric receiver. Omitting the time dependence, the signal wave may be represented by

$$p_s(z) = P_s e^{-jk_s z}, \quad (A6.1)$$

where the symbols are defined in connection with Eq. (4.1).

The pump transducer is approximated by a plane wave having a Gaussian shaded transverse amplitude function; i.e., the pressure amplitude at a point (ρ, θ_p) on the face of the pump transducer is assumed to be given by

$$P_p(\rho, \theta_p) = P_o e^{-(\rho^2/b^2)}, \quad (A6.2)$$

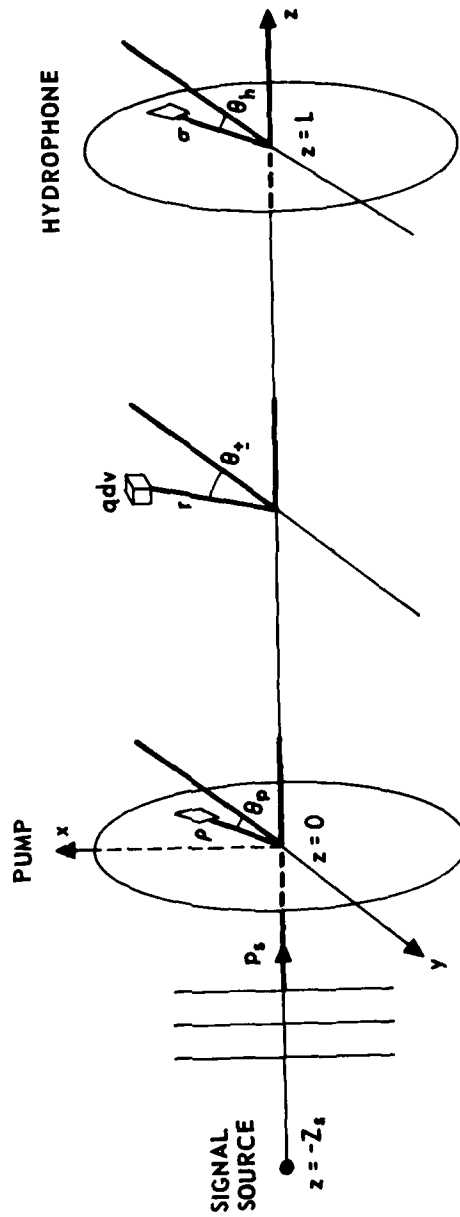


FIGURE A6.1
MODEL OF THE NEARFIELD PARAMETRIC RECEIVER

where

ρ and θ_p are coordinates on the face of the transducer, as shown in Fig. A6.1,

P_o is the pressure amplitude at the center of the transducer, and b is the characteristic radius of the transducer.

The pump signal at some point (r, θ_{\pm}, z) in the interaction region is the sum of contributions from all elemental surfaces on the face of the piston, and can be shown to be

$$p_p(r, \theta_{\pm}, z) \doteq P_o \int_0^{2\pi} \int_0^{\infty} \frac{1}{z} \exp \left[-\left(\frac{\rho}{b} \right)^2 - jk_p \left(z + \frac{R}{2z} \right) \right] d\theta_p \rho d\rho \quad (\text{A6.3})$$

where $R = r^2 + \rho^2 - 2r\rho \cos(\theta_{\pm} - \theta_p)$, and it is assumed that $R \ll z$.

The second-order pressure at a point (σ, θ_h, L) on the face of the hydrophone can be found from Eq. (2.7) to be

$$p_{\pm}(\sigma, \theta_h, L) = \int_0^{\infty} \int_0^{2\pi} \int_0^L \frac{-j\omega_{\pm}^2 \rho_o}{4\pi(L-z)} q_{\pm}(r, \theta_{\pm}, z) \times \exp \left\{ -jk_{\pm} \left[L - z + \frac{R'}{2(L-z)} \right] \right\} r dr d\theta_{\pm} dz, \quad (\text{A6.4})$$

where

$$q_{\pm} = \frac{j\beta P_s P_o \omega_{\pm}}{\rho_o c_o} e^{-jk_{\pm} z} \int_0^{2\pi} \int_0^{\infty} e^{-\rho^2/b^2} \exp \left\{ \frac{-jk_p R}{2z} \right\} d\theta_p \rho d\rho, \quad \text{and}$$

$$R' = r^2 + \sigma^2 - 2r\sigma \cos(\theta_h - \theta_{\pm})$$

It is also assumed that the voltage response of the hydrophone has Gaussian shading in the transverse dimension, so that

$$M(\sigma, \theta_h) = M_o \exp(-\sigma^2/h^2),$$

where M is the voltage response in V/Pa, and

M_0 is the voltage response at the center of the hydrophone. The voltage produced at the hydrophone by the second-order pressure at $z = L$ will therefore be

$$v_H = M_0 \int_0^\infty \int_0^{2\pi} p_{\pm}(\sigma, \theta_h, L) \exp(-\sigma^2/h^2) \sigma d\sigma d\theta_h \quad (A6.5)$$

Substitution of Eq. (A6.4) for p_{\pm} allows the hydrophone voltage to be written as

$$v_H = A \int_0^\infty \int_0^{2\pi} \int_0^L \frac{1}{z(L-z)} I_1 I_2 \exp\left\{-jr^2 \left[\frac{k_p}{2z} + \frac{k_{\pm}}{2(L-z)}\right]\right\} r dr d\theta_{\pm} dz \quad (A6.6)$$

where $A = \frac{\omega_{\pm}^2 M_0 \beta P_s P_o}{4\pi \rho_o c_o^4} e^{-jk_{\pm}L}$,

$$I_1 = \int_0^{2\pi} \int_0^\infty \exp\left[-\left(\frac{\rho}{b}\right)^2 - jk_p \frac{\rho^2 - 2r\rho\cos\psi}{2z}\right] \rho d\rho d\psi \quad ,$$

$$I_2 = \int_0^{2\pi} \int_0^\infty \exp\left[-\left(\frac{\sigma}{h}\right)^2 - jk_{\pm} \frac{\sigma^2 - 2r\sigma\cos\phi}{2(L-z)}\right] \sigma d\sigma d\phi \quad ,$$

$$\psi = \theta_{\pm} - \theta_p \quad , \text{ and}$$

$$\phi = \theta_{\pm} - \theta_h \quad .$$

Equation (A6.6) can be greatly simplified with the aid of tabulated integrals, and by using the definition of the Bessel function. The angular integration of I_1 and I_2 may be written in the form

$$I = \int_0^{2\pi} e^{j\beta\cos u} du \quad , \quad (A6.7)$$

where

$$\beta = \begin{cases} k_p r \rho / z & \text{for } I_1 \\ k_{\pm} r \sigma / (L - z) & \text{for } I_2. \end{cases}$$

The definition of the Bessel function of the first kind is¹¹¹

$$J_n(\beta) = \frac{1}{2\pi} \int_{-\pi}^{\pi} e^{j(\beta \sin x - nx)} dx \quad (A6.8)$$

Using the change of variables, $u = x - \frac{\pi}{2}$, and taking the case for which $n = 0$, Eq. (A6.8) becomes

$$J_0(\beta) = \frac{1}{2\pi} \int_{-\frac{3\pi}{2}}^{\frac{\pi}{2}} e^{j\beta \cos u} du \quad (A6.9)$$

From Eqs. (A6.7) and (A6.9) we can write

$$I = 2\pi J_0(\beta)$$

so that I_1 and I_2 become

$$I_1 = 2\pi \int_0^{\infty} J_0\left(\frac{k_{\pm} r \rho}{z}\right) \exp\left[-\left(\frac{\rho}{b}\right)^2 - jk_{\pm} \rho^2 / 2z\right] \rho d\rho$$

and

$$I_2 = 2\pi \int_0^{\infty} J_0\left(\frac{k_{\pm} r \sigma}{L-z}\right) \exp\left[-\left(\frac{\sigma}{h}\right)^2 - jk_{\pm} \sigma^2 / 2(L-z)\right] \sigma d\sigma$$

Now I_1 and I_2 are in the form of a tabulated¹¹² integral, viz,

$$\int_0^{\infty} x^{v+1} e^{-\alpha x^2} J_v(\beta x) dx = \beta^v (2\alpha)^{-(v+1)} \exp(-\beta^2 / 4\alpha) \quad (A6.10)$$

Evaluation of I_1 and I_2 using Eq. (A6.10) gives

$$I_1 = \frac{\pi b^2}{\left[1 + \frac{jk_{\pm} b^2}{2z}\right]} \exp\left\{-\left(\frac{k_{\pm} r}{z}\right)^2 \frac{b^2}{4\left(\frac{1}{b^2} + \frac{jk_{\pm}}{2z}\right)}\right\} \quad (A6.11)$$

and

$$I_2 = \frac{\pi h^2}{\left[1 + \frac{jk_{\pm} h^2}{2(L-z)}\right]} \exp\left\{-\left(\frac{k_{\pm} r}{L-z}\right)^2 \frac{h^2}{4\left[\frac{1}{h^2} + \frac{jk_{\pm}}{2(L-z)}\right]}\right\} \quad (A6.12)$$

By substituting Eqs. (A6.11) and (A6.12) into Eq. (A6.6), the hydrophone voltage can be expressed as

$$v_H = A_{\pm} \int_0^L \int_0^{\infty} \frac{1}{C_2} e^{-C_1 r^2} 2r dr dz \quad (\text{A6.13})$$

$$\text{where } A_{\pm} = \frac{\pi \omega_{\pm}^2 \beta_S^P P_O M_O}{2 \rho_O c_O^4} e^{-jk_{\pm} L}$$

$$C_1 = j \left(\frac{k_P}{2z} + \frac{k_{\pm}}{2(L-z)} \right) + \frac{k_P^2 b^2}{4 \left(1 + \frac{jk_P b^2}{2z} \right)} + \frac{k_{\pm}^2 h^2}{4 \left(1 + j \frac{k_{\pm} h^2}{2(L-z)} \right) (L-z)^2}$$

$$\text{and } C_2 = 4z(L-z) \left(1 + j \frac{k_P b^2}{2z} \right) \left(1 + j \frac{k_{\pm} h^2}{2(L-z)} \right) \frac{1}{b^2 h^2}$$

As C_1 and C_2 are independent of r , the integration with respect to r can be done by the change of variable, $u = r^2$. The result is

$$v_H = A_{\pm} \int_0^L \frac{1}{C_1 C_2} dz \quad (\text{A6.14})$$

Equation (A6.14) represents the hydrophone voltage produced by the second-order pressure field in a homogeneous medium. In the next section this result will be used to determine the amplitude fluctuations in the second-order pressure when inhomogeneities are present in the medium.

A6.2 Amplitude Fluctuations in an Inhomogeneous Medium

In an inhomogeneous medium the hydrophone voltage will fluctuate in amplitude and phase, and may be written in a form similar to Eq. (4.14), viz,

$$v_{\pm} = v_H (1 + B_{PR} - jS_{PR}) \quad (\text{A6.15})$$

where B_{PR} and S_{PR} are the amplitude and phase fluctuations, respectively,

of the interaction frequency pressure at the hydrophone. A development similar to that in Section 4.2 gives the following expression for v_{\pm} in terms of the total amplitude and phase fluctuations, B and S:

$$v_{\pm} = A_{\pm} \int_0^L (1 + B - jS) \frac{1}{C_1 C_2} dz \quad . \quad (A6.16)$$

Following the methods used in Section 4.2, we substitute Eq. (A6.16) for v_{\pm} in Eq. (A6.15), and at the same time write v_H in terms of its magnitude and phase:

$$|v_H| e^{j\theta} (1 + B_{PR} - jS_{PR}) = A_{\pm} \int_0^L (1 + B - jS) \frac{dz}{C_1 C_2} \quad . \quad (A6.17)$$

Subtracting the homogeneous solution, Eq. (A6.14), from both sides of Eq. (A6.17), and dividing by the hydrophone voltage v_H , we obtain

$$\begin{aligned} B_{PR} - jS_{PR} &= \frac{A_{\pm}}{|v_H|} \int_0^L (B - jS) e^{-j\theta} \frac{dz}{C_1 C_2} \\ &= |v_H|^{-1} \int_0^L (B - jS) K(z) dz \quad , \end{aligned} \quad (A6.18)$$

$$\text{where } K(z) = \frac{A_{\pm} e^{-j\theta}}{C_1 C_2} \quad .$$

The amplitude fluctuation term can be found by taking the real part of Eq. (A6.18), and is

$$B_{PR} = |v_H|^{-1} \int_0^L [B \operatorname{Re}(K) + S \operatorname{Im}(K)] dz \quad .$$

The mean-squared amplitude fluctuations of the second-order pressure at the hydrophone are therefore

$$\langle B_{PR}^2 \rangle = |v_H|^{-2} \int_0^L \int_0^L \langle [B_1 \operatorname{Re}(K_1) + S_1 \operatorname{Im}(K_1)] \times [B_2 \operatorname{Re}(K_2) + S_2 \operatorname{Im}(K_2)] \rangle dz_1 dz_2$$

Writing this result in terms of the coefficient of amplitude variation, and expanding the terms in angular brackets, we obtain

$$\begin{aligned} \text{CAV}_{PR}^2 = |v_H|^{-2} \int_0^L \int_0^L \left\{ \operatorname{Re}(K_1) \operatorname{Re}(K_2) \langle B_1 B_2 \rangle \right. \\ \left. + \operatorname{Im}(K_1) \operatorname{Im}(K_2) \langle S_1 S_2 \rangle + \operatorname{Re}(K_1) \operatorname{Im}(K_2) \langle B_1 S_2 \rangle \right. \\ \left. + \operatorname{Im}(K_1) \operatorname{Re}(K_2) \langle S_1 B_2 \rangle \right\} dz_1 dz_2, \end{aligned}$$

which appears in the text as Eq. (5.12).

REFERENCES

1. G. G. Stokes, *Phil. Mag. (Series 3)*, 33, 349 (1848).
2. For example, D. T. Blackstock, "History of Nonlinear Acoustics and a Survey of Burgers' and Related Equations," Nonlinear Acoustics, Proceedings of the 1969 Symposium held at Applied Research Laboratories, The University of Texas at Austin (1970).
3. For example, T. G. Muir, "Nonlinear Acoustics: A New Dimension in Underwater Sound," a paper submitted by its author to the Office of Naval Research for inclusion in a collection entitled "Research Perspectives" (1976).
4. For example, R. T. Beyer and S. V. Letcher, Physical Ultrasonics, Chapter 7 (New York, 1969).
5. Lord Rayleigh, The Theory of Sound, Vol. II, Section 297 (Dover Publications, New York, 1945).
6. G. A. Sorge, Anwesung zur Stimmung der Orgelwerke und des Claviers, (Hamburg, 1744). Cited in Ref. 8.
7. G. Tartini, Trattato di Musica (Padua, 1754). Cited in Ref. 8.
8. R. T. Beyer, Nonlinear Acoustics, pp. 9-10 (Naval Ship Systems Command, Department of the Navy, 1974).
9. V. M. Albers, Underwater Sound, Benchmark Papers in Acoustics, p. 415 (Dowden Hutchinson and Ross, Inc., 1972).
10. P. J. Westervelt, "Parametric Acoustic Array," *J. Acoust. Soc. Am.* 35, 535 (1963). Presented at the 59th A.S.A. Meeting, 1960.
11. For example, T. G. Muir, "An Analysis of the Parametric Acoustic Array for Spherical Wave Fields," Applied Research Laboratories Technical Report No. 71-1, Chapter 4 (1971). (Dissertation presented to the University of Texas at Austin for Ph.D.)
12. For example, R. J. Urick, Principles of Underwater Sound for Engineers, Section 6.4 (McGraw-Hill Book Company, New York, 1967).
13. W. H. Munk and F. Zachariassen, "Sound Propagation through a Fluctuating Stratified Ocean: Theory and Observation," *J. Acoust. Soc. Am.* 59, 818 (1976).
14. D. C. Whitmarsh, E. Skudrzyk, and R. J. Urick, "Forward Scattering of Sound in the Sea and its Correlation with the Temperature Microstructure," *J. Acoust. Soc. Am.* 29, 1124 (1957).
15. P. G. Bergmann, "Propagation of Radiation in a Medium with Random Inhomogeneities," *Phys. Rev.* 70, 486 (1946).
16. D. Mintzer, "Wave Propagation in a Randomly Inhomogeneous Medium. I," *J. Acoust. Soc. Am.* 25, 922-927 (1953). "Part II", 25, 1107-1111 (1953). "Part III", 26, 186 (1954).
17. E. Skudrzyk, "Scattering in an Inhomogeneous Medium," *J. Acoust. Soc. Am.* 29, 50 (1957).

REFERENCES (cont'd)

18. L. Chernov, Wave Propagation in a Random Medium (McGraw-Hill Book Co., 1960; reprinted by Dover Publications, New York, 1967).
19. V. I. Tatarski, Wave Propagation in a Turbulent Medium (McGraw-Hill Book Co., 1961; reprinted by Dover Publications, New York, 1967).
20. M. J. Lighthill, "On Sound Generated Aerodynamically I. General Theory," Proc. Roy. Soc. (London) A211, 564-587 (1952).
21. M. J. Lighthill, "On Sound Generated Aerodynamically II. Turbulence As a Source of Sound," Proc. Roy. Soc. (London) A222, 1-32 (1954).
22. P. J. Westervelt, "Scattering of Sound by Sound," J. Acoust. Soc. Am. 48, 199-203 (1957).
23. P. J. Westervelt, "Scattering of Sound by Sound," J. Acoust. Soc. Am. 49, 934-935 (1957).
24. For example, Reference 11, p. 6.
25. B. V. Smith, "Nonlinear Acoustics, Transmitting Applications," p. 44 (Ph.D. Thesis, The University of Birmingham, 1965). Supplemented by private communication.
26. P. J. Westervelt, "Virtual Sources in the Presence of Real Sources," Nonlinear Acoustics, Proceedings of the 1969 Symposium held at Applied Research Laboratories, The University of Texas at Austin (1970).
27. P. M. Morse, Vibration and Sound, Second Edition, p. 313 (McGraw-Hill Book Company, New York, 1948).
28. J. L. S. Bellin and R. T. Beyer, "Experimental Investigation of an End-Fire Array," J. Acoust. Soc. Am. 34, 1051 (1962).
29. H. O. Berkta, "Possible Exploitation of Non-Linear Acoustics in Underwater Transmitting Applications," J. Sound Vib. 2, 435 (1965).
30. H. O. Berkta and B. V. Smith, "End Fire Array of Virtual Sound Sources Arising from the Interaction of Sound Waves," Electronic Letters I, 6 (1965).
31. H. Hobaek, "Experimental Investigation of an Acoustical End Fired Array," J. Sound Vib. 6, 460 (1967).
32. V. A. Zverev and A. I. Kalachev, "Measurements of the Scattering of Sound by Sound in the Superposition of Parallel Beams," Soviet Phys. Acoust. 14, 173 (1968).
33. T. G. Muir and J. E. Blue, "Experiments on the Acoustical Modulation of Large Amplitude Waves," J. Acoust. Soc. Am. 46, 227 (1969).
34. B. V. Smith, "An Experimental Study of a Parametric End-Fire Array," J. Sound Vib. 14, 7 (1971).
35. H. O. Berkta, "Parametric Amplification by the Use of Acoustic Non-Linearities and Some Possible Applications," J. Sound Vib. 2, 462 (1965).

REFERENCES (cont'd)

36. J. J. Truchard, "A Theoretical and Experimental Investigation of the Parametric Acoustic Receiving Array," Applied Research Laboratories Technical Report No. 74-17, Chapter 2 (1974). (Also Ph.D. Thesis, The University of Texas at Austin, 1974).
37. H. O. Berkday and C. A. Al-Temimi, "Virtual Arrays for Underwater Reception," J. Sound Vib. 9, 295 (1969).
38. H. O. Berkday and C. A. Al-Temimi, "Up-Converter Parametric Amplifications of Acoustic Waves in Liquids," J. Sound Vib. 13, 67 (1970).
39. G. R. Barnard, J. G. Willette, J. J. Truchard, and J. A. Shooter, "Parametric Acoustic Receiving Array," J. Acoust. Soc. Am. 52, 1437 (1972).
40. W. L. Konrad, R. H. Mellen, and M. B. Moffett, "Parametric Sonar Receiving Experiments," Naval Underwater Systems Center, Technical Memorandum PA4-304-71 (1971).
41. V. A. Zverev and A. I. Kalachev, "Modulation of Sound by Sound in the Intersection of Sound Waves," Soviet Phys. Acoust. 16, 204 (1970).
42. H. O. Berkday and T. G. Muir, "Arrays of Parametric Receiving Arrays," J. Acoust. Soc. Am. 53, 1377 (1973).
43. H. O. Berkday and J. A. Shooter, "Parametric Receivers with Spherically Spreading Pump Waves," J. Acoust. Soc. Am. 54, 1056 (1973).
44. J. J. Truchard, "Parametric Acoustic Receiving Array. I. Theory," J. Acoust. Soc. Am. 58, 1141 (1975). "II. Experiment," 1146.
45. A. Freedman, "Sound Field of a Rectangular Piston," J. Acoust. Soc. Am. 32, 197 (1960).
46. H. O. Berkday, "A Study of Travelling-Wave Parametric Amplification Mechanism on Nonlinear Acoustics," J. Sound Vib. 5, 155 (1967).
47. C. A. Al-Temimi, "Non-Linear Acoustics Receiving Applications and Signal Processing," (Ph.D. Thesis, The University of Birmingham, 1968).
48. D. F. Rohde, T. G. Goldsberry, W. S. Olsen, and C. R. Reeves, "Band Elimination Processor for an Experimental Parametric Acoustic Receiving Array," J. Acoust. Soc. Am. 66, 484-487 (1979).
49. R. A. Lamb, "Investigation of a Phase-Locked Loop Receiver for a Parametric Acoustic Receiving Array," (MS Thesis, The University of Texas at Austin, 1980).
50. C. R. Reeves, "A Mixer-Receiver for the Parametric Acoustic Receiving Array," Technical Report ARL-TR-78-33, Applied Research Laboratories, The University of Texas at Austin (1978).

REFERENCES (cont'd)

51. C. A. Al-Temimi, "Effects of Acoustic Shadows on the Performance of a Parametric Receiving System," *J. Sound Vib.* 13, 415 (1970).
52. D. T. Blackstock, "Nonlinear Acoustics (Theoretical)," Section 3n in American Institute of Physics Handbook, Third Edition (McGraw-Hill Book Company, New York).
53. D. T. Blackstock, "On Plane, Spherical, and Cylindrical Sound Waves of Finite Amplitude in Lossless Fluids," *J. Acoust. Soc. Am.* 36, 217 (1964).
54. D. T. Blackstock, "Thermoviscous Attenuation of Plane Periodic Finite-Amplitude Sound Waves," *J. Acoust. Soc. Am.* 36, 534 (1964).
55. H. Merklinger, "High Intensity Effects in the Nonlinear Acoustic Parametric End-Fire Array," (Ph.D. Thesis, The University of Birmingham, 1971).
56. H. O. Berktaay, "Finite-Amplitude Effects in Acoustic Propagation in Fluids," Memorandum, Dept. of Electronic and Electrical Engineering, University of Birmingham.
57. H. O. Berktaay, "The Use of Parametric Receivers for the Reception of Low-Frequency Signals," Memorandum, Dept. of Electronic and Electrical Engineering, University of Birmingham.
58. H. O. Berktaay, "On the Noise-Rejection Properties of Parametric Receivers," Memorandum, Dept. of Electronic and Electrical Engineering, University of Birmingham.
59. T. G. Goldsberry, "Parameter Selection Criteria for Parametric Receivers," Paper presented at the 88th Meeting of the Acoustical Society of America (November 1974).
60. T. G. Goldsberry, "Noise in Parametric Receivers," Paper presented at the 98th Meeting of the Acoustical Society of America (April 1975).
61. T. G. Goldsberry, "The PARRAY as an Acoustic Sensor," Paper 4.1, Proceedings of the Conference Underwater Application of Non-Linear Acoustics held at School of Physics, University of Bath, England (1979).
62. W. S. Olsen, T. G. Goldsberry, C. R. Reeves, and D. F. Rohde, "A Crystal Controlled Pump Signal Source for an Experimental Parametric Acoustic Receiving Array," Paper presented at the 92nd Meeting of the Acoustical Society of America (November 1976).
63. C. R. Reeves, T. G. Goldsberry, V. E. Maki, and D. F. Rohde, "Vibration Sensitivity of the Parametric Acoustic Receiving Array," paper presented at the International Conference on Acoustics, Speech, and Signal Processing, IEEE, Tulsa, Oklahoma, 10-12 April 1978. (Published in the Conference Record.)
64. C. R. Reeves, T. G. Goldsberry, D. F. Rohde, and V. E. Maki, "Parametric Acoustic Receiving Array Response to Transducer Vibration," *J. Acoust. Soc. Am.* 67 (1980).

REFERENCES (cont'd)

65. H. O. Berkday and J. A. Shooter, "Nearfield Effects in End-Fire Line Arrays," *J. Acoust. Soc. Am.* 53, 550 (1973).
66. M. J. Sheehy, "Transmission of 24 kc Underwater Sound from a Deep Source," *J. Acoust. Soc. Am.* 22, 24 (1950).
67. R. G. Stone and D. Mintzer, "Range Dependence of Acoustic Fluctuations in a Randomly Inhomogeneous Medium," *J. Acoust. Soc. Am.* 34, 647 (1962).
68. V. N. Karavainikov, "Fluctuations of Amplitude and Phase in a Spherical Wave," *Soviet Phys. Acoust.* 3, 175 (1957).
69. L. J. Liebermann, "The Effect of Temperature Inhomogeneities in the Ocean on the Propagation of Sound," *J. Acoust. Soc. Am.* 23, 563 (1951).
70. H. Medwin, "Sound Phase and Amplitude Fluctuations Due to Temperature Microstructure in the Upper Ocean," *J. Acoust. Soc. Am.* 56, 1105 (1974).
71. V. I. Tatarski, The Effects of the Turbulent Atmosphere on Wave Propagation (Published for the National Oceanic and Atmospheric Administration, U. S. Department of Commerce, and the National Science Foundation, Washington, DC, by the Israel Program for Scientific Translations, 1971. Reproduced by National Technical Information Service, Springfield, Va., as Document Number TT-68-50464.)
72. B. J. Uscinski, The Elements of Wave Propagation in Random Media (McGraw-Hill International Book Company, New York, 1977).
73. A. Ishimaru, Wave Propagation and Scattering in Random Media (Academic Press, New York, 1977).
74. A. Ishimaru, "Theory and Application of Wave Propagation and Scattering in Random Media," *Proc. IEEE* 65, 1030-1060 (1977).
75. Y. N. Barabanenkov, Y. A. Kravtsov, S. M. Rytov, and V. I. Tatarski, "Status of the Theory of Propagation of Waves in a Randomly Inhomogeneous Medium," *Sov. Phys. Uspekhi* 13, 551-680 (1971).
76. R. J. Urick and C. W. Searfoss, "The Microthermal Structure of the Ocean Near Key West, Florida: Part I - Description; Part II - Analysis," *U. S. Naval Res. Lab. Repts.* S-3392 (1948) and S-3444 (1949). Cited in Ref. 12, p. 151.
77. Ref. 18, Chapter 1.
78. G. K. Batchelor, The Theory of Homogeneous Turbulence (Cambridge University Press, Cambridge, 1953).
79. J. O. Hinze, Turbulence (McGraw-Hill Book Company, Inc., New York, 1959).
80. Ref. 71, p. 53 or Ref. 19, p. 29.

REFERENCES (cont'd)

81. Ref. 71, p. 52.
82. Ref. 71, p. 80.
83. A. N. Kolmogorov, "Local Structure of Turbulence in an Incompressible Viscous Liquid at Very Large Reynolds Numbers," C. R. Aca. Sci. USSR, 30, 299-303 (1941). Cited in Ref. 76.
84. N. P. Chotiros and B. V. Smith, "Sound Amplitude Fluctuations Due to a Temperature Microstructure," J. Sound Vib. 64, 349-369 (1979).
85. Y. H. Pao, "Structure of Turbulent Velocity and Scalar Fields at Large Wavenumbers," Physics of Fluids 8, 1063-1075 (1965).
86. Ref. 5, Vol. II, Section 296. Cited in Ref. 17.
87. Ref. 18, Chapter 3.
88. Ref. 18, Section 16.
89. Ref. 18, Chapter 5.
90. V. N. Karavainikov, "Fluctuations of Amplitude and Phase in a Spherical Wave," Sov. Phys. Acoust. 3, 175-186 (1957).
91. N. P. Chotiros, "The Parametric Array in Inhomogeneous Medium" (MScQ Thesis, Dept. of Electronic and Electrical Engineering, The University of Birmingham, 1978). Equation (3.1.11).
92. Ref. 18, Chapter 6.
93. Ref. 91, Appendix II.
94. V. A. Eliseevnin, "Longitudinal Frequency Correlation of Fluctuations of the Parameters of Plane Waves Propagating in a Turbulent Medium," Sov. Phys. Acoust. 19, 533-538 (1974).
95. B. V. Smith and W. Weston-Bartholomew, "An Investigation of a Parametric Array in a Random Medium," Dept. of Electronic and Electronic Engineering, University of Birmingham, England.
96. B. V. Smith, "A Theoretical Study of the Effect of an Inhomogeneous Medium upon a Transmitter which Exploits the Non-Linear Properties of Acoustic Propagation," J. Sound Vib. 17, 129 (1971).
97. N. P. Chotiros and B. V. Smith, "The Parametric End-Fire Array in a Random Medium," Proceedings of the Conference Recent Developments in Underwater Acoustics held by the Institute of Acoustics (31 March 1976).
98. E. O. Lacasce, Jr., R. G. Stone, and D. Mintzer, "Frequency Dependence of Acoustic Fluctuations in a Randomly Inhomogeneous Medium," J. Applied Phys. 33, 2710-2714 (1972).

REFERENCES (cont'd)

99. R. G. Stone and D. Mintzer, "Transition Regime for Acoustic Fluctuations in a Randomly Inhomogeneous Medium," *J. Acoust. Soc. Am.* 38, 843-846 (1965).
100. W. J. Sederowitz and A. G. Favret, "Covariance Between Acoustic Signals Travelling Diverging Paths in a Random Medium," *J. Acoust. Soc. Am.* 45, 386-391 (1969).
101. S. J. Campanello and A. G. Favret, "Time Autocorrelation of Sonic Pulses Propagated in a Random Medium," *J. Acoust. Soc. Am.* 46, 1234-1245 (1969).
102. Ref. 47, p. 25.
103. E. L. Crow, F. A. Davis, and M. W. Maxfield, Statistics Manual, p. 152 (Dover Publications, New York, 1960).
104. Ref. 91, Section 4.2.1.
105. Ref. 91, Appendix II.
106. N. P. Chotiros, "Parametric Receiver: Calculation of Difference Frequency Signals for Gaussian Shaded Circular Transducers and an Axial Plane Wave Signal" (unpublished).
107. H. O. Berktaf, "Nearfield Effects in Parametric End-Fire Arrays," *J. Sound Vib.* 20, 135-143 (1972).
108. R. T. Aiken, "Propagation from a Point Source in a Randomly Refracting Medium," *Bell Sys. Tech. Journal*, 1129-1165 (May 1969).
109. K. F. Knott, "Sensitive Wideband Linear A.C.-D.C. Convertor," *Proc. IEE* 122, 249-252 (1975).
110. Ref. 91, Appendix III.
111. M. Schwartz, Information Transmission, Modulation, and Noise, p. 243 (McGraw-Hill Book Company, Inc., New York, 1970).
112. I. S. Gradshteyn and I. M. Ryzhik, Table of Integrals, Series, and Products, Fourth Edition, p. 717, Eq. 4 (Academic Press, New York, 1965).

18 August 1980

DISTRIBUTION LIST FOR
ARL-TR-80-44
UNDER CONTRACTS N00024-79-C-6358 and N00014-75-C-0161
UNCLASSIFIED

Copy No.

Commander
Naval Sea Systems Command
Department of the Navy
Washington, DC 20362
1 Attn: Mr. C. D. Smith, Code 06R/63R
2 Dr. E. Liszka, Code 63R
3 Mr. D. E. Porter, Code 63R
4 CAPT R. H. Scales, PMS 402
5 Mr. D. L. Baird, Code 63X3
6 CDR D. F. Bolka, Code 63G
7 Mr. D. M. Early, Code 63D
8 Mr. John Neely, Code 63X3

Commander
Naval Electronic Systems Command
Department of the Navy
Washington, DC 20360
9 Attn: CAPT H. Cox, PME 124
10 Dr. J. A. Sinsky, Code 320A

Defense Advanced Research Projects Agency
1400 Wilson Boulevard
Arlington, VA 22209
11 Attn: CDR V. P. Simmons (TTO)
12 Dr. T. Kooij

13 Chief of Naval Material
Department of the Navy
Washington, DC 20360

Director
Naval Research Laboratory
Department of the Navy
Washington, DC 20375
14 Attn: Dr. M. Potosky, Code 5109
15 Dr. J. Jarzynski, Code 5131
16 Dr. R. D. Corsaro, Code 5131

Distribution List for ARL-TR-80-44 under Contract N00024-79-C-6358,
Item 0021 (Cont'd)

Copy No.

Naval Research Laboratory
Underwater Sound Reference Division
P. O. Box 8337
Orlando, FL 32806
17 Attn: Dr. J. E. Blue
18 Dr. Lee Van Buren
19 Dr. Peter H. Rogers

Commanding Officer
Naval Ocean Systems Center
Department of the Navy
San Diego, CA 92152
20 Attn: Dr. H. Schenck, Code 71
21 Mr. M. Akers, Code 724
22 Dr. H. P. Bucker, Code 5311

Office of the Chief of Naval Operations
The Pentagon
Washington, DC 20350
23 Attn: CAPT Bruce Gilchrist, OP-95T

Office of the Chief of Naval Operations
Long Range Planning Group
2000 North Beauregarde St.
Alexandria, VA 22311
24 Attn: CAPT J. R. Seesholtz

Officer-in-Charge
New London Laboratory
Naval Underwater Systems Center
Department of the Navy
New London, CT 06320
25 Attn: M. B. Moffett, Code 313
26 W. L. Konrad
27 R. H. Mellen

Chief of Naval Research
Department of the Navy
Arlington, VA 22217
28 Attn: Mr. R. F. Obrochta, Code 464
29 Dr. L. E. Hargrove, Code 421

Commander
Naval Ocean Research and Development Activity
NSTL Station, MS 39529
30 Attn: Dr. A. L. Anderson
31 Dr. S. W. Marshall

Distribution List for ARL-TR-80-44 under Contract N00024-79-C-6358.
Item 0021 (Cont'd)

Copy No.

| | |
|-------|--|
| 32 | Commanding Officer USCG Research and Development Center Avery Point Groton, CT 06340 Attn: CAPT M. Y. Suzich |
| 33-43 | Commanding Officer and Director Defense Technical Information Center Cameron Station, Building 5 5010 Duke Street Alexandria, VA 22314 |
| 44 | Battelle Columbus Laboratories 505 King Avenue Columbus, OH 43201 Attn: TACTEC |
| 45 | Applied Research Laboratory The Pennsylvania State University State College, PA 16801 Attn: Dr. F. H. Fenlon |
| 46 | Westinghouse Electric Corporation P. O. Box 1488, MS9R40 Annapolis, MD 21404 |
| 47 | Attn: Mr. A. Nelkin Dr. P. J. Welton |
| 48 | Raytheon Company P. O. Box 360 Portsmouth, RI 02871 Attn: Mr. J. F. Bartram |
| 49 | Mr. E. P. Aurand 19 Hanapepe Place Honolulu, HI 96825 |
| 50 | Department of Engineering and Applied Science Yale University New Haven, CT 06520 Attn: Dr. P. M. Schultheiss |
| 51 | RAMCOR, Inc. 800 Follin Lane Vienna, VA 22180 Attn: Mr. V. J. Lujetic |

Distribution List for ARL-TR-80-44 under Contract N00024-79-C-6358,
Item 0021 (Cont'd)

Copy No.

| | |
|----|--|
| 52 | Systems Planning Corporation 1500 Wilson Blvd., Suite 1500 Arlington, VA 22209 Attn: Mr. Jack Fagan |
| 53 | Bolt, Beranek, and Newman, Inc. 50 Moulton Street Cambridge, MA 02138 Attn: Dr. J. E. Barger |
| 54 | Dr. F. J. Jackson |
| 55 | Marine Physical Laboratory of The Scripps Institution of Oceanography San Diego, CA 92152 Attn: Dr. William S. Hodgkiss |
| 56 | TRACOR, Inc. 6500 Tracor Lane Austin, TX 78721 Attn: Mr. J. Dow |
| 57 | Mr. D. F. Rohde |
| 58 | Radian Corporation 8500 Shoal Creek Blvd. Austin, TX 78758 Attn: Mr. Jerry L. Bardin |
| 59 | Dr. C. Richard Reeves |
| 60 | Office of Naval Research Resident Representative Room 582, Federal Building Austin, TX 78701 |
| 61 | General Physics Corporation 10630 Little Patuxin Turnpike Columbia, MD 21044 Attn: Dr. Frank Andrews |
| 62 | Commanding Officer Naval Postgraduate School Monterey, CA 93940 Attn: Prof. G. Sacklman |
| 63 | Prof. A. B. Coppens |
| 64 | Prof. J. V. Sanders |

Distribution List for ARL-TR-80-44 under Contract N00024-79-C-6358,
Item 0021 (Cont'd)

Copy No.

| | |
|----|---|
| 65 | Trans World Systems, Inc. 1311A Dolly Madison Blvd. McLean, VA 22101 Attn: Mr. Sam Francis |
| 66 | Department of Physics Hendrix College Conway, AR 72032 Attn: Prof. R. L. Rolleigh |
| 67 | Department of Physics Brown University Providence, RI 02912 Attn: Prof. P. J. Westervelt |
| 68 | Prof. R. T. Beyer |
| 69 | Department of Electrical Engineering The University of Texas at Austin Austin, TX 78712 Attn: Prof. E. L. Hixson |
| 70 | Prof. W. C. Duesterhoeft |
| 71 | Prof. E. J. Powers |
| 72 | Department of Mechanical Engineering The University of Texas at Austin Austin, TX 78712 Attn: Prof. R. L. Panton |
| 73 | Physical Sciences Group, ARL:UT |
| 74 | G. R. Barnard, ARL:UT |
| 75 | D. T. Blackstock, ARL:UT |
| 76 | J. Byers, ARL:UT |
| 77 | C. R. Culbertson, ARL:UT |
| 78 | T. G. Goldsberry, ARL:UT |
| 79 | J. M. Huckabay, ARL:UT |

Distribution List for ARL-TR-80-44 under Contract N00024-79-C-6358,
Item 0021 (Cont'd)

Copy No.

| | |
|--------|-------------------------|
| 80 | R. A. Lamb, ARL:UT |
| 81 | T. G. Muir, ARL:UT |
| 82 | M. W. Widener, ARL:UT |
| 83 | R. H. Wallace, ARL:UT |
| 84 | J. R. Clynch, ARL:UT |
| 85 | L. D. Hampton, ARL:UT |
| 86 | Library, ARL:UT |
| 87 | Physical Sciences Group |
| 88-100 | ARL:UT Reserve |

ATE
LMED
8